Università
Ca'Foscari
Venezia

Laurea Magistrale in Scienze e Tecnologie dei Bio e Nano Materiali

Anno 2018-2019

Synthesis and structural characterization of Gadolinium oxide and Lanthanide doped gadolinium oxide anisotropic nanoparticles.

Laureando: Franceschin Matteo   Relatore: prof.ssa Canton Patrizia

Matricola 845395

Sommario

LIST OF TABLES

LIST OF FIGURES

LIST OF SCHEMES

What are Nanoparticles?

In the technological field the term "nanoparticle" is a source of ambiguity since a definition that includes the different facets of the term itself isn't well defined.

*The term was born towards the end of twentieth century as a composition of nano- and particle and is defined as "**atomic or molecular aggregate, present in nature or produced by means of nanotechnologies, characterized by chemical and physical properties and by size of the order of nanometer"**.*

Subsequently the ISO and ASTM experts have coined several definitions, some of which are reported below.

*The Nanoscale newspaper defines a nanoparticle as "**particle of size between 1 nm and 100 nm**" (ISO/TS 27687)* [1].

In this definition the dimensional limits are approximated because, it doesn't include system whose dimension develop more along one direction than another (such as rods and plate); while the lower limit is set so as to prevent groups of single object constituting nanostructures or individual atoms from being called "nano-object". This incomplete definitions was soon implemented so that in it are considered mono-, bi- and tri-dimensional structure included in the range 1-100 nm [2]*, emphasizing the dimensions linked to the particular application of the nanostructured material and not to its properties.*

In 2010, the Scientific Committee on Emerging and Newly Identified Health Risks (SCENIHR) provided a complete definition of the term "nanoparticle" [3]*. This document divides the nanoparticles into three categories respect to the dimension, on the basis of which a risk assessment is provided:*

- *Category 1, size > 500 nm: average dimensions are taken into consideration. The high deviation from the limit value (100 nm) indicates than probably the dimensions of the single particles are greater than the upper limit itself. The classification is then performed based on the specific properties with respect to the nature of the material constituting the nanoparticles.*

- *Category 2, 100 < size < 500 nm: the probability that a part of the material has dimensions of approximately 100 nm is taken into consideration. The "middle" category refers to the previous one if the dimensional distribution of the sample approaches the value of 500 nm. On the contrary, if it is close to the lower limit of the dimensional interval defined by category 2, the system can be considered a nanomaterial and the risk classification must be performed according to the guidelines identified by category 3.*

- *Category 3, 100 < size < 1 nm: the system is considered as a nanomaterial and the risk assessment must be performed using the scheme provided by the cited document.*

This definition, therefore, not only provides a dimensional limit, but also makes it possible to classify a nanomaterial, formed by nanoparticles, through a thorough evaluation of the specific properties of the material.

*According to these considerations, the definitions given for the term "**nanoparticle**" don't include the infinite space of the possibility that the implementation of a nano-structured system offers. In the next paragraphs we will introduce system based on nanoparticles of a particular subspace, like the one whose application is in the field of nano-biotechnologies.*

INTRODUCTION

1.1 NANOPARTICLES FOR BIOMEDICAL APPLICATIONS: STATE OF THE ART

As it is known, a nano-structured material may exhibit different properties with respect to the same on a macroscopic scale [4]. For example, a property that characterizes metallic nanoparticles, which isn't found in bulk material, is the Surface Plasmon Resonance (SPR). It allows to build optically responsive system, which can be implemented, for example in bio sensor (sensor that detect the presence and concentration of biological component, such as DNA, proteins, within an active biological system) or in system investigated by Raman scattering and fluorescence spectroscopy.

SPR together other chemical-physical characteristics, make a system structure on a nanoscopic scale applicable in many technological fields ranging from electronics to restoration and from non-linear optics to bio-medicine.

In the biomedical field, in recent years, the research has focused on the design and implementation of system capable of allowing the diagnosis of pathologies and subsequently their treatment in a targeted manner and without damaging the areas not affected by the pathology itself.

It's therefore possible to talk about diagnostics and therapy [5]: for example, the aforementioned SPR property can exploited in optical imaging diagnostic techniques accompanied by the use of optically responsive material such as noble metals or rare earths. A second diagnostic technique that could make use of nano-structured system is that of the magnetic resonance imaging; however, the literature is scarce about this topic.

Instead there are countless example of nanoparticles used in therapy, a case is that of the DDS (Drug Delivery System) which envisages the use of mesoporous nanoparticles capable of locally drug releasing [6].

A new frontier is represented by the union of terms "*therapy*" and "*diagnostic*"; we talk about "*teragnostic*". A nano-structured system, to be applied in this field, must have characteristics directly related to the specific technical of the therapy and diagnosis for which it is designed. For example, if we are supposed to design a material suitable for photothermal therapy, we will need to choose a material that, on a nano scale, responds to a physical excitement with the emission of heat. A possible choice could be to use nanoparticles in Ag [7], Au [8] or, more generally, of metallic nanoparticles. To these it is possible to add bi-metallic particles consisting of Fe-Co [9], Fe-Pt [10] and nano-system in metal oxide such as TiO_2 [11], ZnO [12], and CeO_2 [13]. Furthermore, some bi-metallic alloys and metal oxide possess magnetic properties that make these materials suitable for their use as contrast agent in magnetic resonance imaging. For this purpose, the progenitor of the materials used is ferrite (Fe_2O_3) [14], which encompasses the basic chemical and physical properties necessary for biomedical applications.

These characteristics can be divided into two macro sections: general properties (such as biocompatibility, non-toxicity and chemical stability) and specific properties such as high saturation magnetisation and a high

magnetic susceptibility, if the material is to be applied in the magnetic resonance technique. The specific properties largely influence the choice of the material, which as mentioned, must be carried out based on its final application. In the other hand, the general properties can be obtained using appropriate synthetic and post-synthetic techniques.

As reported in the work of McNamara and Tofail [15] a nano-system can be classified based on the nature of the material composing it; recalling the example mentioned above, there are four classes of nano-system: metallic, bi-metallic, magnetic and metal oxides. However, each class of materials can be seen as a closed chamber in which all the existing material possess approximately the same characteristics. This makes these materials specific for a targeted use which is decided at the design stage.

Based on this, a question naturally arises: is it possible to "open the room" by designing a material with greater potential? In other words, would it be possible to produce a nano-scale system with different properties that could be used in more than one field?

Recently, a new class of material has been introduced that responds affirmatively to this question: the material belonging to this new "open chamber" are called **hybrid materials**.

Hybrid material are defined as "*composed of both inorganic and organic components*" [16]; they have an organic part, usually as a coating, which has size control functions, prevents aggregation to macro-particles or as a surface functionalization in order to make the nanoparticles dispersible in hydrophobic or hydrophilic media. A further function of organic components is to make the inorganic part of the nanoparticles compatible with a biological system. The inorganic part, instead, represent the heart of the system; whatever the purpose for which it is designed, its primary structure will be composed of an inorganic material that falls within the four general classes previously presented.

This definition, however, is not complete: in fact, to the hybrid material belong also systems formed by two or more inorganic compounds that provide different characteristics to the heart of the system to which subsequently can be added an organic component. In the literature there are many examples of such materials, some of which find applications in the field of sensor as nano thermometers [17] or as systems for controlled drug release (DDS), photothermal and photodynamic therapy [18]. For these applications, generally, nanoparticles composed of an inorganic matrix on which different elements are added depending on the desired properties; if these elements are added in a much lower quantity than the matrix, we call them **doped materials**. Among the known doping agents there are the lanthanides (or Rare Earths) which, thanks to their peculiar optical and magnetic properties, allow the design of hybrid materials that can be used simultaneously on multiple fronts. In recent years, the research has considered the design of nanoparticles formed mainly of rare earth derivatives [19] [20]; in fact, the known characteristics of these elements are emphasized by the reduced dimensional scale [21].

1.2 INTRODUCTION TO LANTHANIDES

1.2.1 Rare-earth elements: chemistry and spectroscopic properties

In the periodic table of elements, the lanthanides or rare earths, are the fourteen elements comprised between the Lanthanum (La, atomic number 57) and the Lutetium (Lu, atomic number 71). The electronic configuration sees the gradual filling of the 4f orbitals (hence the name "elements of the f block) and of the outermost 6s and 5d orbitals.

Element name	Symbol	Atomic number (Z)	Ln	Ln3+	Ln3+ radius [pm]
Lanthanum	La	57	$[Xe]6s^2 5d^1$	$[Xe]4f^0$	116
Cerium	Ce	58	$[Xe]4f^1 6s^2 5d^1$	$[Xe]4f^1$	114
Praseodymium	Pr	59	$[Xe]4f^3 6s^2$	$[Xe]4f^2$	113
Neodymium	Nd	60	$[Xe]4f^4 6s^2$	$[Xe]4f^3$	111
Promethium	Pm	61	$[Xe]4f^5 6s^2$	$[Xe]4f^4$	109
Samarium	Sm	62	$[Xe]4f^6 6s^2$	$[Xe]4f^5$	108
Europium	Eu	63	$[Xe]4f^7 6s^2$	$[Xe]4f^6$	107
Gadolinium	Gd	64	$[Xe]4f^7 6s^2 5d^1$	$[Xe]4f^7$	105
Terbium	Tb	65	$[Xe]4f^9 6s^2$	$[Xe]4f^8$	104
Dysprosium	Dy	66	$[Xe]4f^{10} 6s^2$	$[Xe]4f^9$	103
Holmium	Ho	67	$[Xe]4f^{11} 6s^2$	$[Xe]4f^{10}$	102
Erbium	Er	68	$[Xe]4f^{12} 6s^2$	$[Xe]4f^{11}$	100
Thulium	Tm	69	$[Xe]4f^{13} 6s^2$	$[Xe]4f^{12}$	99
Ytterbium	Yb	70	$[Xe]4f^{14} 6s^2$	$[Xe]4f^{13}$	99
Lutetium	Lu	71	$[Xe]4f^{14} 6s^2 5d^1$	$[Xe]4f^{14}$	98

Table 1*: Electronic configuration of lanthanide elements and its trivalent ions*

Observing their electronic configuration (table 1) it is evident that the external orbitals (6s and 5d) are not complete and therefore, the lanthanides are easily ionisable. In fact, these elements are commonly found in the oxidation state 3+ except for Ce and Tb which possess the state 4+ and Eu, Sm and Yb which can present in the form of bivalent ions. The cerium ion (Ce^{3+}) has only one electron in the 4f orbital, which being the most external and easily removable gives consequently rise to the oxide element in the tetravalent state. Europium, Samarium and Ytterbium, on the other hand, possess the closed 6s shell, so their oxidation can lead to the removal of only two electrons leaving the element in the oxidation state 2+.

The chemistry of lanthanides is strongly influenced by their electronical structure both for elementary and trivalent ions: in figure 1 the energy scheme of the orbitals 4f, 5d and 6s is reported. Since the 4f orbitals turn out to be internal respect to the 5d and 6s ones, and since these are partially (Ox state 0) or totally (Ox state 3+) empty they aren't involved in the formation of the chemical bond [22]
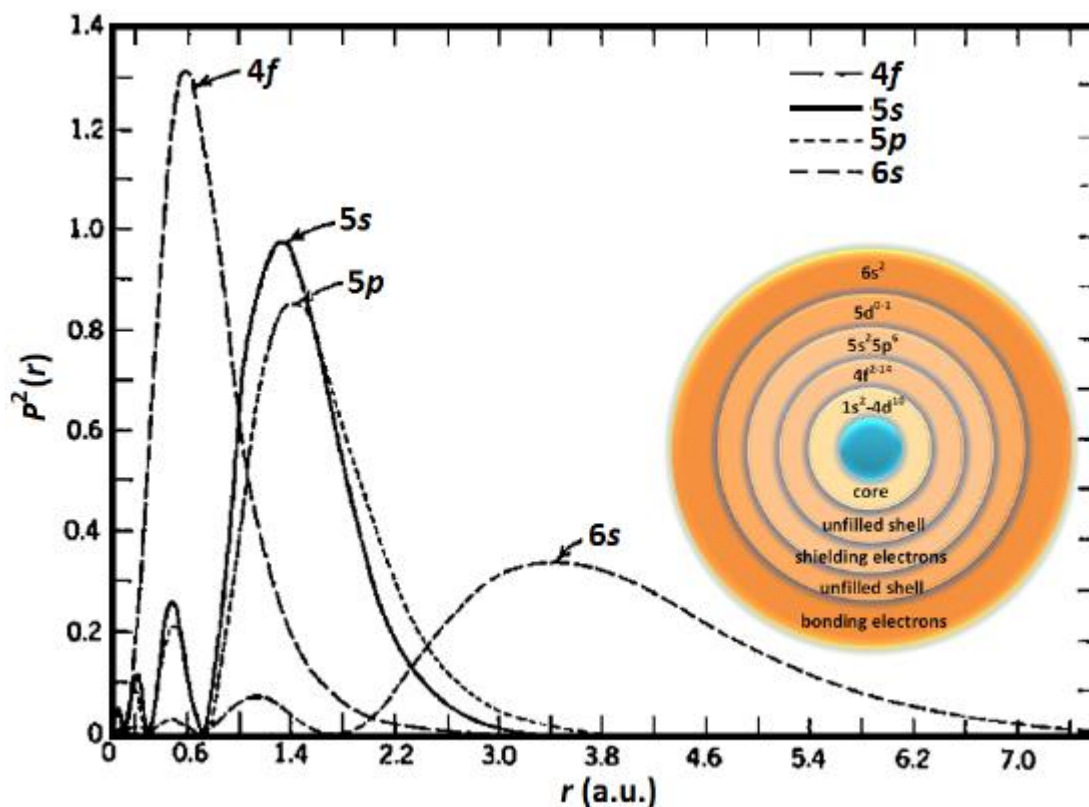
Figure 1: Square of the radial wave functions for the 4f, 5d and 6s energy level from Hartree-Fock. Inset shows a schematic representation of atomic orbitals and their roles [23]

The non-participation in any type of bond by the 4f orbitals makes the partially populated levels to electronic transition available, where these transitions are induced by electromagnetic waves (photons)at well-defined wavelengths.

In general, the seven orbitals should possess the same energy, however the electron-electron repulsive interaction induces a first energy separation between the levels quantifiable of the order of 10^2 cm^{-1}. A second division of energy levels is due to the interaction between angular momentum and spin angular momentum. This very intense interaction is described by the quantum number J whose values depend on the quantum number S and L respectively relative to the vector combination of all the spin moments of the Ln^{3+} ion considered and to the total orbital angular momentum deriving from the composition of the orbital angular moments of single electron.

The electronic states of lanthanides in the oxidation state 3+ are determined by the quantum numbers S, L and J; being numerous, they are represented in a scheme known as the Dieke diagram (figure 2) [24].
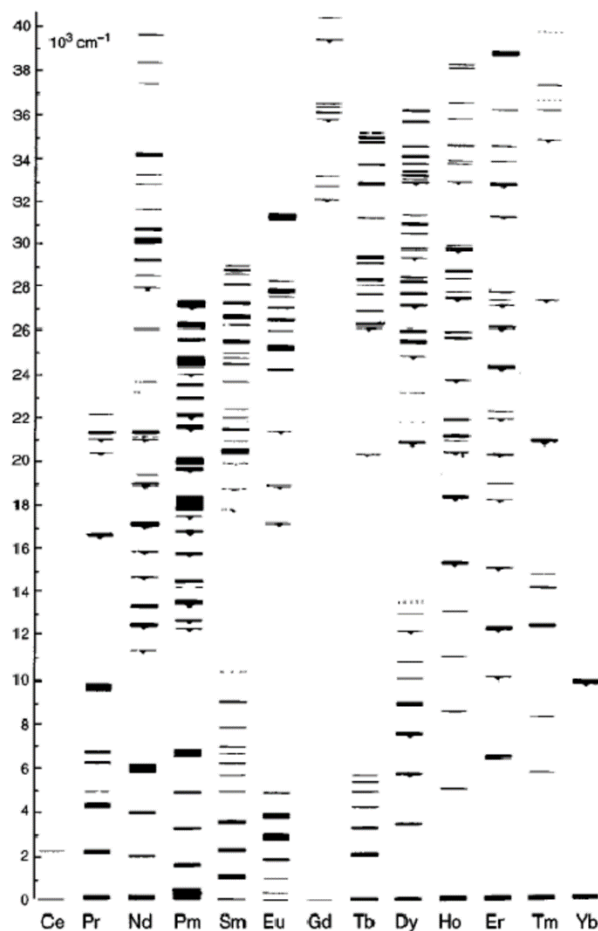
Figure 2: Dieke diagram - energy level of lanthanide in oxidation state 3+

As previously mentioned, the 4f orbitals are not involved in the formation of chemical bond, therefore the different energy levels aren't affected by the influence of the chemical environment (for example the presence of an organic binder or an inorganic matrix). This makes the electrons present in the 4f levels free and susceptible to light or electrical excitation; in other words this makes possible the f → f electronic transition whose intensity in strongly influenced by the symmetry of the ligand field (when the Ln^{3+} is in an organic complex) and by the symmetry of the crystal lattice when it is inserted into an inorganic matrix. Thus, by irradiating an Ln^{3+} ion with electromagnetic radiation, the electrons populating the ground state are excited at higher energy levels determining the excited state. If there weren't intermediate levels between the excited state and the fundamental one, the only relaxation channel would be the radiative one with emission of photons similar to those used for excitation.

In the f group this circumstance is verified only in the case of Gadolinium (Gd^{3+}) which, as it can be seen from the Dieke diagram (figure 2) has a single electronic level at about 5.2 eV from the ground state. This high energy gap value translates into absorption and emission in the ultraviolet region (at about 238 nm). In all the other elements, belonging to the lanthanide family, between the ground state and the excited state there are many levels of intermediate energies that can behave like traps for the electrons making some electronic

transition impossible. A second property that allows the use of these materials, is given by the fact that the intermediate levels constitute an alternative radiative relaxation channel for the f → f transition.

The f to f transition, present in each of the fourteen elements, identifies the excitation wavelength to promote the electrons from the ground state to the highest energy levels corresponding to the excited states. This transition can take place in three different ways:

- For direct excitation, with photons of specific wavelength in relation to the element;
- By combination of photons absorbed at a shorter wavelength than the one required for the f → f transition;
- As a result of an internal energy transfer to the system containing the trivalent ion.

In this last mechanism an "antenna" molecule is exploited that absorbs and transfer energy to the lanthanide indirectly inducing an electron transition [25]; similarly the direct absorption by light irradiation leads to the same results. From this excited state, the system can relax in the fundamental state or relax non-radiatively at a lower energy level from which the transition to the ground state takes place radiatively. In this mechanism the emitted photons will have a longer wavelength than the excitation one (since the energetic distance between the ground and excited state is smaller) which in some cases is located in the visible region (Eu^{3+}, Er^{3+}, Tb^{3+} and Sm^{3+}) or in the near infrared region (Nd^{3+}, Pr^{3+}, Ho^{3+} and Yb^{3+}). This relaxation way is known as Down Conversion (DC, figure 3a) and can also occur when the role of "antenna" is covered by a lanthanide ion; this is the case of bi-doped system. For example, a pair often used to obtain DC is that formed by Eu^{3+} and Tb^{3+}: by exciting Tb^{3+} directly, we obtain a high intensity emission in red region (616 nm) identifiable in the main transition of the Europium ion [26].
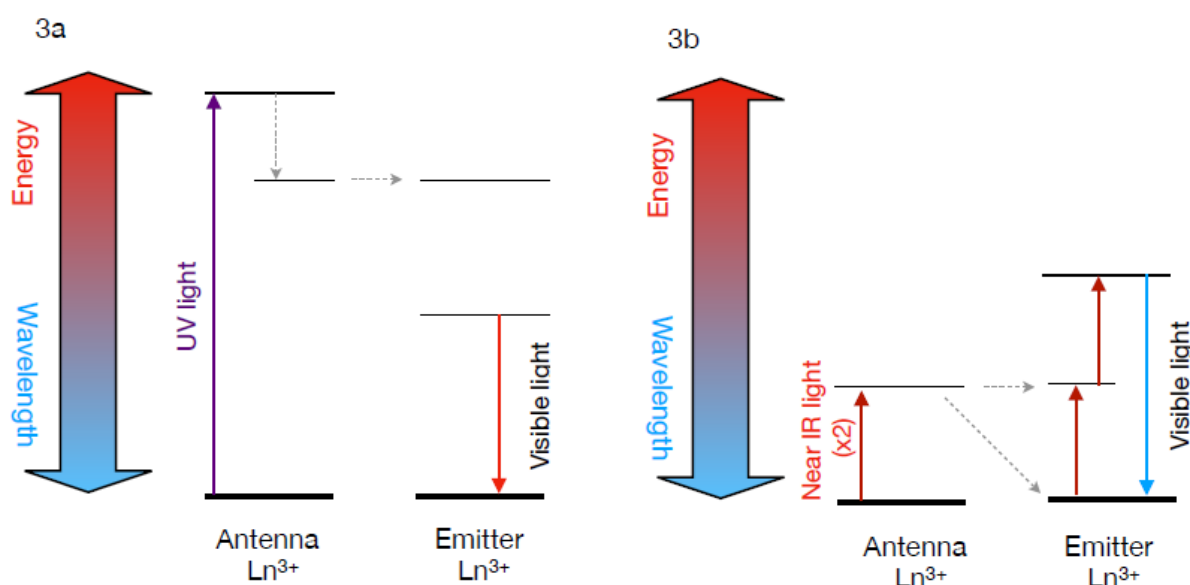
Figure 3: Down Conversion (a) and Up Conversion(b) mechanism in bi-doped system

Some lanthanides have near-infrared emission, such as Yb^{3+} ion: this channel of relaxation, that is the associated electronic transition, is also feasible in the opposite direction. It can be used to promote electron

from the ground state to an intermediate excited one and subsequently to the second excited state with higher energy by the absorption of photons with wavelength belonging to the near-infrared region. From the second excited state, the energy, can be transferred to another lanthanide, present in the chemical environment, or it can be released as photon with a shorter wavelength. This mechanism is called Up Conversion (UC, figure 3b) and can be used in photo thermal therapy and in medical diagnostic system [27] while system that exploit the down conversion mechanism are used in biomedical application and mainly in solar cells [28].

1.2.2 Magnetic properties

The presence of 4f energy level populated by unpaired electrons (with the exception of La^{3+} and Lu^{3+}) gives to the Ln^{3+} ions paramagnetic properties which are determined solely by the fundamental state since the excited one is energetically well separated due to the interaction already discussed in the previous paragraph. For each element, the magnetic momentum can be calculated using the quantum numbers S, L and J relative to the ground state [22]. The magnetic properties may not be transferred to the material containing a Ln^{3+} ions: for example, the Eu^{3+} ion is paramagnetic while its compounds are diamagnetic. This is due to the fact that the levels $^7F_1$ and $^7F_2$, immediately following the ground state ($^7F_0$), are thermally accessible and this results in a significant reduction of the magnetic moment which can be cancelled when it is inside a material. In general, any elements of the periodic table have magnetic properties that can manifest themselves in the form of ferro-magnetism, para-magnetism or diamagnetism. In the specific case of the lanthanide series the "degree of para-magnetism" and the intensity of the magnetic moment is accentuated when the excited state isn't thermally accessible; that is, there is a direct link between energy gap and magnetic moment. Using the following formula [22], it is possible to calculate the effective magnetic moment, expressed respect to the Bohr's magneton, for each of the fourteen lanthanides.

$$\mu_{eff} = \frac{3/2 + [S(S+1) - L(L+1)]}{2J(J+1)} \cdot \frac{1}{\sqrt{J(J+1)}} \qquad (1)$$

Element name	f^n	Ground term	Predicted μ_{eff} (μ_B)
Lanthanum	0	$^1S_0$	0.00
Cerium	1	$^2F_{5/2}$	2.54
Praseodymium	2	$^3H_4$	3.58
Neodymium	3	$^4I_{9/2}$	3.68
Promethium	4	$^5I_4$	2.83
Samarium	5	$^6H_{5/2}$	0.85
Europium	6	$^7F_0$	0.00
Gadolinium	**7**	$^8S_{7/2}$	**7.94**
Terbium	**8**	$^7F_6$	**9.72**
Dysprosium	**9**	$^6H_{15/2}$	**10.63**
Holmium	**10**	$^5I_8$	**10.60**
Erbium	**11**	$^4I_{15/2}$	**9.59**
Thulium	**12**	$^3H_6$	**7.57**
Ytterbium	13	$^2F_{7/2}$	4.53
Lutetium	14	$^1S_0$	0.00

__Table 2__: effective magnetic moments calculated by formula (1)

As it can be observed from the values expressed in table 2, the ions with the greatest magnetic dipole are Gd^{3+}, Tb^{3+}, Dy^{3+}, Ho^{3+}, Er^{3+} and Tm^{3+}. Since the magnetic properties are emphasized when the system is designed on a nano scale, these elements are used in the design of magnetic nanomaterials.

1.2.2.1 Magnetism: a brief introduction

The classic theory, developed by Weiss in the 1906 [29], shows how the macroscopic property that gives rise to magnetism is present in all materials and only if some "environmental" conditions are present, it occurs. In general, any macroscopic material (ie with dimension > 500 nm) can be divide into small regions in which a magnetic dipole is present: these regions are known as the magnetic domains (figure 4).
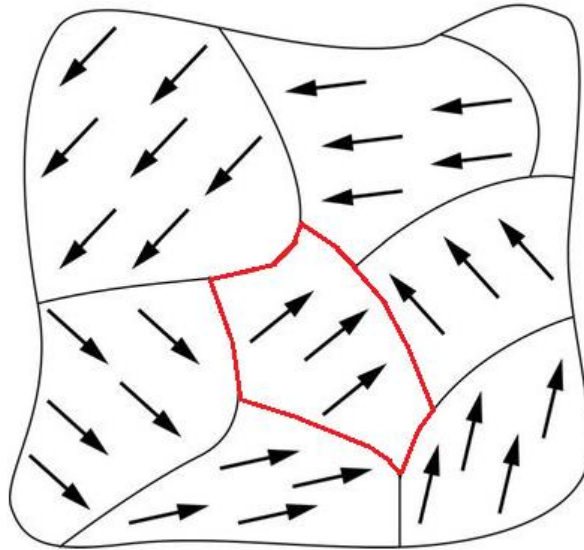
Figure 4:*schematic representation of magnetic domains*

Each of these magnetic moments, at certain temperature, is randomly oriented and their vector sum constitutes the magnetic moment of the material that is observed macroscopically. Random orientation can bring at null magnetic moment: in this case the material, at the working temperature, doesn't have any magnetic properties. However, by changing the temperature the thermal agitation could modify the random orientation of the domains implying a total non-zero moment: the material acquires magnetic characteristics. Experimentally, the magnetic moment of a material isn't directly measurable, therefore the classification of these materials is performed on a basis of a measurable physical quantity: the magnetic susceptibility, χ, it is a constant that provides information on the ability of a material to be magnetized [30]. Considering the subdivision into magnetic domains, when an external magnetic field is applied, the dipole moments of each single domain will be oriented parallel to it. If this doesn't happen the material is called diamagnetic and the susceptibility value χ < 0. On the contrary if the material is magnetized by external field and, when the external field is turned off, it maintains a value of magnetization the material under examination in called ferro-magnetic and his χ >> 0.

In addition to these two classes, the magnetic materials that have a χ > 0 are called para-magnetic: they respond transiently to the perturbation of an external magnetic field. This means that, as long as the field is active, the material is magnetized; when the external field is turned off the magnetization disappears. At the microscopic level, this results in a return to the equilibrium condition of each magnetic domain after the induced magnetic perturbation.

Each magnetic domain can therefore be considered as if it contains a switch that can be controlled by applying an external magnetic field. In order to maximize the magnetization, it is possible to engineer a nanomaterial containing only one or few magnetic domains. In this way, the macroscopic effect will appear amplified if compared to a bulk material.

1.3 LANTHANIDE BASED NANOPARTICLES

The nanotechnology market is rich in materials based on rare earth compounds; this is due to their specific properties so that they can be used in many different fields of application. The use of Ceria (CeO_2) nanoparticles in the field of catalysis is, in fact, well known [31], as well as the use of trivalent ions as doping agent for nanophosphors (on a matrix of $NaYF_4$, Y_2O_3 LnF_3) applicable in biomedical diagnostic techniques and in the industrial field as optically active elements in photovoltaic system.

Recently, the implementation of new synthetic techniques capable of providing precise control of shape, size and dimensional distribution, has quickly led to an increase in research activity towards this type of nanomaterials.

1.3.1 Synthesis method to produce Ln-based nanoparticles

When designing a new material, it is necessary to set an application target where to use the system under study. The field of applications, in fact, requires the presence of specific characteristics that the material must possess. This, when considering a nano-structured system, becomes of fundamental importance: supposing we want to construct a nano-material that is able to convert an electric impulse into electromagnetic wave with a definite wavelength (applicable in the technological field as pixel for high efficiency screen) it is necessary to have a high conversion efficiency. It will therefore be mandatory to design an inert matrix doped with rare earths in proper concentration so that to maximize the photoluminescence quantum yield.

In general, for each field of application the required characteristics can be divided into two classes: general and specific.

The specific characteristics, like the one in the example described a few lines above, strongly depend on the foreseen application and can usually be included with post-synthetic treatments.

As for the general characteristics, such as shape and dimension, they are closely linked to the synthetic technique used.

The traditional techniques used for the synthesis of nanomaterials, led to the production of samples with problems relating to the shape, size and size distribution. These problems have been partially solved with new synthetic chemical techniques known as "soft chemical routes" [32]. The soft chemical routes possess an enormous potential, as they foresee one or more chemical reactions among solid or liquid reagents, they are conducted in controlled environments and have in common the following aspects:

they represent an easy strategy to coordinate ligands on the surface of nanoparticles already in the synthesis phase, allowing the control of the particle size and preventing the aggregation of the particles; moreover, as the second but no less important advantage, they make the system dispersible both in polar or non-polar organic solvents depending on the nature of the binder used during the synthesis.

Another aspect that characterizes these techniques are the so-called "synthesis factor", consisting in modulable parameters such as concentration of reagents, type of solvent, pH, temperature and reaction

time. The synthesis factor can be easily controlled and manipulated in order to direct the synthetic process towards a final product with morphological characteristics (size and shape) decided in the design phase. Finally, the soft chemical routes allow to work at relatively low temperatures < 400° C, with simple and inexpensive devices and allow the application of post-synthetic techniques. The soft chemical routes can also be applied both at laboratory and industrial level, i.e. it allows the scaling-up in continuous production line (this is perhaps the main problem when one wants to produce the nanomaterial at a large-scale).

The set of soft chemical routes includes the following synthetic techniques: thermal decomposition method [33], Hydro/Solvothermal method [34], Co-precipitation method [35], Sol-Gel process [36], Micro-emulsion method [37], Microwave-assisted method [38] and Ionic-liquid-based synthesis [39]. In the following pages the seven techniques listed are schematized indicating, for each of them, the precursors reagents, the type of nanoparticles that are produced and the advantages/disadvantages of the described technique.
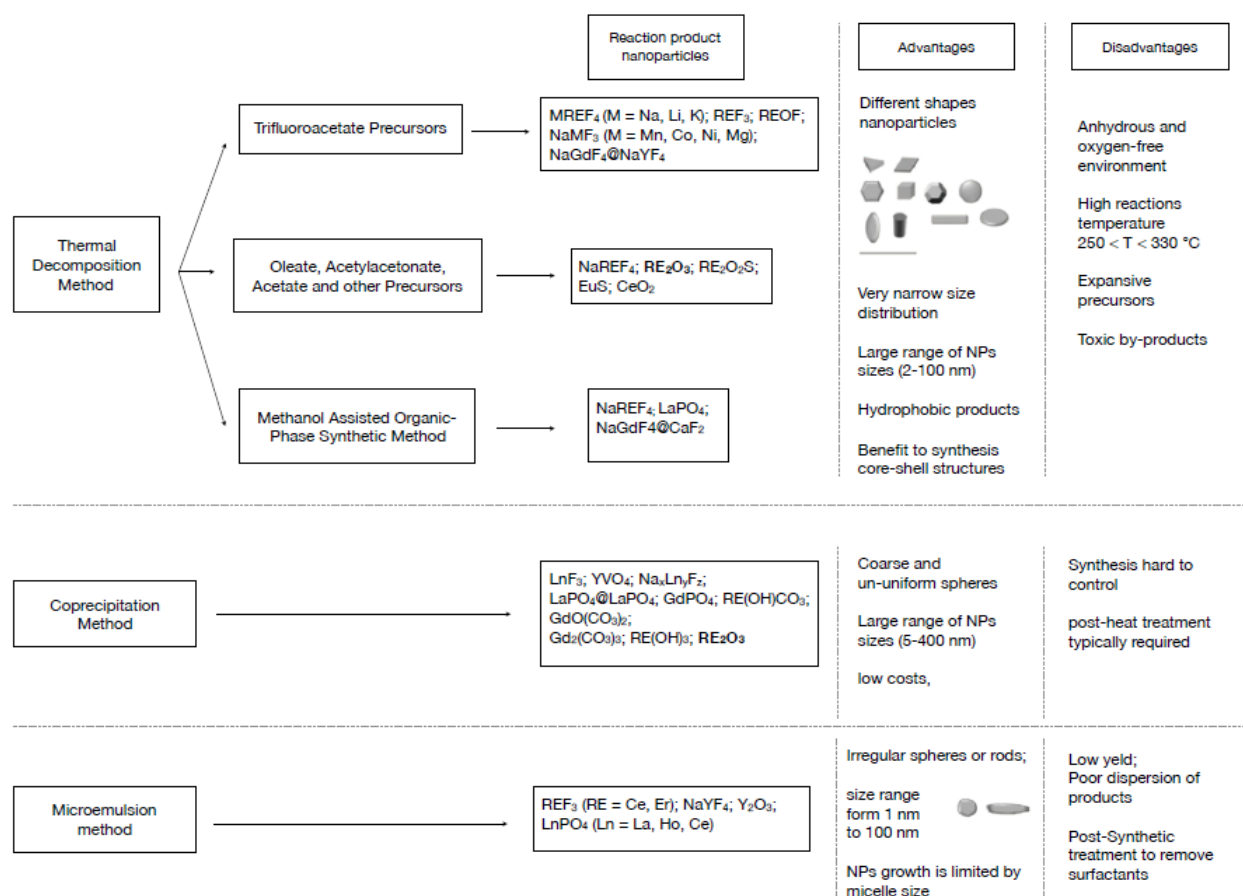
Scheme 1: *Soft Chemical Route (a) Thermal decomposition method, Co-precipitation and Micro emulsion method*
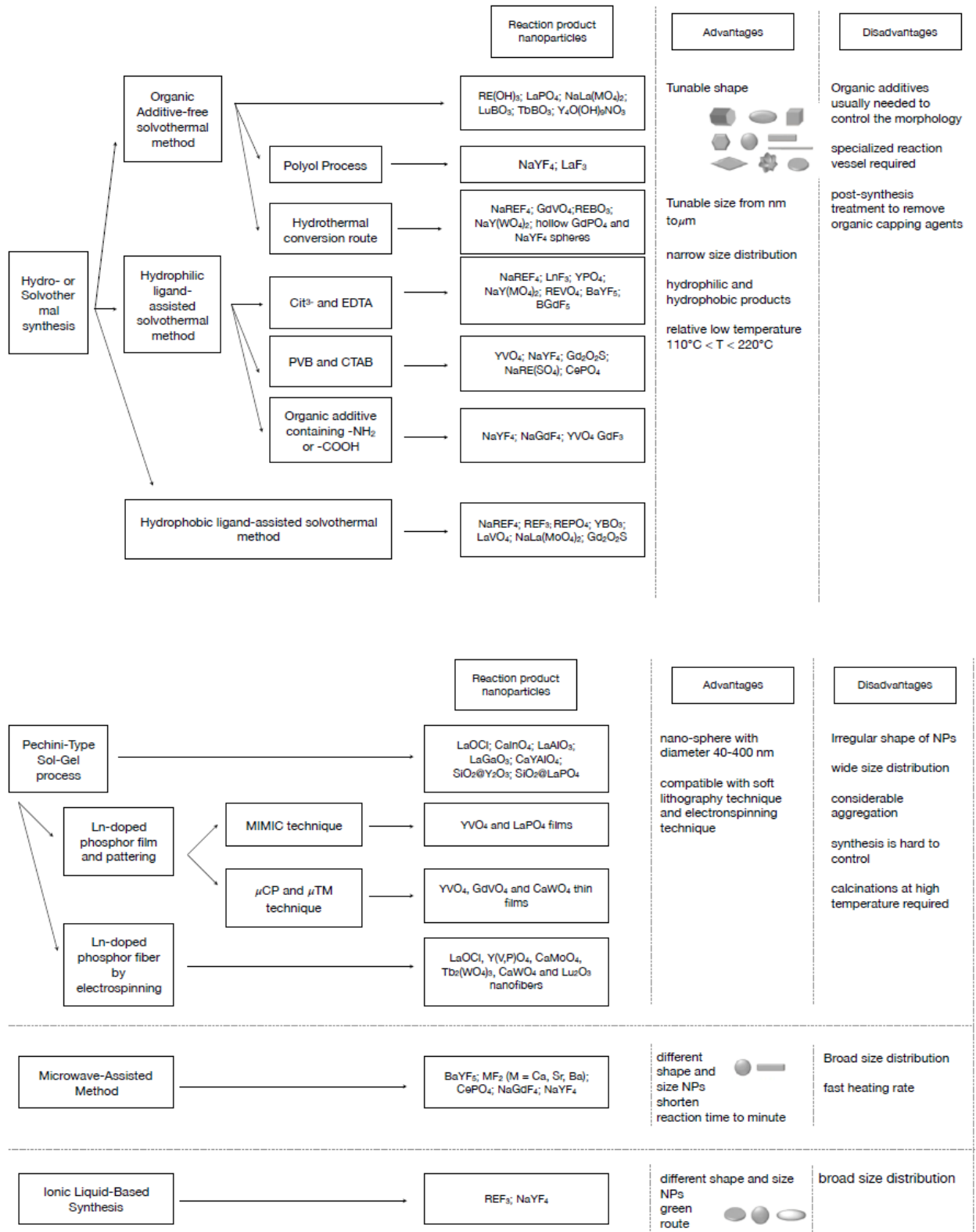
Scheme 2: *Soft Chemical Routes (b) Hydro/Solvothermal synthesis, Sol-Gel process, Microwave-assisted method and Ionic-Liquid-Based synthesis.*

As it can be seen in the representative schemes of the synthetic techniques presented above, only some of them allow to obtain systems with different shapes and sizes, while others lead to the formation of nanoparticles with unique and well-defined morphology.

The final shape and size of nanomaterial depend on the chosen technique and it is strongly influenced by reaction parameters such as concentration of reagents, type of binder, lanthanide/binder ratio, temperature, reaction time and, last but not least, the type of material chosen for the formation of the nano-structured system. Moreover, from the dimensional point of view, among the illustrated techniques only the ones that work at high temperature allow to obtain a controlled dimensional distribution. This characteristic is fundamental because the properties of the nanoparticles depend on it (as described in the previous paragraph) and, consequently their effectiveness in application for which they were designed.

Recently, a new synthetic technique has appeared in literature that allows to obtain particles of different materials with a narrow dimensional distribution and with a well-defined shape. It is known as "Modified Digestive Ripening Method".

1.3.2   From digestive ripening process to digestive ripening method

The most famous and most used chemical synthesis techniques lead to the formation of polycrystalline nanoparticles which are formed and grow according to the known processes of LaMer [40] and Ostwald [41]. The latter is a maturation process that is divided into two phases: the first one consists on the formation of a high number of small particles called "nucleation centers"; subsequently some of these nuclei grow to form larger nanoparticles. In other words, the Ostwald Ripening process sees the sacrifice of small particles as to form a larger system. Form this brief explanation it is evident that some "environmental" conditions are necessary for this process to take place: high concentration of nuclei (and therefore, of a precursor reagents), a non-solvent for the particles in formation and an accurate control of the temperature in the different phases of the process.

However, even using the most sophisticated and accurate synthesis control devices, the synthetic techniques that use Ostwald maturation often produce a poly-disperse system.

The researchers' work has developed toward the search for methods able to control the size of the nanoparticles; the revolution came with the implementation of the methods such as the hot-injection [42] and Brust-Schiffrin [43]. In addition, in 2000, the "Journal of Nanoparticle Research" published a paper where a post-synthetic treatment was described which made possible to standardize the final size distribution starting from a dimensional colourful system. This post-synthetic strategy is called Digestive Ripening Process [44]. Seven years later Lee at al. published a theoretical model describing the mechanism by which this process operates [45].

The digestive ripening process can be described as the opposite procedure to Ostwald's maturation; in fact, it uses an organic binder to tear atoms or cluster of atoms from the surface of large particles and build much

smaller particles, finally obtaining a uniform dimensional distribution. This mechanism has been widely applied to colloidal system consisting of nanoparticles of noble metals (such as Au and Ag) and for the formation of AuSn alloys.

In 2017, the Langmuir journal published an article summarizing the main aspects of this process [46] where the finally dimension of nanoparticles is compared to the nature of the binder used and the temperature at which digestion process occurs. Furthermore, Prasad et al. proposed a modification to the operative protocol suggesting the possibility of applying the post-synthetic treatment directly on the nanoparticles produced thus eliminating the first step of isolation and purification of the nanoparticles. The variation to the experimental procedures has seen the introduction of an ion of the group of halogens (Br^- in particular) which, thanks to its properties of electron-donor, is able to sequestrate ligand molecules to the reaction environment causing a significant reduction in particle size. For example, a sample of nanoparticles treated with and without Br^- shows average dimension of 6 nm and 1.8 nm respectively [47]. In accordance with the cited papers the digestive ripening process has a high application potential; can it be applied as a synthetic method?

The answer to this question was provided by Kim et al. who, in 2016, developed a synthetic protocol for the production of lanthanide oxide based nanoparticles applicable in the field of medical diagnosis [48]. The modified digestive ripening process proposed by Kim is based on the combination of three different synthetic protocols: thermal decomposition at high temperature, hot-injection and finally digestive ripening process. In the first step, large particles are produced by thermal decomposition of the lanthanide acetylacetonate complex. This first step of reaction is carried out in oleylamine which has the dual role of solvent (in that the organic complexes used are perfectly soluble) and of binder which limits, albeit weakly, the growth of the particles and defines their morphologies. Shape and dimension are also controlled by the introduction of a transition metal (Co or Cd) in trivalent ion form coordinated by the same binder forming the complex of the rare earth used. The thermal decomposition reaction is carried out at 280°C in an N_2 atmosphere; at this temperature the second step of the synthesis procedure takes place which consists in the hot-injection of oleic acid in a ratio of 1:3 respect to the volume of oleylamine used. The injection of organic acid causes a lowering of the reaction temperature and consequently the nucleation and growth of the nanoparticles. The oleic acid represents the digestive agent in the last step of the reaction. In their work, Kim's group, focused attention on the application of the method described in the synthesis of the sesquioxide of nine lanthanides (La, Eu, Gd, Tb, Dy, Ho, Er, Tm and Yb); while the role of the transition metal and the effect of the binder are only partially investigated. However, the modified Digestive Ripening process is a revolutionary synthetic method that allows to obtain nanoparticles with anisotropy of shape (disk-like) and narrow size distribution (diameter < 10 nm and thickness about 1 nm). These particular features make this type of nanoparticles the ideal candidates for application in diagnostic techniques such as magnetic resonance imaging.

1.4   SCOPE OF THIS THESIS

In biomedical field, in particular in the diagnostic technique as magnetic resonance imaging, the use of a contrast agent is often required in order to highlight the tissue or organs affected by a pathology. The contrast agent commonly used are Gadolinium-based organic complexes which, thanks to the paramagnetic properties of the rare earth, allow detailed images to be obtained. However, the efficiency is proportional to Gadolinium concentration, in fact to obtain a high contrast image a high dose of the organic complex is required. On the other hand, the high concentration could cause negative effects for the biological system under investigation. The research turned its attention to the study of system capable of providing images with high contrast using a relatively low dosage. In this context, nanotechnologies have made possible the approaching of the objective: in particular, several studies consider Gadolinium oxide in the form of nanoparticles [49] revealing a better contrast power with much lower doses than those of the same lanthanide underneath organic complex form.

The efficiency of these particles is strongly influenced by the topology of the surface of the nanoparticles both from the point of view of its functionalization with bio-compatible organic molecules and with respect to the morphology of the nanoparticles. By morphology, we mean shape and size of nanoparticles which are determined by the crystalline structure of the particles and in addiction, they determine the macroscopic properties of the particles.

In order to build a nano-scale system that can maximize contrasting power (or any other property for which it was developed), researchers need a preliminary work to study the relationships between the macroscopic property requested and the morphology of the system.

In this context, this thesis project is about the development of nanoparticles based on Gadolinium sesquioxide (Gd_2O_3) and lanthanide doped Gadolinium oxide nanoparticles produced chemically through the m-DR method. The samples produced have been characterized by XRD and TEM morphological-structural analyses in order to determine the crystal structure, shape, size and dimensional distribution and to observe whether the introduction of a doping agent (such as Pr^{3+}, Eu^{3+}, Yb^{3+} and Er^{3+}) modifies or not the characteristic of the pure matrix. Finally, this work will represent a starting point for the construction of a nanomaterial with high application potential: in fact, it can be used as a multifunctional contrast agent (in the magnetic resonance imaging and in the photoluminescence applications) or in the field of photo-thermal and magneto-thermal therapies.

1.4.1 Physical and chemical properties of Gadolinium oxide nanoparticles

Gadolinium oxide, also known as Gadolinia, is an inorganic compound consisting of the rare earth Gadolinium (symbol Gd) and oxygen in the ratio 2 to 3 (formula Gd_2O_3). It appears as a white odourless powder and it is soluble in acids. This material, both in bulk and in the form of nanoparticles, has mainly two crystal structures: cubic and monoclininic (C2/m). The cubic structure is, between the two, the thermally stable one in fact, at

room temperature the Gadolinia presents a Body Centered Cubic phase (BCC, Ia-3) where the Gd^{3+} ions occupy two different sites both with a coordination number equal to six. This difference between the lattice sites is the source of the spectroscopic properties of the material: observing the energy gap of the material (5.2 eV) it is natural to expect the complete absence of excitation lines in the near ultraviolet region. However, observation conduced on both macro and nanoparticles have demonstrated the presence of two main spectral lines at 232 and 275 nm respectively [50]. This intrinsic characteristics of the material doesn't involve changes to its ability to accommodate dopant ions (such as lanthanide or transition metal) rather it combined with a low phononic energy (about 600 cm^{-1}) [51] could increase the energy transfer efficiency between antenna ions and emitting ions favouring photoluminescence. Moreover, Gadolinia thanks to the electronic configuration of the Gd^{3+}, possesses paramagnetic properties at room temperature.

All these characteristics make this material an ideal candidate to be used for the design of nano-system both as a pure material and as a matrix for hosting doping lanthanide ions in order to be used in various medical therapy and diagnostic techniques.

EXPERIMENTAL SECTION

Chapter 2

INSTRUMENTATIONS, PROCEDURES, CHEMICALS AND SYNTHESIS

This section describes the materials (such as chemicals), the synthesis method and analytical instruments that have been used to produce and characterize Gadolinium Oxide and lanthanide-doped Gadolinium Oxide nanoparticles.

2.1 INSTRUMENTATIONS

2.1.1 UV Visible spectroscopy

UV-Visible spectra of solutions were recorded with an Agilent diode array spectrometer 8453 using a 1 mm quartz cell at room temperature. All the spectra were recorded in a range between 200 nm and 1000 nm using Tungsten lamp for the visible light range and a Deuterium lamp for ultraviolet radiation.

2.1.2 Fourier Transform Infrared spectroscopy (FT-IR)

Fourier Transform infrared spectra were recorded with FT-IR Nicolet Nexus spectrometer. All the spectra were collected in range 400-4000 cm^{-1}.

2.1.4 X-ray powder diffraction

X-ray powder diffraction patterns were recorded by Philips X'Pert with Bragg-Brentano geometry in a 2 theta range from 1.2 to 140 degrees, with a step size of 0.05 degree, counting time 10 s and a total of 3 runs.

2.1.5 Transmission Electron Microscopy

TEM measurements were performed by using a Jeol JEM-3010 Transmission Electron Microscope with a point to point resolution of 1.7 Å at Scherzer defocus.

2.2 PROCEDURES

2.2.1 UV Visible

UV Visible spectra were collected preparing a toluene solution for each sample. A solid sample was dispersed in toluene and sonicated for 3 minutes to obtain an homogenous solution. Then, 2 mL of this solution were transferred to a 1 mm quartz cell and the UV-Vis spectra collected.

2.2.2 FT-IR

The same solutions used for UV-Vis spectra have been used for collecting FT-IR spectra; a drop of this solution was deposited on the surface of Potassium Bromide tablet.

The background was automatically subtracted from the sample spectrum by the spectrophotometer software.

2.2.4 X-Ray powder diffraction patterns

Samples have prepared depositing a homogenous layer of toluene solution on the surface of a zero-background sample holder.

XRPD patterns have been elaborated with a "home-made" software to search how many phases were present in the powder sample.

Rieltveld method for refinement of structural information such as lattice parameters and crystallite dimensions has been performed using GSAS software [52].

2.2.5 Transmission electron microscopy (TEM)

The samples for TEM analysis were prepared by dispersing the nanoparticles in toluene and depositing a drop of this solution on TEM grid in nickel or copper. The choice of the material of the grid was based on the nature of the sample to be observed.

The acquired images were processed with ImageJ software in order to determine the particle size and their size distribution.

2.3 CHEMICALS

Gadolinium Chloride hexaydrate (99%, Sigma-Aldrich)

Erbium Chloride hexahydrate (99.9%, Sigma-Aldrich)

Ytterbium Chloride hexahydrate (99.9%, Sigma-Aldrich)

Praseodymium acetylacetonate hydrate (99%, Sigma-Aldrich)

Zinc acetylacetonate di-hydrate (Sigma-Aldrich)

Nickel acetylacetonate (Sigma-Aldrich)

Oleylamine (70%, Sigma-Aldrich)

Oleic Acid (90%, Sigma-Aldrich)

Absolute ethanol (99.9%, Sigma-Aldrich)

Toluene (99.9% for HPLC, Sigma-Aldrich)

Acetone (90%, Sigma-Aldrich)

All the reagents and solvents were used as received.

2.4 SYNTHESIS METHODS

2.4.1 Synthesis lanthanide acetylacetonate complexes

The following method [53] has been used to synthetize the precursors, that is acetylacetonate complexes of several lanthanides, which were then used to synthetize the nanoparticles.

This method consists of three different steps: preparation of 5 M ammonia solution; preparation of ligand solution and synthesis of the lanthanide complexes.

The ammonia solution was prepared by adding 8 mL of a 30%v/v ammonia solution in a 25 mL flask and then bringing to volume with distilled water (a qualitative control of the correct concentration of solution has been done by checking the pH).

The Second step consist in the preparation of the ligand solution: to this purpose, 500 μL (0.5 mL) of acetyl acetone and 2 mL of distilled water were added to a 10 mL beaker (reaction scheme 3); the 5 M ammonia solution was then added under magnetic stirring until the solution became homogenous.

The third and last step, consists in the synthesis of $Ln(Acac)_3$ complexes (reaction scheme 4); 1 mmol of $LnCl_3$ x n H_2O with 2 mL of distilled water were dissolved, under magnetic stirring, in a 10 mL beaker. The ligand solution was added drop by drop and a precipitate was formed, this solid product was then filtered through a Büchner funnel under vacuum, washed thrice with 2-3 mL of cold distilled water and allowed to dry.

The product was transferred into a vial for the characterization steps and synthesis of nanoparticles.

2.4.2 Synthesis of Gadolinium oxide nanoparticles

Gadolinium Oxide nanoparticles were prepared according to the method by Kim et al. [54]; 0.066 mmol of Gadolinium acetylacetonate hydrate, 5 mL of Oleylamine (OAm, as solvent) and 0.033 mmol of Zinc acetylacetonate or Nickel acetylacetonate were added to a 50 mL three neck round bottom flask. The flask was equipped with a reflux condenser, a thermometer and pierceable rubber stopper.

The solution was heated under N_2 atmosphere; as soon as the temperature reached 280 °C, 1.67 mL of Oleic Acid (OA) was injected into the reaction flask and the solution was held at 280°C for 1 hour. After the reaction, the solution was left to cool down at room temperature. Nanoparticles were precipitated by adding 15 mL of ethanol to the solution followed by centrifugation at 10000 rpm for 10 minutes. The pellets were dispersed in 8 mL of washing solution (toluene/acetone 1:3) and then the obtained solution was precipitated by centrifugation at 10000 rpm for 3 minutes. This washing procedure was repeated thrice. The obtained nanoparticles were dispersed in toluene for subsequent characterization.

Regarding the synthesis where nickel acetylacetonate was used, the precipitate was dispersed in the lowest amount of toluene as possible for the washing procedure; the obtained nanoparticles were separated by centrifugation at 3000 rpm for 10 minutes. In this case, the nanoparticles remained into the supernatant solution.

2.4.3 Synthesis of Lanthanide doped gadolinium oxide nanoparticles

Lanthanide doped Gadolinium oxide nanoparticles were synthetized by two different methods: the first one is the very same procedure used in the synthesis of the pure gadolinium oxide NPs where, in the three neck round bottom flask was also added the chosen lanthanide doping ions (such as Er^{3+}, Yb^{3+} and Pr^{3+}). While, for the second method the doping ions have been added after heating at 170°C by the injection of a solution previously prepared. The doping solution was obtained by dissolving 0.1 mmol of $Ln(Acac)_3$ x 3 H_2O (where Ln = Pr, Er, Yb) in 2 mL of Oleylamine.

After the reaction, nanoparticles were washed using toluene/acetone (1:3) solution followed by centrifugation at 10000 rpm for 10 minutes. Nanoparticles were dispersed in toluene for subsequent characterizations.

LANTHANIDE ACETYLACETONATE COMPLEXES LIKE OXIDE NANOPARTICLES PRECURSORS

This chapter briefly describes the synthesis and characterization of acetylacetonate complexes of lanthanides. In particular, the Gadolinium acetylacetonate will be used as a source of rare heart in the synthesis of nanoparticles (chapter 4). The spectra of the all complex acetylacetonate synthesized, with their main signals highlighted, and their structure are reported instead in appendix A.

3.1 SYNTHESIS

Lanthanide acetylacetonate complexes were synthetized following the previously described method (see paragraph 2.4.1). The following table shows quantity, expresses in mmol (10^{-3} mol) and in milligrams or millilitres, purity and molecular mass of each chemicals that have been used.

Chemicals	Purity	M.M	Density [g/mL]	mmol	quatity
GdCl$_3$	0,99	371,7007		1	375,5 mg
AcacH		100,116	0,98	3	500 mL
NH$_3$	0,3	17,031	0,898	3	1.5 mL
ErCl$_3$ x 6 H$_2$O	0,999	381,7097		1	382,1 mg
YbCl$_3$ x 6 H$_2$O	0,999	387,5047		1	387,9 mg

Table 3: *Chemicals, quantity used for synthesis of Ln(Acac)$_3$ x 3 H$_2$O*

The reaction process is divided into two different steps: the first one consists on the preparation of the ligand solution; 500 μL of acetylacetone were mixed with 2 mL of distilled water and a 5 M ammonia solution is added dropwise until a homogenous solution is obtained (scheme 3), the acetylacetone loses a β-proton after the basic attack of ammonia, the negative charge, stabilized by resonance, gives the molecule stability and chelating properties.
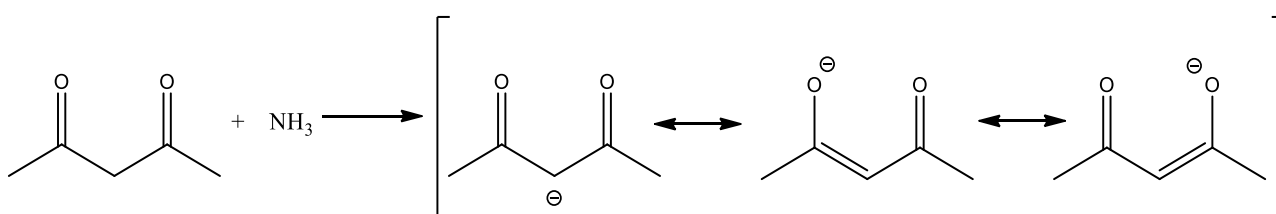
Scheme 3: *Acid-base reaction between acetyacetone and ammonia solution*

The second step of reaction is illustrated in scheme 4 corresponding to the synthesis of acetylacetonate lanthanide complexes; when the ligand solution is added dropwise to the LnCl$_3$ (previously dissolved in

distilled water), the negative charge present in the ligand molecule coordinates Ln^{3+} ion forming an insoluble solid complex.

$$LnCl_3 \quad + \quad 3 \quad \text{[β-diketone]} \quad \xrightarrow{\;H_2O\;} \quad Ln(acac)_3 \quad + \quad 3\,NH_4Cl$$
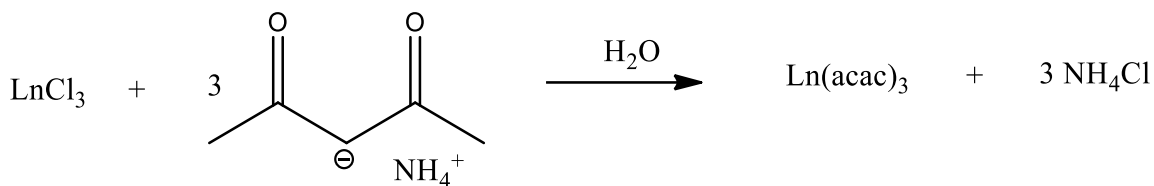
Scheme 4: Synthesis of Ln(Acac)3 complex

The solid product was filtered under vacuum, air dried and stored in plastic vial for subsequent characterization.

3.2 SPECTROPHOTOMETRIC CHARACTERIZATION

This paragraph reports the results of the spectrophotometric characterization of Gadolinium Acetylacetonate; the spectra of Er, Yb and Nd complexes are illustrated in appendix A.

The synthetized acetylacetonate complexes were characterized by means of IR spectrophotometry.

Figure 5 shows the IR spectra of Gadolinium acetylacetonate hydrate and the spectra of pure acetylacetone [55] in region between 4000 cm^{-1} and 350 cm^{-1} where the main signals characterizing the molecules under examination are present; the IR signals relating to the main functional groups, from which it is possible hypothesize the structure of the complex, are highlighted.

The spectrum of Gadolinium acetylacetonate (black line figure 5) indicates that the ligand is in the form of enolate, signals at 1607 cm^{-1} and 1523 cm^{-1}, therefore a negative charge is present and shared between the two oxygen atoms of the β-diketone. The second signal that allows to hypothesize the structure of the complex is the one at 536 cm^{-1} and indicates the presence of a covalent bond between Gadolinium and Oxygen.
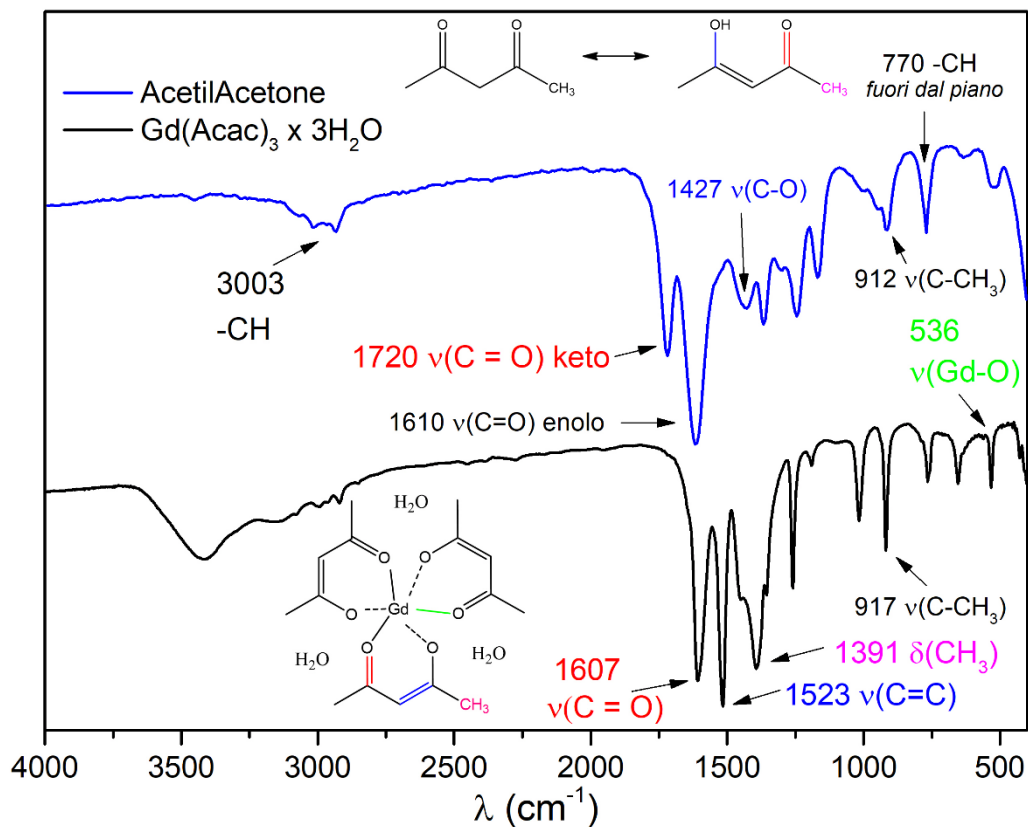
Figure 5: *IR spectra of Gd(Acac)₃ x 3H₂O, the Blu line is the IR spectrum of pure Acetylacetone.*

From these experimental results, the structure of the complex can be extrapolated: three ligand molecules coordinate a trivalent lanthanide ion located at the centre of the complex through alternating dative and covalent bond. The signal present at about 3500 cm^{-1} is caused by the presence of water of crystallization. Our results are in agreement with the work performed by Fengzhu et al. [56].

SYNTHESIS AND CHARACTERIZATION OF GADOLINIUM OXIDE AND LANTHANIDE DOPED GADOLINIUM OXIDE NANOPARTICLES

This chapter describes the main syntheses of this thesis work, whose goal is to produce a hybrid system applicable in medical diagnostics.

First of all, the synthesis of Gadolinium Oxide nanoparticles is described by discussing a new synthetic method to obtain small particles with a uniform dimensional distribution; then the doping of these NPs with specific lanthanide ions is treated.

For both synthesis, the products obtained were characterized by x-ray powder diffraction and transmission electron microscopy (TEM) to determine their size, crystal structure and morphology, by FT-IR spectroscopy to evaluate the degree of cleanliness and to identify the capping agents, by spectrophotometric analysis (UV-Vis and Photoluminescence) to study the optical properties.

4.1 GADOLINIUM OXIDE NANOPARTICLES

4.1.1 Synthesis

Gadolinium Oxide nanoparticles were synthetized following the previously described method (see paragraph 2.4.2). Acetylacetonate precursors were added in volume by a 0.1 M stock solution prepared by dissolving the appropriate (table 4) amount of reagent in 2 mL of oleylamine.

Reagent	Purity	M.M [g/mol]	Concentration of stock solution [M]	Volume of solution [mL]	Quantity [mg]
$Gd(Acac)_3$ x $3H_2O$	--	508,6195	0,1	2,00	101,7
$Er(Acac)_3$ x $3H_2O$	--	518,6285	0,1	2,00	103,7
$Zn(Acac)_2$ x $2H_2O$	--	299,6263	0,1	2,00	59,9
$Ni(Acac)_2$	0,96	256,9092	0,1	2,00	53,5

Table 4: Amount of Acetylacetonate precursor to prepare the stock solutions.

In a typical process 0.066 mmol of gadolinium acetylacetonate hydrate and 0.033 mmol of Zinc acetylacetonate or Nickel acetylacetonate and 5 mL of Oleylamine were added into a three neck round bottom flask. The solution was then heated to 280°C under nitrogen atmosphere, as soon as the temperature

was reached, 1.67 mL of Oleic Acid were rapidly injected and the solution was kept at 280°C for 1 hour, then the solution was naturally cooled down to room temperature and the nanoparticles were precipitated by the addition of 15 mL of absolute ethanol. To separate the nanoparticles from the liquid phase (which contains unreacted precursors) a centrifuge was performed at 10000 rpm for 10 minutes.

After the first centrifugation the supernatant was removed and the precipitate washed thrice with different solvents such as toluene, solution of toluene/acetone (1:3), hexane, ethanol and diethyl ether with the initial aim of determining the solvent capable of eliminating most of the impurities.

Each washing cycle was performed by dispersing the solid phase in the appropriate solvent with the help of a sonicator. The dispersion was separated by centrifugation at 10000 rpm for 10 minutes; the solid pellet was stocked in a solution of toluene for the subsequent characterizations.

The same synthesis method was used to produce two different oxide materials: Gd_2O_3 and Er_2O_3. Nanoparticles based on gadolinium oxide were synthetized with and without metal ions, such as Zinc and Nickel (table 5). Zinc and Nickel have been used to obtain a uniform size and shape of the nanoparticles [54]. These two elements have been chosen because they form an acetylacetonate complexes which are easy to eliminate during the first washing step.

Both nanoparticle families were characterized by x-ray powder diffraction, transmission electron microscopy, Fourier Transform Infrared spectroscopy and UV-Visible spectroscopy.

#	Sample name	Composition	Reaction parameters		Volume of 0.1 M solution of acetylacetonate precursor [μL]				Volume of ligands/solvents [mL]	
			Temperature [°C]	Time [minutes]	Gd	Er	Zn	Ni	OAm	OA
1	MFGdO1	Gd_2O_3	280	60	667	--	--	--	4,4	1,67
2	MFGdO2	Gd_2O_3	280	60	667	--	333	--	4,0	1,67
3	MFGdO3	Gd_2O_3	280	60	667	--	333	--	4,0	1,67
4	MFGdO_Ni	Gd_2O_3	280	60	667	--	--	333	4,0	1,67
5	MFErO	Er_2O_3	280	60	--	667	333	--	4,0	1,67

Table 5: Samples synthetized and amounts of reagents (OAm = Oleylamine; OA = Oleic Acid).

4.1.2 Results and discussion

This paragraph will present and discuss the results of analyses carried out on the sample listed in table 5: in particular, the tests performed on the sample 5 (Erbium Oxide nanoparticles) will be illustrated to determine the best solvent capable of removing the impurities present in the reaction product.

The result of the morphological and optical analyses of the five aforementioned samples will then be presented.

4.1.2.2 Fourier Transform Infrared (FT-IR) spectroscopy characterization

This synthesis process uses oleylamine both as solvent and capping agent and oleic acid which has the role of digestive agent. The reaction product is therefore rich in organic material that coats the nanoparticles. As reported in literature [46], the nanoparticles should be coated only by the digestive agent and not by the synthetic solvent; to verify it, FT-IR analysis was performed on the first sample produced to identify the organic molecules present in a fast and effective way. Furthermore, there is the possibility of understanding which organic compound is bound to the particles and which instead can be considered as an impurity and must therefore be removed.

Figure 6 shows the IR spectra of gadolinium oxide nanoparticles (sample 1 in table 5); the graph shows many signals corresponding to vibrational modes of the main functional groups present in the organic compound. The spectrum can be divided into three regions, each of them contains signals that allow the identification of the organic compound present. Comparing the experimentally acquired spectrum with the ones of oleylamine and oleic acid obtained from literature [55] it is possible to assign each signal to the parent molecule.

Starting from the left of the spectrum we find an extended signal located at 3466 cm^{-1} originating from the –OH groups. The doublet placed at 2922 cm^{-1} and 2850 cm^{-1} is related to the stretching of the CH_3 and CH_2 groups, respectively, of the aliphatic chain present in both organic molecules. The signals that allow us to discriminate the two organic compounds are those located in the region between 1720 cm^{-1} and 1200 cm^{-1} (insert of figure 5). Starting from left a signal is found at 1633 cm^{-1} corresponding to the stretching of –NH, at 1539 cm^{-1} is placed the asymmetric stretching of the COO- group and at 1468 cm^{-1} is present the C-N stretching.
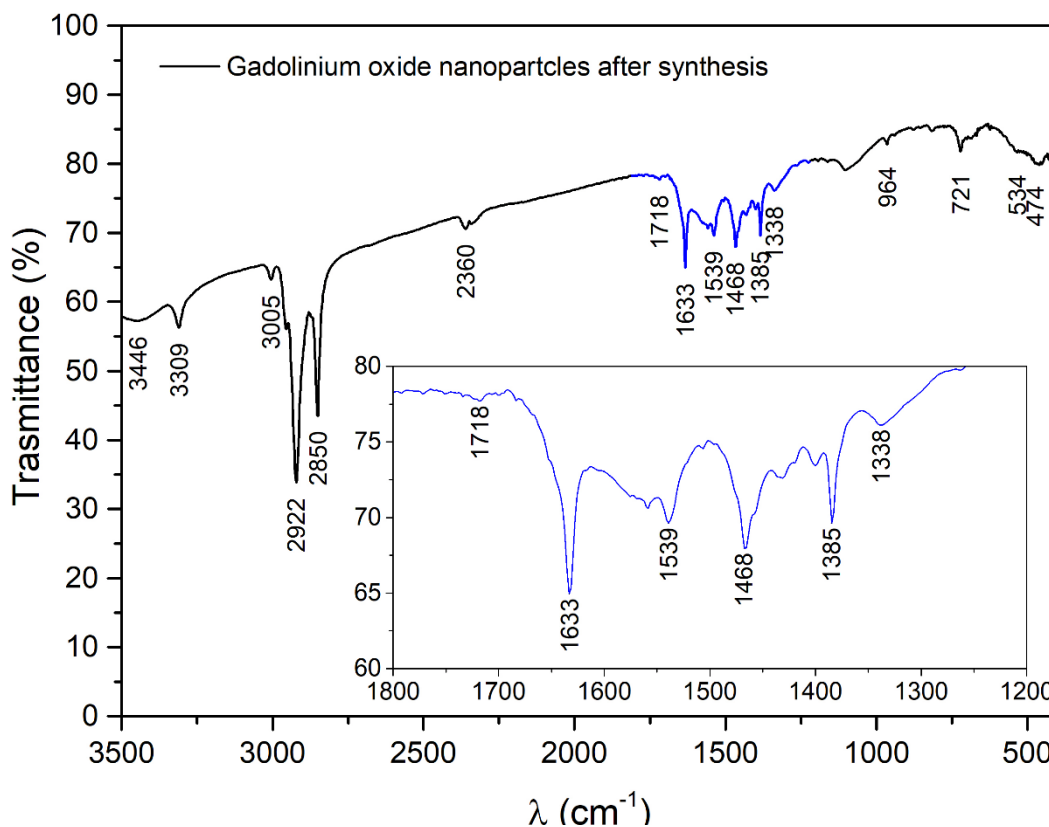
Figure 6: *IR spectra of gadolinium oxide nanoparticles (sample MFGdO1) after synthesis with the positions of the main signals assigned*

The stretching of the –NH and C-N groups identify the presence of oleylamine, while the asymmetric stretching of the COO- is significant in the presence of oleic acid in its deprotonated form [57]. It allows to discriminate which of the two identified organic molecules is linked to nanoparticles.

Observing the terminal part of the fingerprint region (1500-500 cm^{-1}) we observe the presence of a signal at 534 cm^{-1}. This weak signal is related to the stretching of the covalent bond between the gadolinium ion and the oleic acid oxygen, as foreseen in literature, binds to the nanoparticles forming a coating which prevents their aggregations.

On the other hand, oleylamine is not directly associated with the particles produced and can be considered a product that must be eliminated by the washing procedure that will be the subject of the next paragraph.

4.1.2.2 Washing test procedures

The synthetic method suggested by Kim et al. aims at washing the nanoparticles by dispersing them in toluene followed by spinning at low (3000) rpm. In this way, only the impurities should precipitate while the nanoparticles remain in solution. However, by recording the IR spectra of the sample before and after three

washing cycles it is observed that the reaction product still has a high quantity of oleylamine (synthesis solvent) which hinders the isolation of the nanoparticles; in fact, we obtain an oily solid.

In order to find the best solvent capable of removing most of the amine present, five washing tests were performed using solvents with increasing polarity: hexane, toluene, diethyl ether, ethanol and using a solution composed of toluene and acetone in a ratio 1:3.

These tests have been carried out on the sample formed by Er_2O_3 as it has an absorption in visible region (521 nm) that allows to quickly evaluate if the NPs, after centrifuge, remain dispersed in the solvent or if they precipitate together with the impurities. The degree of cleanliness of Erbium oxide nanoparticles was evaluated by FT-IR spectroscopy.

The first solvent to be tested was the hexane (non-polar solvent): it is not a good solvent as the dispersion is very difficult and, after three washing cycles there is no improvement in the degree of cleaning.

The second test was performed using Kim's solvent: toluene. It has shown interesting results already from the first step of the cleaning process, in fact the dispersion of the nanoparticles was very fast.

Figure 7 shows the UV-visible spectra, of the Erbium oxide nanoparticles, recorded after precipitation by ethanol (P0) and after each washing cycle (centrifugation at 10000 rpm) P1 and P2 respectively.
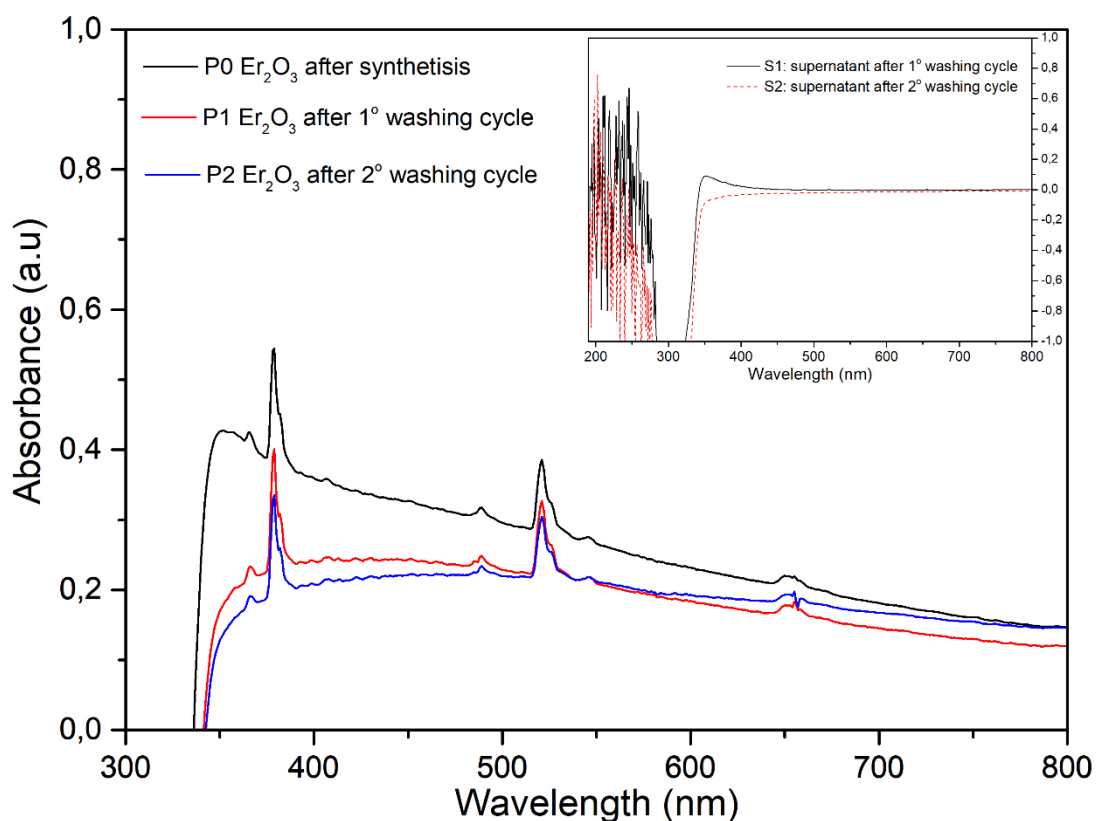
Figure 7: UV-Visible spectra of Erbium oxide nanoparticles in toluene as washing solvent.

Looking at the figure we note the presence of three main signals: one band at 350 nm relative to the impurities present and two signals placed at 379 nm and 521 nm respectively of the erbium oxide.

Comparing the spectra collected after each washing cycle, a clear decreasing in the band intensity at 350 nm is observed, while the absorption related to the main product of the synthesis does not undergo any variations. These considerations provide the first evidence of the effectiveness of toluene as a solvent for the cleaning of the nanoparticles.

UV-Visible spectra also suggest the mechanism by which the elimination of secondary reaction product occurs: the toluene dissolves only the impurities that are eliminated with the supernatant. This mechanism is supported by the spectra shown in the insert of figure 7 which illustrates the absorption of the supernatant after two washing cycles. The image clearly shows that the first washing is the one that removes almost all of the reaction by-products.

The analysis of UV-Visible spectra allows to assess the degree of cleanliness of the nanoparticles, yet it does not provide any information about the nature of the impurities that make the solid oily. Considering that the synthesis method uses oleylamine as a solvent we can hypothesize that it is this compound that pollutes the reaction product.

The confirmation that it is indeed the amine of oleic acid is provided by the IR spectrum (figure 8): in fact, observing the central region of the spectrum (between 1800 cm^{-1} and 1200 cm^{-1}) we may note the presence of signals relating to the stretching of the –NH and –CN groups of the amine.
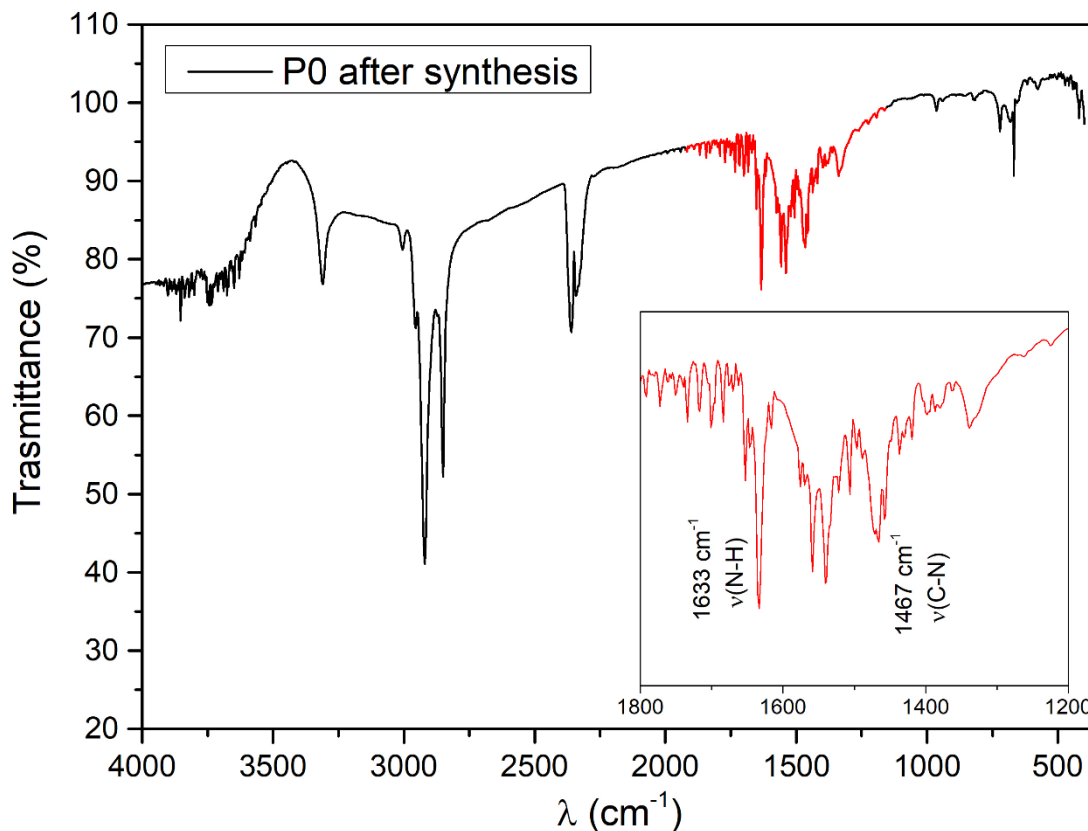
Figure 8: IR spectra of Er2O3 after synthesis. Insert shows a magnification of region between 1800 cm^{-1} and 1200 cm^{-1}.

In order to demonstrate the efficacy of toluene in the elimination of oleylamine from nanoparticles, the IR spectra of the same five samples used in the previous spectrophotometric analysis were recorded. Figure 9 shows the comparison between the spectra focusing the attention in the region where the signals relative to the vibrations of the functional groups characterizing the oleylamine and oleic acid molecules are positioned.
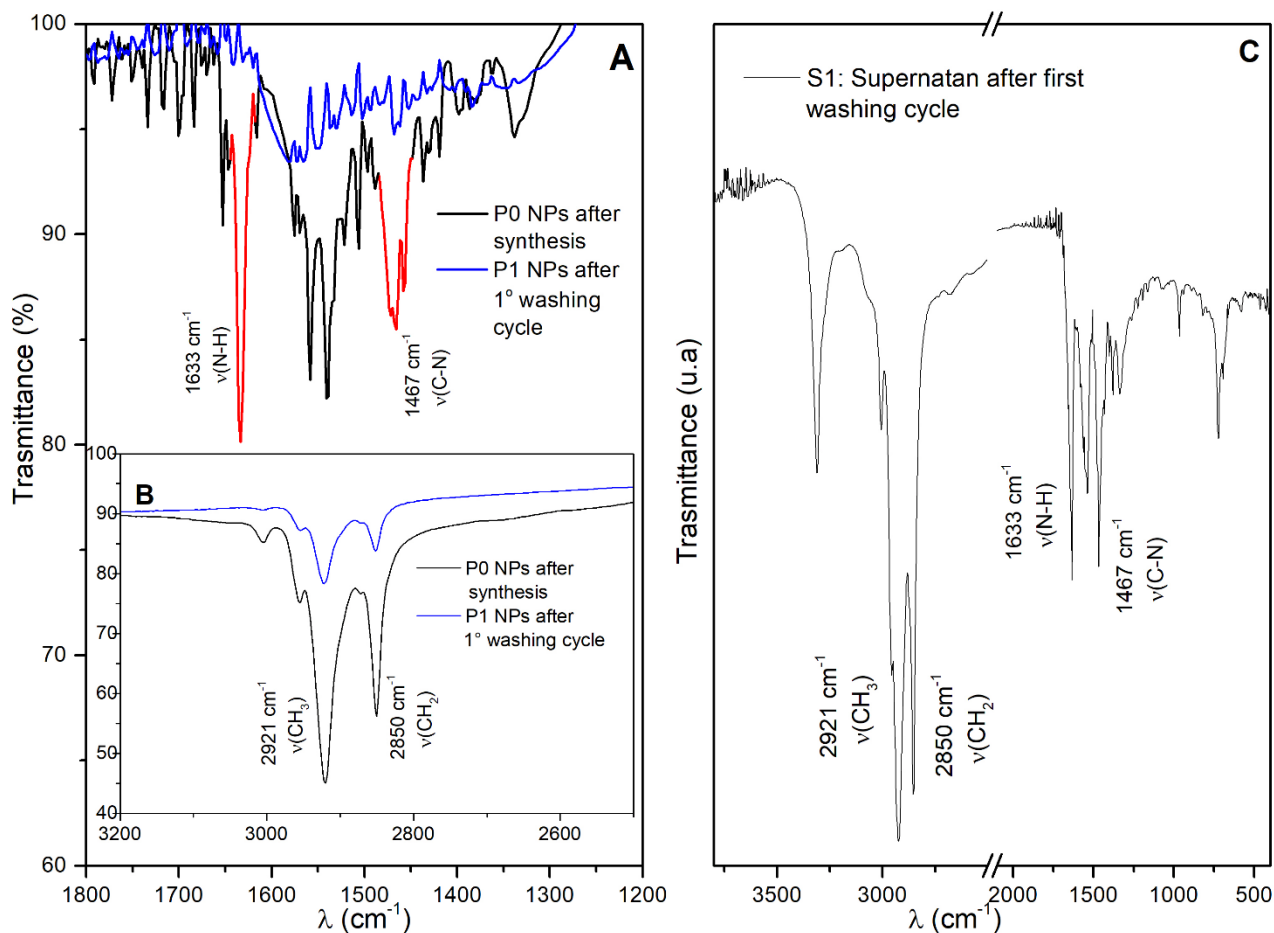
Figure 9: *IR spectra of nanoparticles A: after synthesis (P0), after first wash (P1); insert B: magnification of the region 3200-2500 cm^{-1}; C: supernatant after first wash.*

From the comparison of the spectra of the nanoparticles recorded immediately after the synthesis (P0) and after the first washing cycle (P1) it is evident that the toluene is able to remove the oleylamine. This is indicated by the disappearance of the signal relative to the –NH vibration in the P1 spectrum with respect to the P0 spectrum and by the significant reduction of the signals positioned at 2921 cm^{-1} and 2850 cm^{-1} relative to the stretching –CH$_3$ and –CH$_2$ respectively.

Finally, the spectrum of the supernatant analyzed after the first washing cycle (figure 9C) provides a further confirmation of the fact that the toluene is an excellent solvent.

Although the use of toluene has provided excellent results, it does not allow to obtain a final product free from impurities; the oleylamine residues, in fact, form an oily matrix that must be removed as it could interfere with the optical characterizations.

To this end, multi-polarized solvents, such as ethyl ether and ethanol, have been used which did not lead to any improvement.

A great step forward was made using a 1:3 solutions of toluene and acetone as a washing solvent. The oleylamine shows a greater affinity with the acetone which is therefore able to solubilize a considerable quantity than the toluene. The latter, thanks to reduced polarity, acts as a solvent for the nanoparticles (coated with oleic acid) separating them from the amino matrix and therefore increasing the cleaning effectiveness.

4.1.2.3 Morphological characterization

The study of the morphology and structure of the synthetized nanoparticles was performed by x-ray powder diffraction (XRPD) and transmission electron microscopy (TEM).

This paragraph will discuss the results of these analyses carried out on the samples listed in table 5.

Sample MFGdO1, composed of nanoparticles in Gadolinium oxide coated with oleic acid, was analyzed by XRPD and observed by TEM.
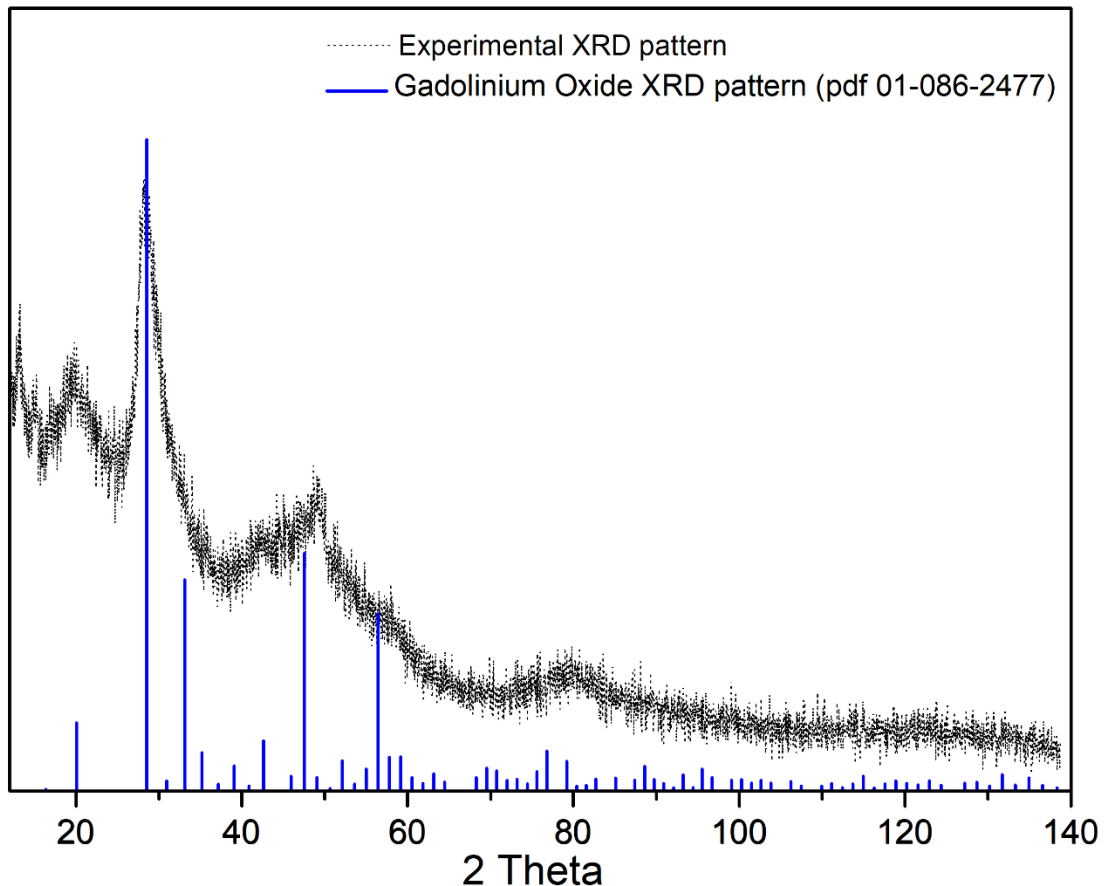
Figure 10: XRD pattern of MFGdO1 - Gadolinium oxide synthetized without any metal ions

The XRD profile of the nanoparticles, illustrates in figure 10, shows the presence of a crystalline structure that was identified in the cubic one (bcc: body centered cubic) of the gadolinium oxide bulk materials (pdf 01-086-2477, figure 10). Observing the diffractogram, we may note that the signals present are slightly

shifted towards greater angles. This is linked to the lattice parameters, specifically to the one that describe the cell edge as it is a cubic lattice. This has been evaluated by applying the Rietveld's method to the experimental profile, the peaks are able to provide information on particle sizes. The refinement was initially done assuming the presence of a single family of crystalline particles with cubic phase, however the results obtained showed substantial differences between the experimental and the calculated profile.

This first analysis is meaningful that the synthesis has led to the formation of particles of a single crystalline phase, however the method applied in not able to provide structural information. By carefully observing the diffraction profile we note that are two different types of signals: some reflections are wide (such as the signal relative to (211) plane at 2θ of about 20 degree) others instead are narrow as the reflection located at 2θ of about 47 degrees relative to (440) crystallographic plane.

Since the widening of the diffraction signal is caused by instrumental factors (which are eliminated during refinement and are the same for the whole spectrum) and mainly by the size of the crystallites it is possible to make two hypothesizes: the presence of two population of nanoparticles with the same crystallographic structure but of different dimensions and the presence of two population of nanoparticles with different crystallographic structure and size.

In order to verify the first hypothesis, the Rietveld's method was applied by inserting two population of particles without obtaining any improvement in the calculated profile. Observing the position of the reflexes in detail, has been hypothesized the presence of a second crystalline structure that it is identified in the monoclinic one (pdf 00-012-0474).

On the basis of this new hypothesis, the experimental profile was again subjected to refinement with the Rietveld method which led to the confirmation of the hypothesis and also providing an estimation of the size of the particles.

Figure 11 shows the experimental profile and the calculated one using the aforementioned method. The results obtained see the presence of two populations of nanoparticles with the following characteristics: the larger particles have a cubic structure (BCC type) with a cell parameter **a** of 10.82 ± 0.01 Å and an average size of 9 ± 1 nm; the second population instead has a smaller average size 6.2 ± 0.9 nm and a monoclinic structure.
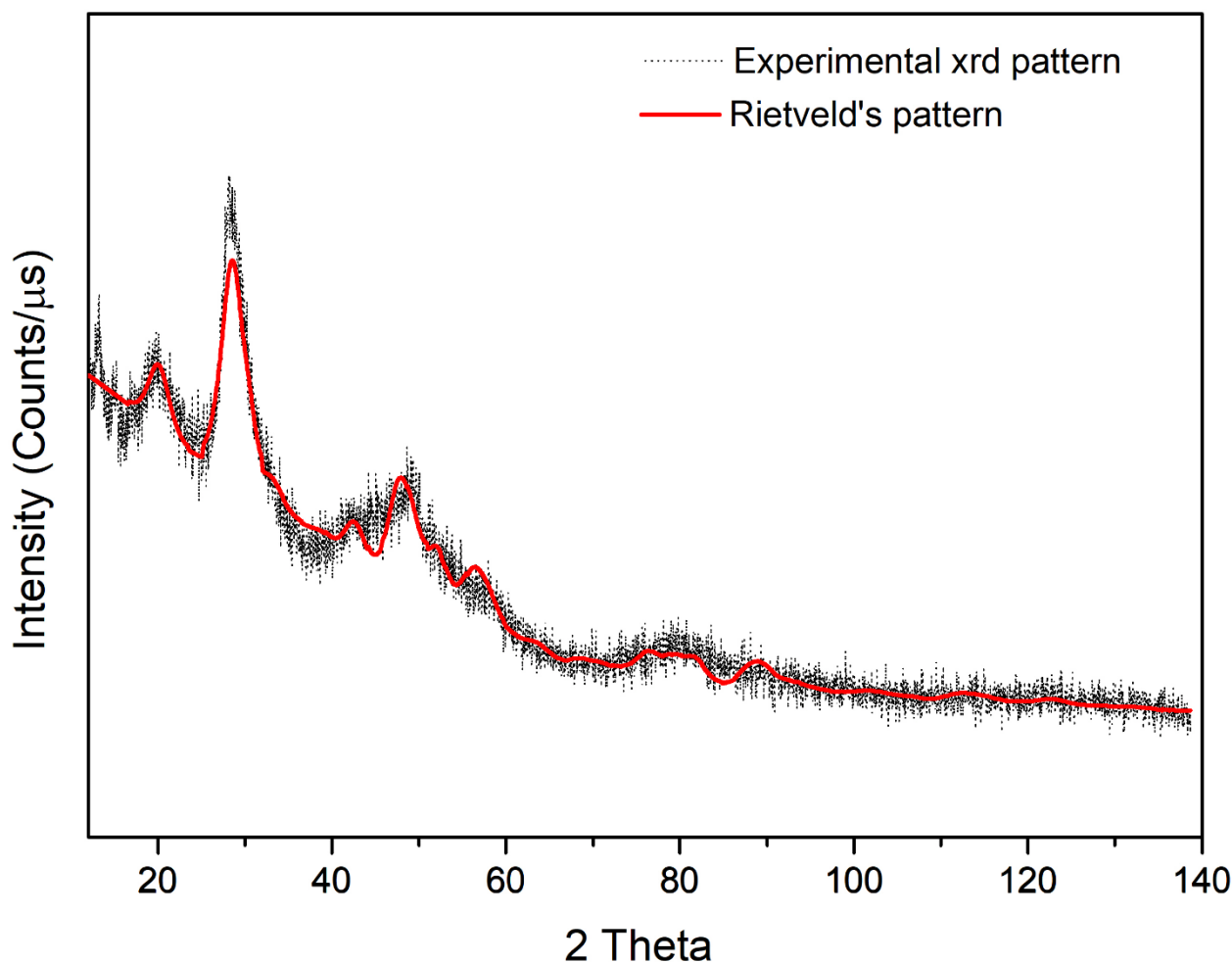
Figure 11: xrd of MFGdO1 sample synthetized without any metal ions; red line shows calculated profile with Rietveld's methods

The analysis of the diffraction spectrum of this sample does not provide any information about the morphology of the synthetized nanoparticles. According to the literature, the use of oleylamine/oleic acid such as solvent/ligand pair should lead to the formation of discoid systems. The morphology of the particles was then investigated by TEM (figure 12) which confirmed the expected anisotropic form. In particular, in the image, we note the presence of particles arranged in columns (A) and particles that instead show the face of the disk. This arrangement is caused by the presence of oleic acid, as established by the FT-IR analysis, which coats the particles preventing their aggregation and favouring the self-assembling in conformation at lower energy.

To explain this statement, we can consider the shape of the nanoparticles, it can be schematized as a disk which shows two structurally different surfaces: the up and down faces and the face corresponding to the thickness of the disk; the up and down faces, that are indistinguishable, have a surface greater than the one corresponding to the thickness, this implies that the larger surfaces receive a greater number of ligand molecules than the one with a smaller surface. A high number of organic molecules makes the interaction between adjacent particles more probable, since they are repulsive nature, the particles are arranged in such

way as to minimize energy, by giving the system the equilibrium disposition seen in the images acquired with the electron microscope.
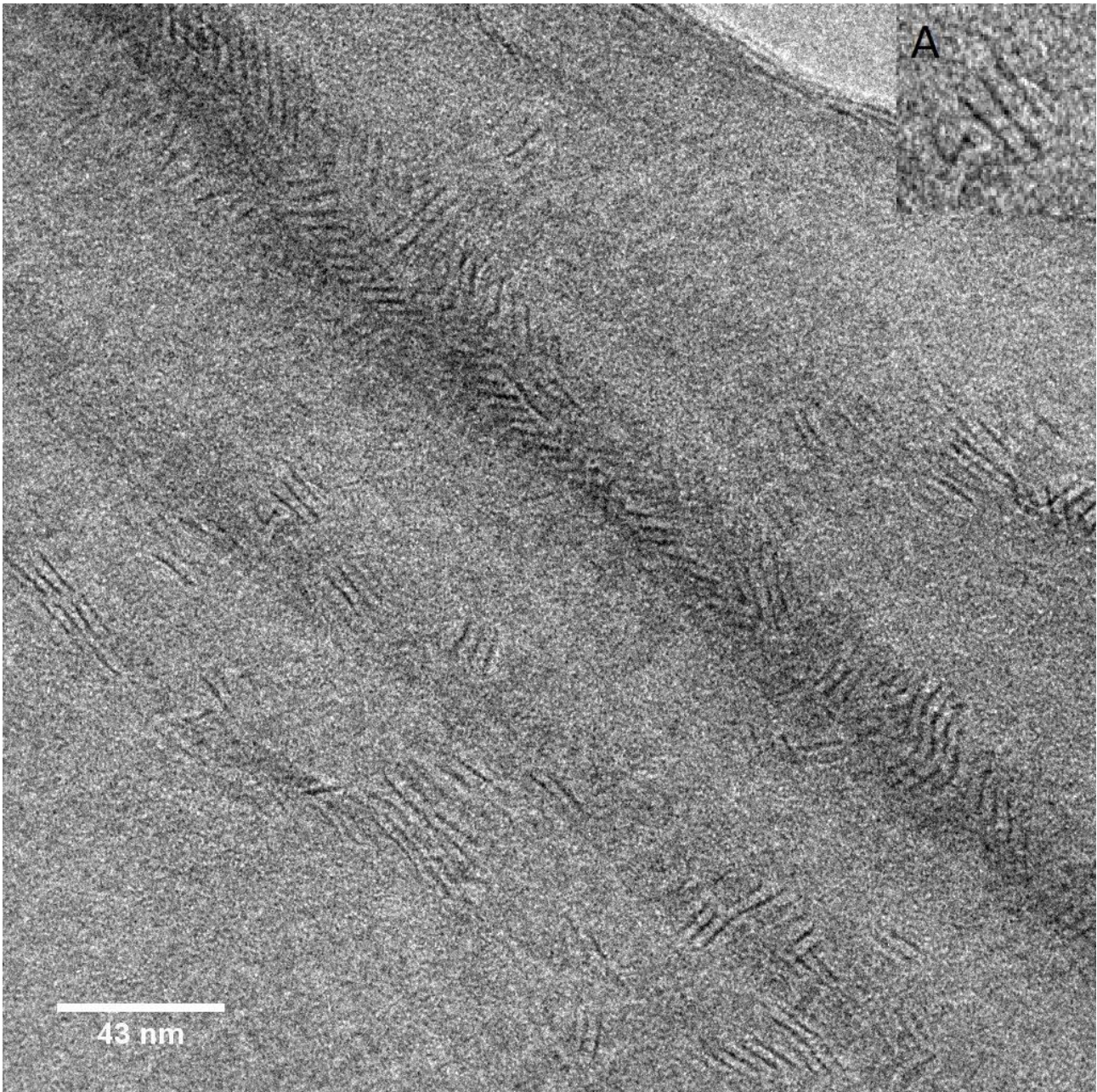
Figure 12: *Gadolinium oxide nanodisk (magnification 60k). Inset A illustrates self-assembly*

The TEM images, not only show the morphology and self-assembly characterizing the system, but they also allow an estimate of the size distribution of the nanodisks. The image in figure 12 has been analysed by using ImageJ software [58] to extrapolate the afore mentioned information. Figure 13 shows the graph representing the size distribution of the nanoparticles of the first synthesized sample labelled with the name of MFGdO1.
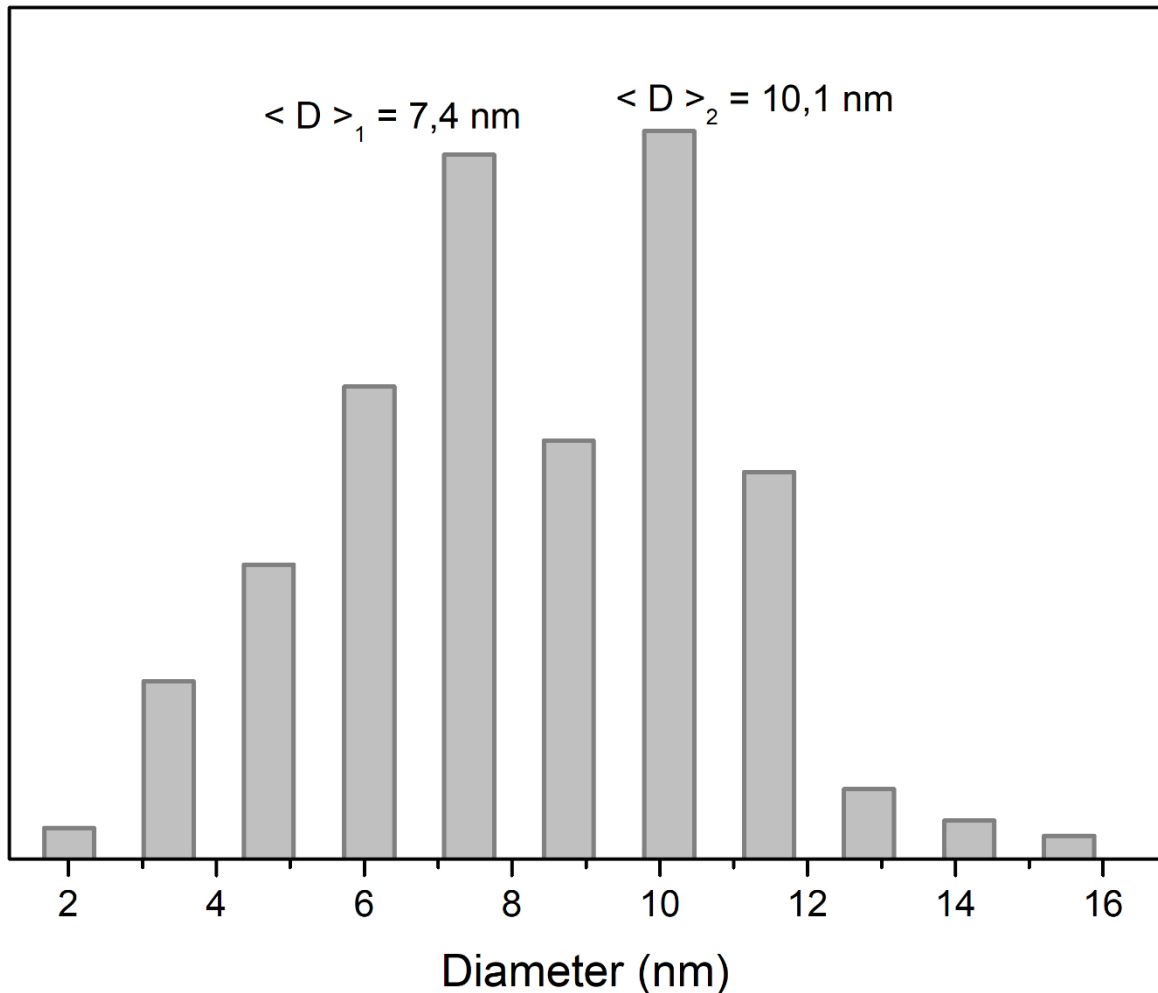
Figure 13: Size distribution of Gadolinium oxide nanodisk (MFGdO_1 sample)

It is evident that both XRD and TEM characterization methods show that the synthesis led to the formation of two distinct populations of gadolinium oxide nanoparticles regarding both crystal structure and size. Looking at the size distribution (figure 13), we may note that there are two maximums respectively at 7.4 nm and 10.1 nm representing the average diameter of the nanoparticles.

Comparing the data obtained from the two characterization techniques, it is possible to state that the synthesis, carried out without the use of a transition metal as a competing ion, sees the formation of two distinct types of particles: a family with a monoclinic structure and larger size (9 nm) and another one with size equal to 6.2 nm and with cubic phase. According to these results, it is possible to suppose that the metal ion has an active role in the synthesis: in fact, it could drive the digestive ripening process towards the formation of particle with a well-defined crystalline structure and narrow size distribution.

Furthermore, observing the sample at higher magnifications (figure 14) we note that there is a heterogeneity of shape, that is not all the particles have a well-define discoid shape.
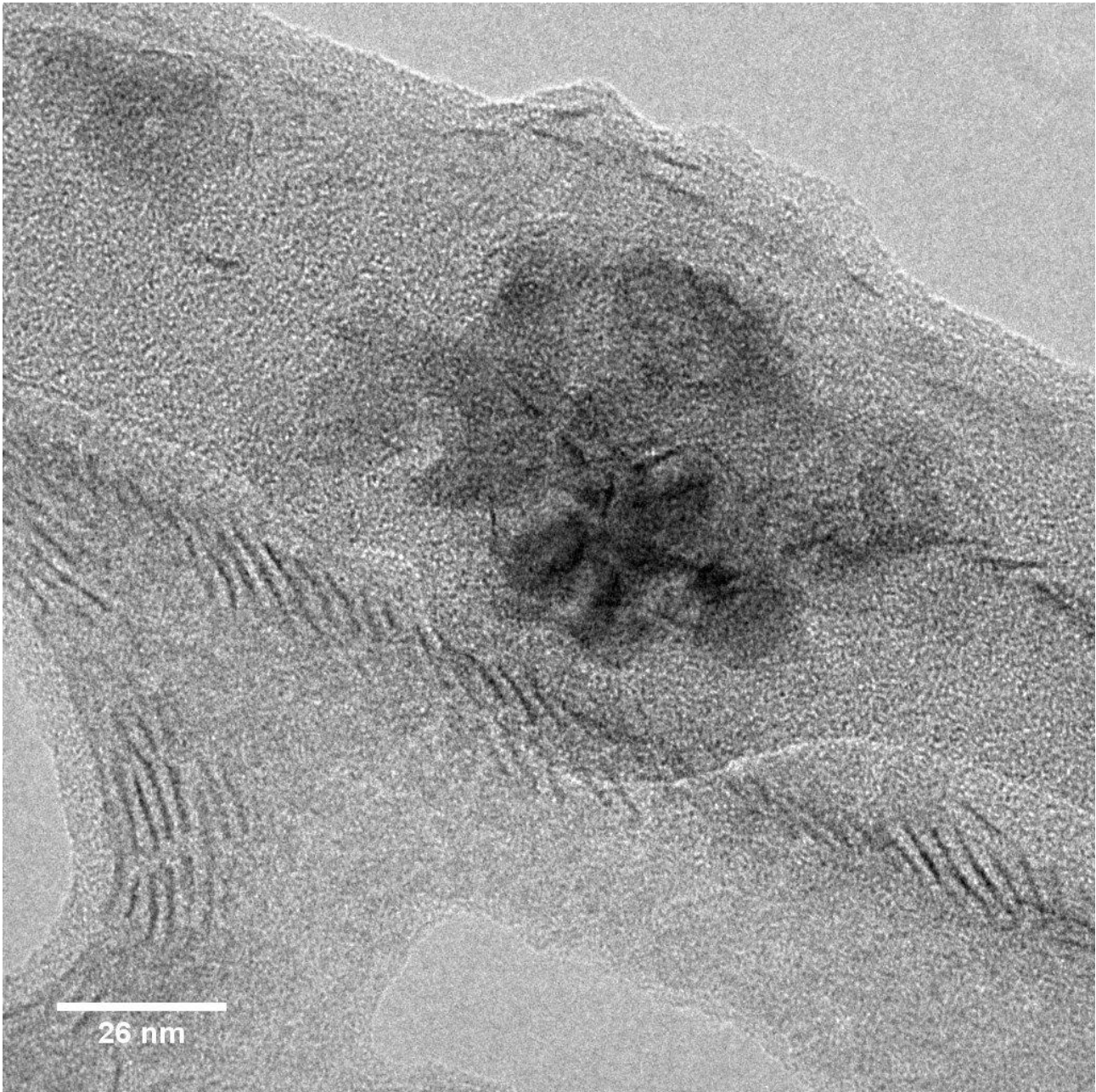
Figure 14: Gd$_2$O$_3$ NPs at magnification of 100k.

These observations are positively reflected in the work we used as a reference (Kim et al); therefore, on the basis of this assumption, a new set of specimens was produced by carrying out the synthesis with the introduction of a transition metal, as an expendable agent, in the process of digestion. Using this approach, two samples were prepared, labelled as MFGdO2 and MFGdO3, for which Zinc (such as Zn(II)-acetylacetonate) was chosen as metal ion.

Figure 15 reports the experimental diffractogram of MFGdO2 sample, compared with the ones of ZnO and Gd$_2$O$_3$ bulk materials obtained from the Pattern Diffraction Files (PDFs) number 01-079-2205 and 01-086-2477.
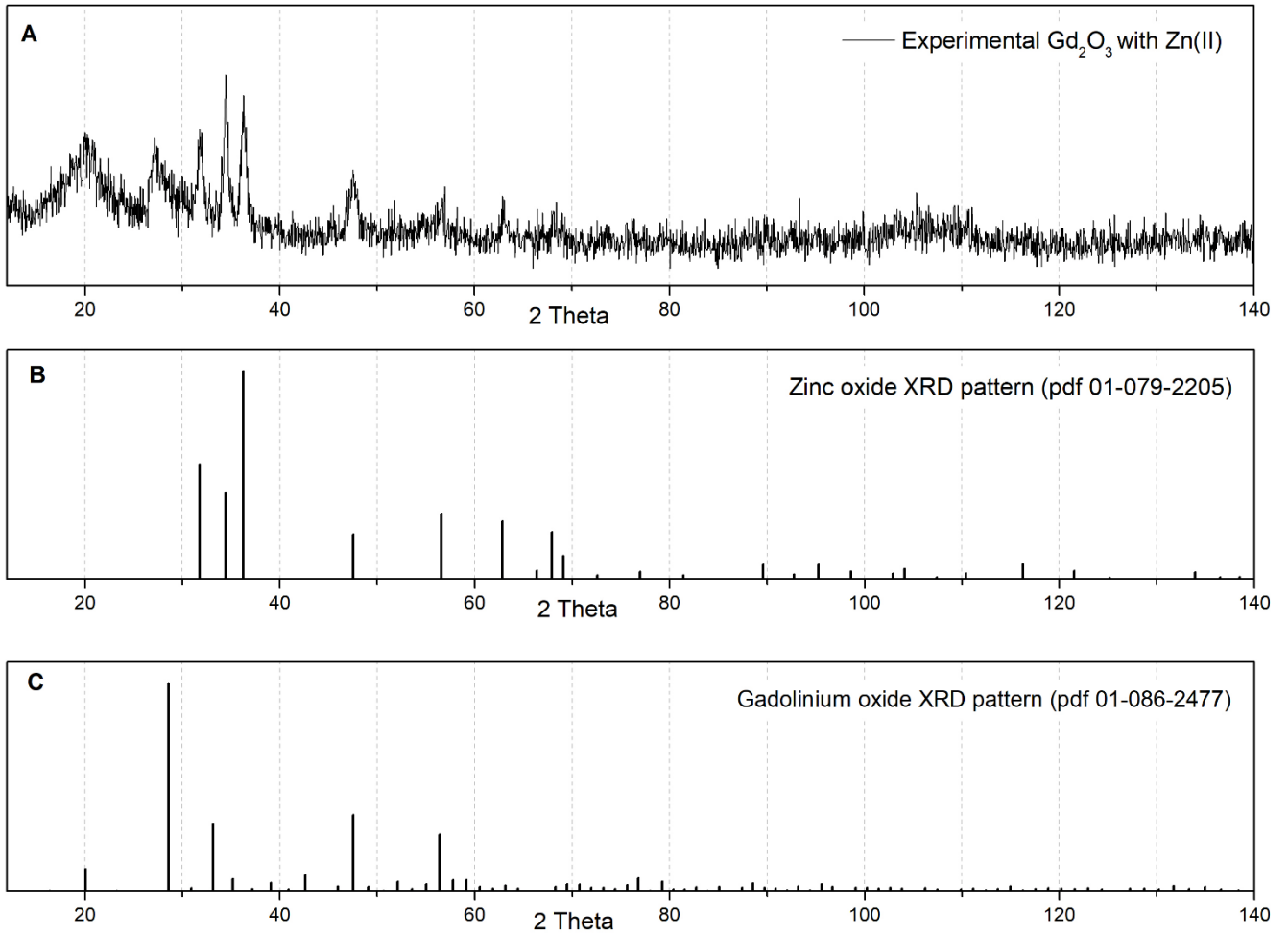
Figure 15: Experimental xrd pattern of Gd₂O₃ with Zn(II) (A); xrd pattern of bulk material of ZnO (B) and Gd₂O₃ (C).

A qualitative observation shows that the first sample synthetized adding the metal ion is composed of two distinct crystalline phases, identified as body centered cubic phase for Gadolinium oxide and an hexagonal one for the ZnO. It is also noted that the hexagonal phase shows narrow signals indicating that the sample is formed by two populations of particles that differ both in chemical composition and in size.

The quantitative analysis, aimed at determining the structure and the average crystallite size, was performed by the Rietveld's method. The diffraction profile was refined following the assumption of the qualitative analysis using two particle populations and leading to the calculated xrd profile reported in figure 16.
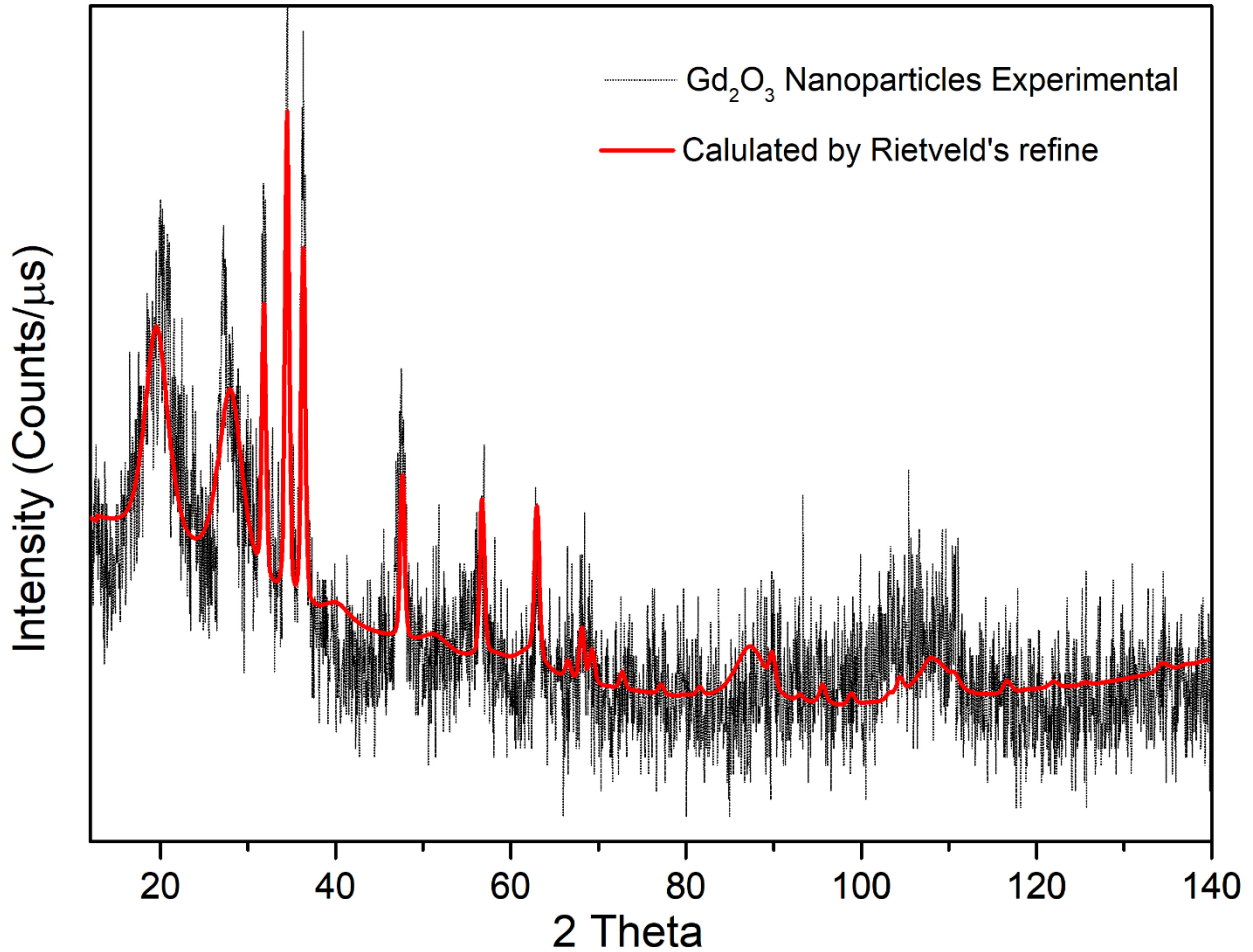
***Figure 16**: Rietveld refinement of gadolinium oxide nanoparticles and experimental ones.*

It perfectly mimics the experimental data giving an estimate of lattice parameters and particle sizes that are reported in table 6.

Sample name	Composition	Phase	Space Group	Edge of cell (Å)	Dimension by Sherrer's equation <D> (nm)
MFGdO2	Gd_2O_3	BCC	Ia-3	a = 10,92 ± 0,02	5,4 ± 0,4
	ZnO	Hex	P63m	a =b = 3,245 ± 0,001	58 ± 9
	ZnO	Hex	P63m	c = 5,201 ± 0,002	

***Table 6**: lattice parameters and average dimension of crystalline phases of the MFGdO2 sample.*

To verify the reproducibility of the synthesis a second sample was produced, called MFGdO3, using the same experimental setup (quantity of reagents, time and reaction temperature). As it can be seen, (figure 17) the experimental data obtained from x-ray diffraction of the two samples differ in position, intensity of the peaks

however the shape of the profile is comparable and both patterns are made of the two phases identified for the MFGdO2 sample.
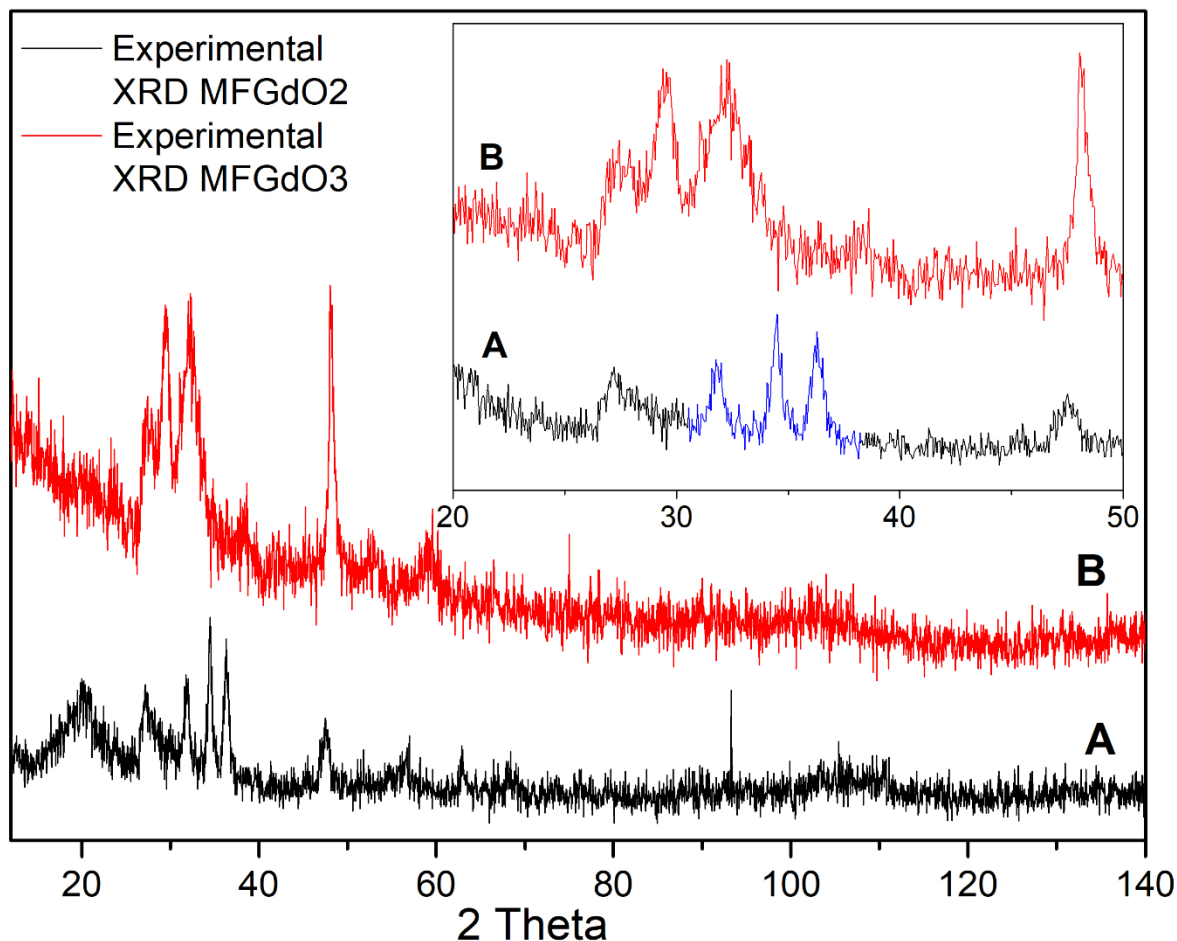
Figure 17: *xrd pattern of MFGdO2 and MFGdO3 samples. Insert shows a magnification of the region between 20 and 50 degrees of the same experimental data.*

Figure 17 shows the diffraction profile of the sample called respectively MFGdO2 (A) and MFGdO3 (B); in whose synthesis Zinc was used as a competitor ion.

The difference in 2θ position suggests a contraction of the elementary cell of the second sample with respect to the first one. The peaks of sample B turned out to be narrower than the ones of specimen A, which implies a greater nanoparticle size produced in the second synthetic run of this series.

The qualitative observation just described are confirmed by the Rietveld's analysis: in table 5 the lattice parameters and the average size obtained from the refinement are illustrated and compared.

Sample name	Composition	Phase	Space Group	Edge of cell (Å)	Dimension by Sherrer's equation <D> (nm)
MFGdO2	Gd_2O_3	BCC	Ia-3	a = 10,92 ± 0,02	5,4 ± 0,4
	ZnO	Hex	P63m	a =b = 3,245 ± 0,001	58 ± 9
	ZnO	Hex	P63m	c = 5,201 ± 0,002	
MFGdO3	Gd_2O_3	BCC	Ia-3	a = 10,62 ± 0,02	10 ± 1
	ZnO	Hex	P63m	a = b = 3,669 ± 0,007	16 ± 3
	ZnO	Hex	P63m	c = 5,41 ± 0,02	

Table 7: *lattice parameters and average size of crystalline phases of the MFGdO2 and MFGdO3 samples*

In fact, the nanoparticles contained in the MFGdO3 sample have a smaller cell parameter (0.3Å) than the MFGdO2 sample. This result may not be entirely correct since the experimental data present a high background noise that could influence the refinement and therefore the calculated profile.

On the other hand, looking at the data of the average size we may note that in the second sample the two phases have comparable dimensions, while this does not happen for the first sample where there is a difference of an order of magnitude concerning the average size.

Comparing the results of the refinement of the experimental data collected for the samples prepared without and with Zinc, respectively (MFGdO1) and (MFGdO2), a significant reduction in the size of crystallite, accompanied by an increase in lattice dimension for the sample produced with assisted metal synthesis is observed.

Table 8 illustrates these differences highlighting what has been hypothesized and reveals that the metal ion plays a fundamental role in controlling dimensions.

Sample name	Composition	Phase	Space Group	Edge of cell (Å)	Dimension by Sherrer's equation <D> (nm)
MFGdO1	**Gd_2O_3**	**BCC**	**Ia-3**	**10,83 ± 0,01**	**19 ± 3**
	Gd_2O_3	BCC	Ia-3	10,71 ± 0,03	15 ± 1
MFGdO2	**Gd_2O_3**	**BCC**	**Ia-3**	**a = 10,92 ± 0,02**	**5,4 ± 0,4**
	ZnO	Hex	P63m	a =b = 3,245 ± 0,001	58 ± 9
	ZnO	Hex	P63m	c = 5,201 ± 0,002	

Table 8: *lattice parameters and average size of crystallite of the MFGdO1 and MFGdO2 (synthetized without any metal ions) samples.*

The aforementioned hypothesis required some checking also for what concerns the effect of the metal ion in the definition of the shape of the nanoparticles. This was verified by acquiring some TEM images at different magnifications.
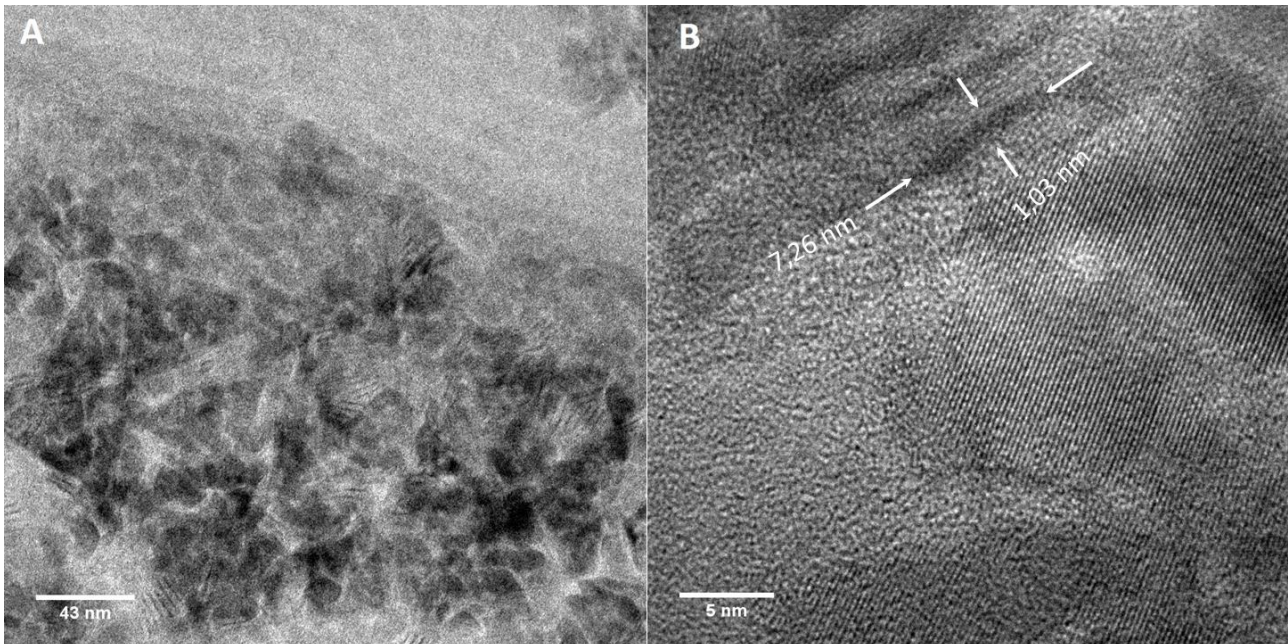
Figure 18: TEM image of Gadolinium oxide nano-disk synthetized with Zn(II) low magnification (A) and high magnification (B)

In figure 18 we can observe disk-shape particles arranged face up and particles edge on the last ones forming a sort of columnar structure. All the nanoparticles are of gadolinium oxide and, as it can be seen from the high resolution image (figure 18b) their morphologies are well defined of a disk shape having size of 7.26 nm (diameter) and thickness of 1.03 nm.

The x-ray diffraction and electron transmission microscope analyses confirm the hypothesis on the role played by the metal in the definition of shape and size of the synthetized nanoparticles. However, both analyses show that the oxide of metal used, which pollutes the sample, is formed during the synthesis; furthermore, ZnO has the ability to reflect the ultraviolet radiation [59] therefore it could prevent the correct evaluation of the optical properties of nanoparticles. For these reasons, it must thus be removed from the sample even if its presence could favour the use of this system in the medical fields as ZnO has interesting antimicrobial properties [60]. Since Zinc oxide is an integral part of the nano-structured system produced, the isolation of nanoparticles of Gd_2O_3 is very difficult.

The possibility of replacing the Zn(II) with another transition metal which is easily removed from the reaction environment and allowing to obtain particles with the same characteristics has been therefore taken into consideration. After careful observations it was chosen to use Nickel, in the form of Ni(II)-acetylacetonate

which led to the synthesis of the sample called MFGdO_Ni, which shows interesting differences with the previous synthesis.

During the synthesis there is a clear variation in colour of the reaction solution when the temperature reaches 170 °C changing from transparent to black, this is an indication of the beginning of the oxidation process by thermal decomposition of the organo-metal precursors. The second difference is observed after the hot injection of oleic acid (carried out at 280°C) where the black colour stays; during the digestive process the reaction mixture becomes more and more transparent while preserving still a dark colour tending to black.

Following the precipitation of the reaction product obtained by adding an excess of ethanol and the subsequent centrifuge, the solid consists of two phases: an oily phase containing the nanoparticles and another phase formed by a black needle-like particulate identified as Nickel oxide.

These first observations show how the use of Nickel, as a metallic assistant, leads to a considerable advantage over the use of Zinc. It is, in fact, sufficient to disperse the solid obtained in toluene and centrifuge at 3'000 rpm for 10 minutes to isolate the Gadolinium oxide nanoparticles from those of Nickel oxide.

The effectiveness of this simple procedure was validated by x-ray diffraction and TEM analysis performed on the isolated solid.

In figure 19 the experimental diffraction pattern of this sample is reported, accompanied by the literature reference of the same bulk material.
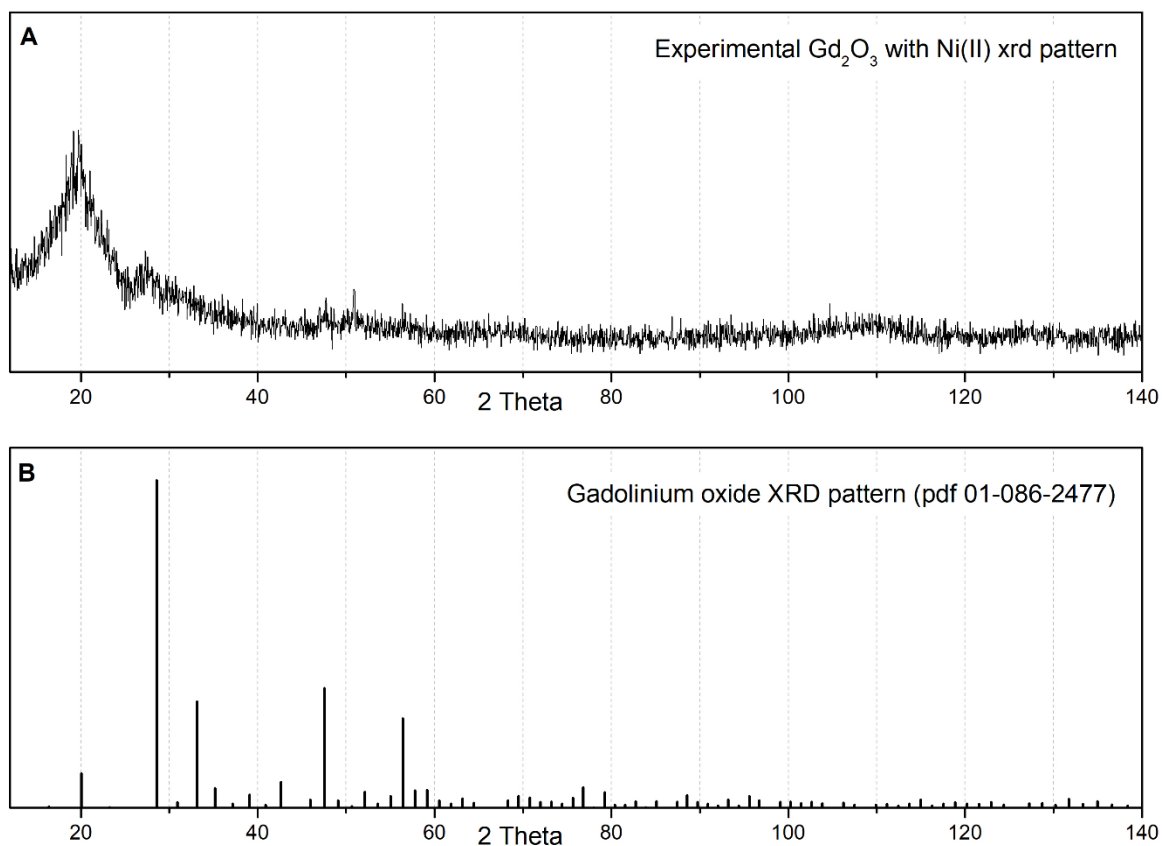
Figure 19: *xrd diffraction pattern of experimental gadolinium oxide nanoparticles (A) and bcc phase of the same bulk material (pdf 01-086-2477) (B).*

The diffractogram shows a single crystalline phase of Gadolinium oxide, the only component of nanoparticles. This phase has been identified, according to PDF 01-086-2477 card, as body centred cubic (bcc).

Furthermore, in the diffraction pattern no signals coming from Nickel oxide is evident, confirming the efficiency of the separation procedure.

The XRD pattern is very noisy due to the low amount of specimen present and to the use of an old detector, but this is also present in all the diffraction patterns collected for all our samples, in any case, it is observed that the signal intensities follow a different pattern respect to the profile presented in figure 19B.

As previously stated, the use of the oleylamine/oleic acid pair leads to the preferential formation of disk-shaped nanoparticles. In this thesis the growth kinetics of nanoparticles is not explored, however an explanation is provided by Yan's work [61], stating that the final shape assumed by the particles is guided by the atomic density present in the crystallographic planes, identified by the Miller's indices, of the crystalline structure. For a complete and exhaustive treatment of the subject it is necessary to carry out further analyses which are out of scope of this thesis.

Figure 20 illustrates the experimental XRD pattern in the region between 20 and 60 2θ degrees in which the reflections relative to the crystallographic planes that delimit the surface of the nano-disks are highlighted. Respectively the upper surface of the disk belongs to the plane identified by the indices (-22-2) while the plane (001) delimits the thickness of the particle.
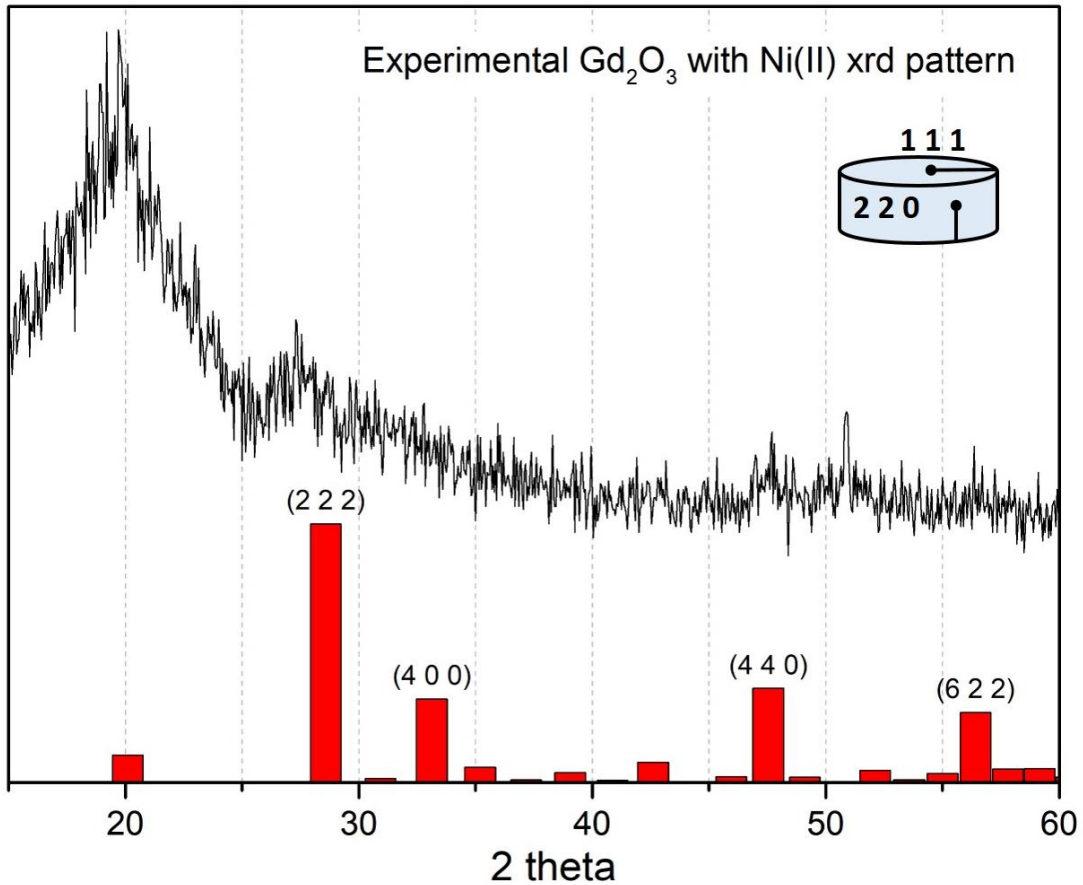
Figure 20: *Experimental xrd patter of gadolinium oxide nanodisk (black line), BCC phase of same bulk material (red histogram), and boundary crystallographic planes of nanodisk.*

Focusing our attention to the reflection (222), a shift towards smaller angles is observed. This difference is also present for all the other reflections but less visible due to the noise that affects the collected data.

This observation leads to the hypothesis that the nanodisk morphology causes an expansion of the elementary cell with respect to the one observed in bulk material. In order to estimate the cell parameters and, therefore, quantify the extent of the cell side increasing, the diffraction pattern was refined by the Rietveld's method.
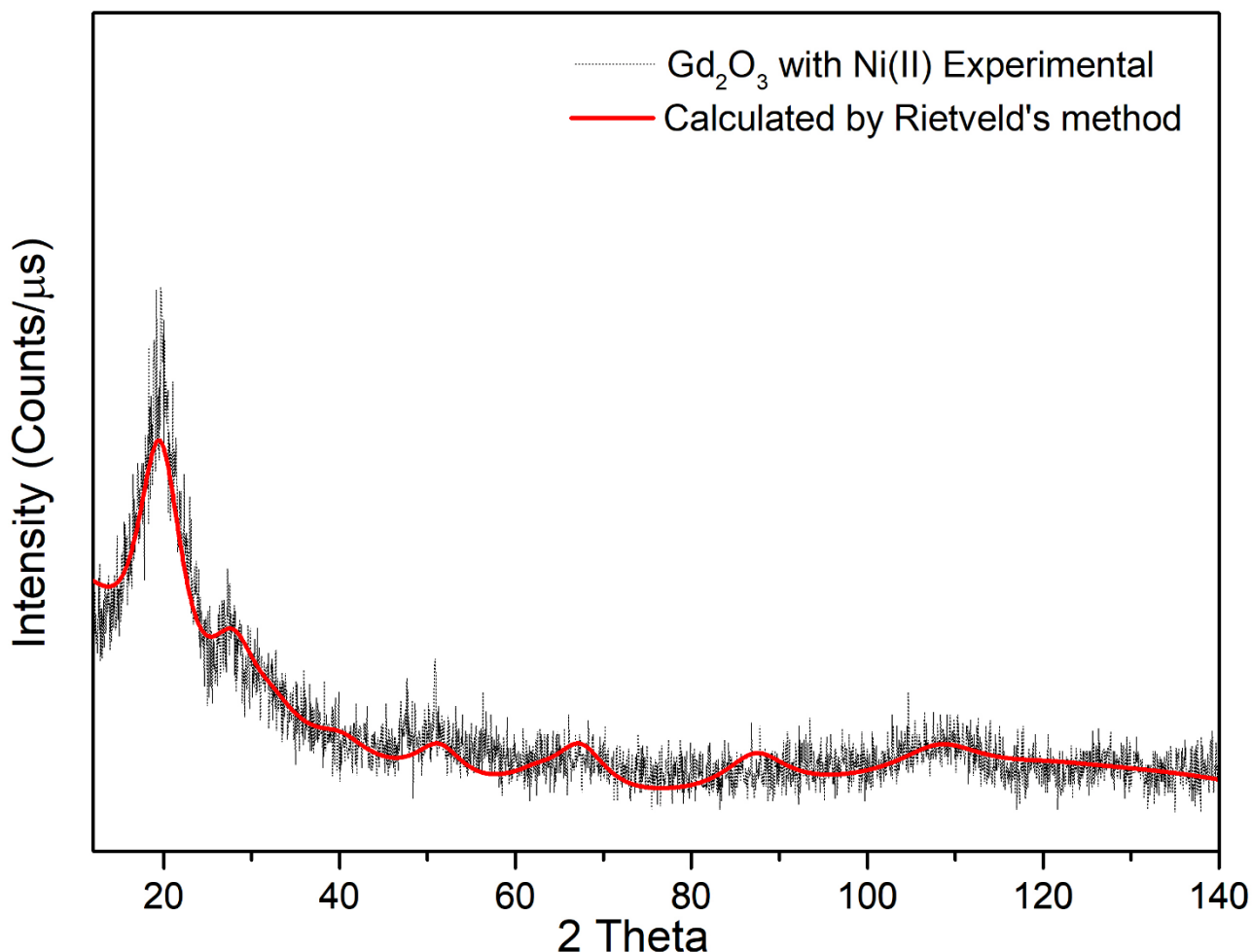
Figure 21: *Experimental xrd pattern and its refinement with Rietveld's method*

The refinement (figure 21) confirms our hypothesis: in fact, the nanodisk have a cubic crystal lattice (BCC type) with an edge of cell equal to 10.92 Å; instead the bulk material has a value of 10.809 Å.

The causes of this expansion are to be found in the formation mechanism of nanoparticles that has not been thoroughly studied in this work. However, Yan et al. provide a general explanation that could be plausible even in the present case: "the bcc structure, characteristic of lanthanide sesquioxide, could derive from a more general fcc cubic structure through the removal of the 25% of oxygen atoms from specific reticular sites".

This mechanism, which must be ascertained, is in line with thermodynamics/kinetics processes that govern the digestive ripening process. In fact, the digestive agent, oleic acid, after its injection into reaction environment, removes cluster of atoms from larger particles formed by the thermal decomposition of metal-organic precursors. The removed atoms form new nucleation centres covered by the same digestive agent which limits their growth, defining their shape and size.

The nanoparticle size obtained by x-ray diffraction is 6.1 ± 0.6 nm. This value refers to the average dimension of the nanodisks as it was obtained by the Scherrer's equation (figure 22A) using a Lorentzian function for the estimation of the peak width, parameter (Lx), during the Rietveld refinement process;

$$<D> = \frac{18000 \cdot K \cdot \lambda}{\pi \cdot Lx} \quad (A) \quad \Delta D^2 = \left(-\frac{18000 \cdot K \cdot \lambda}{\pi \cdot Lx^2} \cdot \Delta Lx \right)^2 \quad (B)$$

Figure 22: *Sherrer's equation (A) and relative error formula (B)*

where K is a proportionally constant, it varies in relation to the shape of the nanoparticles, in this case K = 1 was used; λ is the X-ray wavelength equal to 1.54056 Å ($K_{\alpha 1}$ of Cu). The error estimate was instead performed by applying the error propagation theory at the Scherrer's equation (figure 22B).

Another efficient method of analysing the size, shape and dimensional distribution of nanoparticles is to observe the sample under a Transmission Electron Microscope. In the following lines the image acquired by the TEM will be presented and discussed.

21 nm
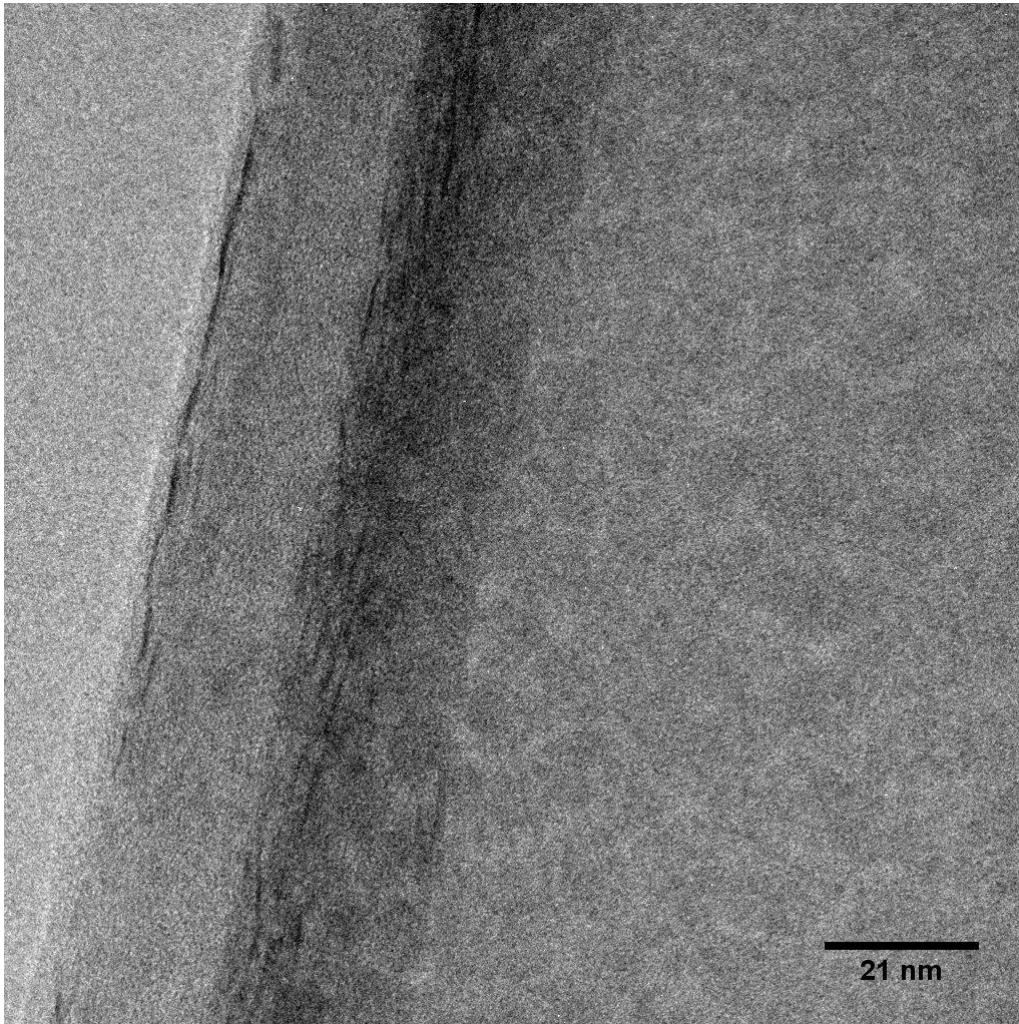
Figure 23: *TEM image of Gadolinium Oxide nanoparticles produced with Nickel*

Figure 23 shows the Gadolinium oxide sample produced with Nickel as a competitor ion: observing the figure, disc-shaped nanoparticles can be seen arranged in orderly manner to form a series of columns and the presence of particles placed on the face (right side of the figure).

Furthermore, the image shows the absence of agglomerations of particles. This confirms the interpretation given to XRD pattern: the sample is formed by a population of disc-shape and small particles. The absence of big particles and agglomerates of their suggest that any Nickel particles have been eliminated during the washing process.

The image acquired at TEM (figure 23) was subjected to a dimensional analysis in order to determinate the dimensional distribution of the nanoparticles.

Figure 24 shows the histogram and the related Gaussian curve resulting from the dimensional analysis.
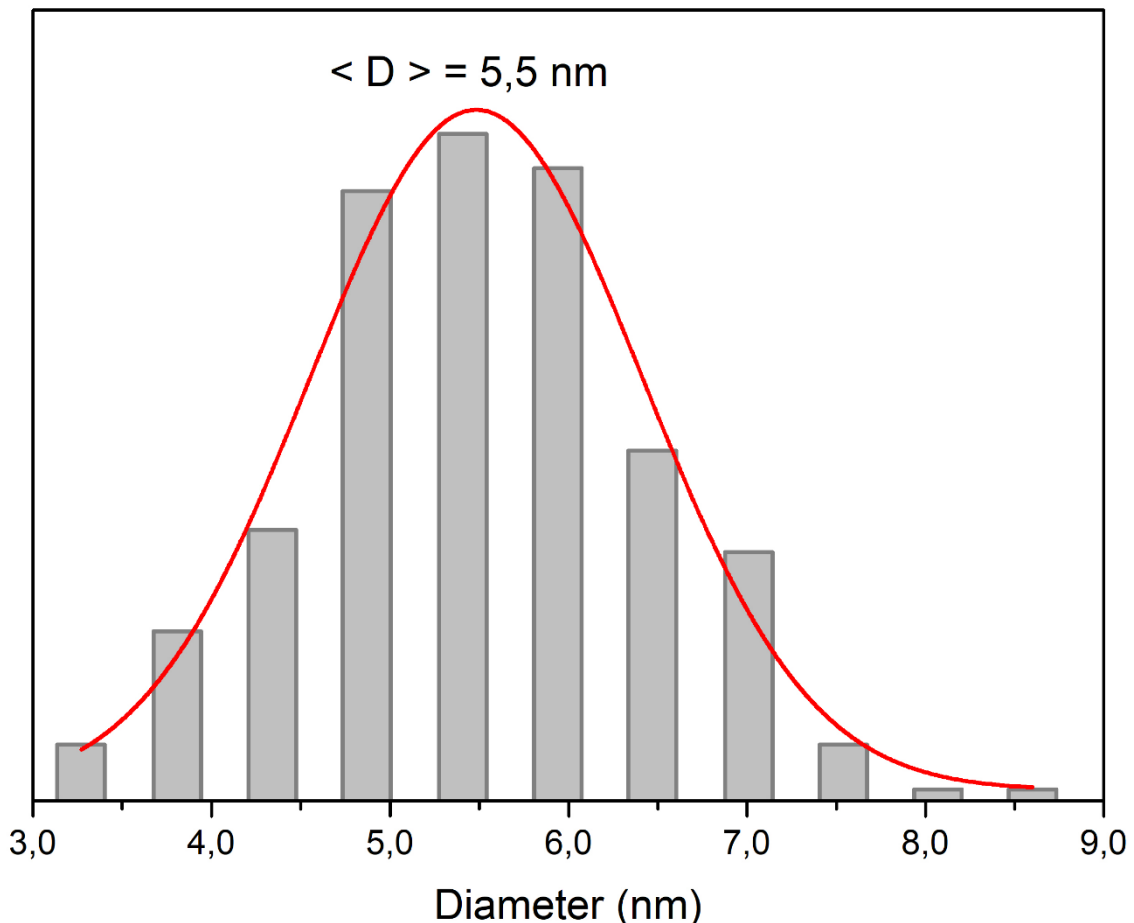
Figure 24: *Dimensional distribution of Gadolinium oxide nanoparticles produced with Nickel as a competitor ion.*

It can be seen, this analysis provides the average size value of 5.5 ± 0.1 nm while the Rietveld method showed a value of 6.1 ± 0.6 nm. The two values determined with two different methods, with respect to their errors, state that the Gadolinium oxide nanoparticles have an average diameter of about 5.5-6 nm.

The characterizations performed on the sample called MFGdO_Ni have shown that it is possible to produce, through the digestive ripening method, a single, mono-phase population of Gd_2O_3 nanoparticles having a

disc-shape morphology, small size and homogeneous dimensional distribution. These characteristics are achieved by using Ni(II) as a competitor ion during the digestion process.

In light of this results it was decided to produce a new series of samples by inserting a doping agent. The dopants chosen are also part of the rare earth family and that elements are: Europium, Ytterbium, Erbium and Praseodymium. The last element was chosen because the literature provides a very few data and it is an excellent candidate to build a hybrid nanomaterial capable of performing Up Conversion from the infrared region.

4.2 LANTHANIDE DOPED GADOLINIUM OXIDE NANOPARTICLES

4.2.1 Synthesis

Lanthanide doped Gadolinium oxide nanoparticles were synthetized following the previously described methods (see paragraph 2.4.3). A stock 0.1 M solution of lanthanide acetylacetonate precursors complexes were prepared in a vial by dissolving the appropriate (table 9) amount of reagent in 2 mL of oleylamine.

Reagents	Purity	M.M [g/mol]	Concentration of stock solution [M]	Volume of solution [mL]	Quantity [mg]
Gd(Acac)$_3$ x 3H$_2$O	--	508,6195	0,1	2,00	101,7
Er(Acac)$_3$ x 3H$_2$O	--	518,6285	0,1	2,00	103,7
Yb(Acac)$_3$ x 3H$_2$O	--	524,4265	0,1	2,00	104,9
Pr(Acac)$_3$ x 3H$_2$O	--	592,2717	0,1	2,00	98,6
Eu(Acac)$_3$ x 3H$_2$O	--	503,3335	0,1	2,00	100,7
Ni(Acac)$_2$	0,96	256,9092	0,1	2,00	53,5

Table 9: *Amount of lanthanide acetylacetonate complexes precursors to prepare the stock solution.*

Samples 7 and samples from 9 to 12 (table 10) have been prepared following the same method used to produce the gadolinium oxide nanoparticles as it is described in the first part of this work.

#	Sample name	Composition	Reaction parameters		Volume of 0.1 M solution of acetylacetonate precursor [µL]						Volume of ligands/solvents [mL]	
			Temperature [°C]	Time [minutes]	Gd	Yb	Er	Pr	Eu	Ni	OAm	OA
7	MFGdOYbEr	$Gd_2O_3{:}Yb_{3\%}Er_{1\%}$	280	60	640	20	6,7			333	4,0	1,67
8	MFGdOPr5	$Gd_2O_3{:}Pr_{5\%}$	280	60	633			33,3		333	4,0	1,67
9	MFGdOPr10	$Gd_2O_3{:}Pr_{10\%}$	280	60	600			66,7		333	4,0	1,67
10	MFGdOPr15	$Gd_2O_3{:}Pr_{15\%}$	280	60	566			100		334	4,0	1,67
11	MFGdOEu10	$Gd_2O_3{:}Eu_{10\%}$	280	60	600				66,7	333	4,0	1,67

Table 10: *Samples synthetized and amount of reagent (OAm = Oleylamine; OA = Oleic Acid)*

The sample 7, called MFGdOYbEr (light blue in table 10) was synthetized with a slight variation to the synthetic method: in three neck round bottom flask, equipped with magnetic stir bar, reflux condenser, thermometer and drillable septum, 640 µL of the stock solution (0.1 M) of Gadolinium acetylacetonate, 333 µL of the stock solution of Ni(Acac)$_2$ and 4.0 mL of oleylamine were added. The reaction mixture, in N$_2$ atmosphere, was heated under magnetic stirring.

The solution of dopant ions was prepared in a vial by adding 20 µL and 6.7 µL of the respective stock solutions of Yb^{3+} and Er^{3+}in 1 mL of oleylamine.

When the temperature of the reaction mixture reached 170°C, the doping solution was quickly injected, and the heating was continued until it reached 280°C. At this temperature 1.67 mL of oleic acid was injected and the reaction solution was left for 1 hour at the same temperature.

After the reaction time has elapsed, the mixture was naturally cooled down to room temperature; subsequently the reaction product was precipitated by adding ethanol. The particles were centrifuged at 10'000 rpm for 10 minutes.

The crude solid was washed thrice with a solution of toluene/acetone (in a ratio of 1:3); finally, the purified nanoparticles were dispersed and preserved in toluene for next characterizations.

4.2.2 Result and discussion

The five samples listed in table 8 were subjected to structural and morphological characterization by X-ray diffraction and Transmission Electron Microscopy while photoluminescence was used for the analysis of the optical properties, deriving from the addition of Lanthanide doping agents.

In the following paragraphs the results of the above characterization will be presented and discussed.

4.2.2.1 Morphological and structural characterization

The results obtained from the structural characterization of the undoped samples show that the synthetic method used leads to the formation of nanodisks formed by Gadolinium sesquioxide having cubic crystal structure of BCC type. By applying the same method, a sample formed of Erbium oxide was produced whose analysis, by x-ray diffraction, highlights a structure similar to that of Gd_2O_3. This makes the Er^{3+} ions an ideal doping agent to give the Gd_2O_3 matrix interesting optical properties.

In order to obtain a system able to perform up-conversion, applying the digestive ripening process, the first doped sample, with 3% of Yb^{3+} and 1% of Er^{3+}, was synthetized (sample 7 of table 8 called MFGdOYbEr).

Figure 25 shows the X-ray diffraction pattern of the doped sample with Yb^{3+} and Er^{3+} ions (black line) and, by way of comparison (in red line) that of the pure Gadolinium Oxide sample.
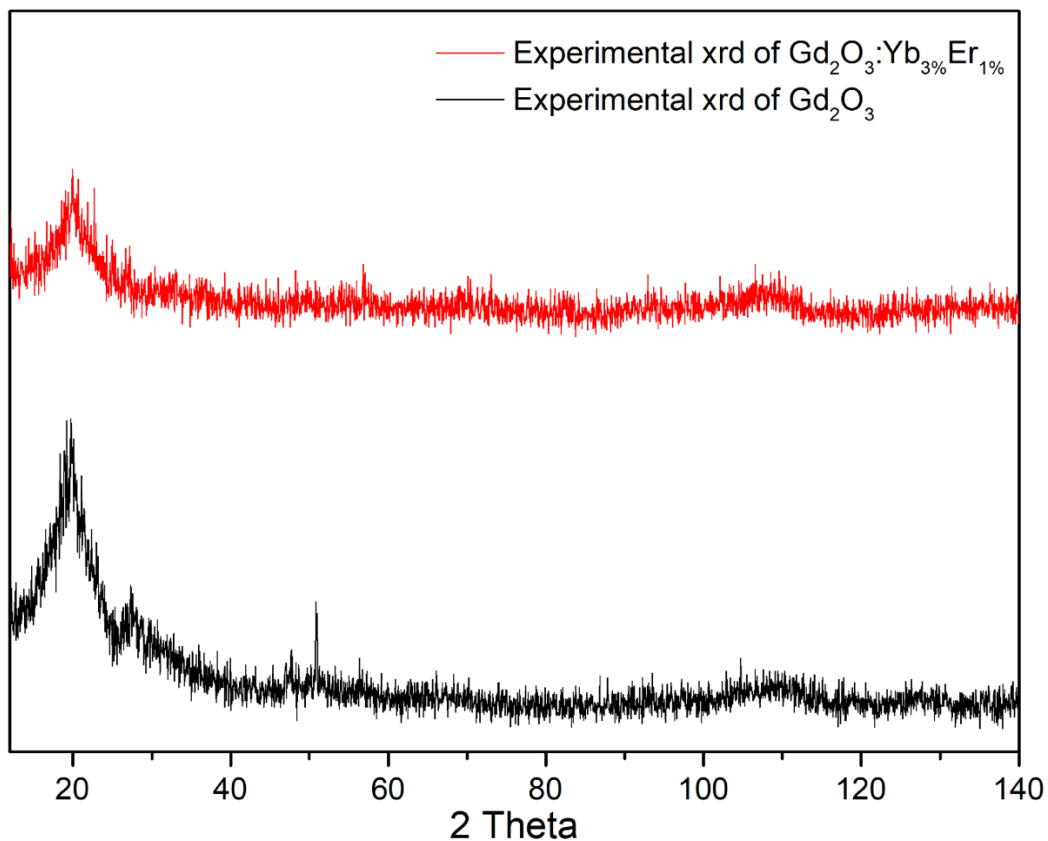

Figure 25*: Comparison between xrd profiles of Gd2O3 (black line) and Gd2O3:Yb3%Er1% (red line) samples.*

Qualitatively comparing the experimental diffraction pattern (the red one in figure 25) with the diffraction profile of bulk Gadolinium oxide (pdf 01-086-2477) it is possible to see that the sample is composed of a single crystalline phase, identified in the body centred ones proper to Gd_2O_3.

From these data, however, no hypothesis can be made about the presence of dopant ions within the crystal lattice. Theoretically, the introduction of substitution dopant ions should cause a deformation of the elementary unit cell visible as a displacement in the position of the diffraction peaks. The presence of such shift toward greater angles would mean a contraction of the unit cell, on the contrary a shift toward smaller angles indicates a reticular expansion.

Taking into consideration the ionic radius of the trivalent ions used as doping agents, respectively equal to 103 pm (Er^{3+}) and 102 pm (Yb^{3+}) and since the ionic radius of Gd^{3+} is equal to 107.8 pm [62] is natural to expect a contraction of the crystal lattice in the doped samples.

Unfortunately, the comparison between the XRD patterns of the doped and un-doped samples does not evidence any shifts in the peaks, in this case the detection of any difference is more complicated due to the high background noise that makes difficult to identify any variations within the sensitivity of the measurement equal to 0.05 degrees.

More detailed information regarding the lattice parameters, as well as the average particle size, is provided by the application of the Rietveld's method on the experimental data. The refinement of the diffraction profile was performed by including the doping atoms in the same stoichiometric quantities used in the synthesis procedure in the cubic phase of Gd_2O_3.

Table 11 compares the results obtained from the refinement of doped sample data with those obtained from the same analysis performed on the XRD pattern of the un-doped sample.

Sample name	Composition	Phase	Space Group	Edge of cell (Å)	Dimension by Sherrer's equation \<D\> (nm)
MFGdO_YbEr	$Gd_2O_3:Yb_{3\%}Er_{1\%}$	BCC	Ia-3	10,910 ± 0,009	8,8 ± 0,1
MFGdO_1	Gd_2O_3	BCC	Ia-3	10,92 ± 0,02	5,4 ± 0,4

Table 11: Comparison of lattice parameter and average size of bi-doped and un-doped Gadolinium oxide nano-disk obtained by Rietveld refinement

As it can be seen, the lattice parameters of the bi-doped sample do not show any variation with respect to the undoped ones; this supports the results of the qualitative analysis which hypothesized the absence of lanthanide ions within the crystal lattice.

The dimensional value extrapolated from the refinement is equal to 8.8 ± 0.1 nm which is perfectly comparable with the size of undoped NPs.

In order to complete the morphological analysis, the sample was analyzed to Transmission Electron Microscopy which clearly shows the disc shape of the nanoparticles (figure 24).
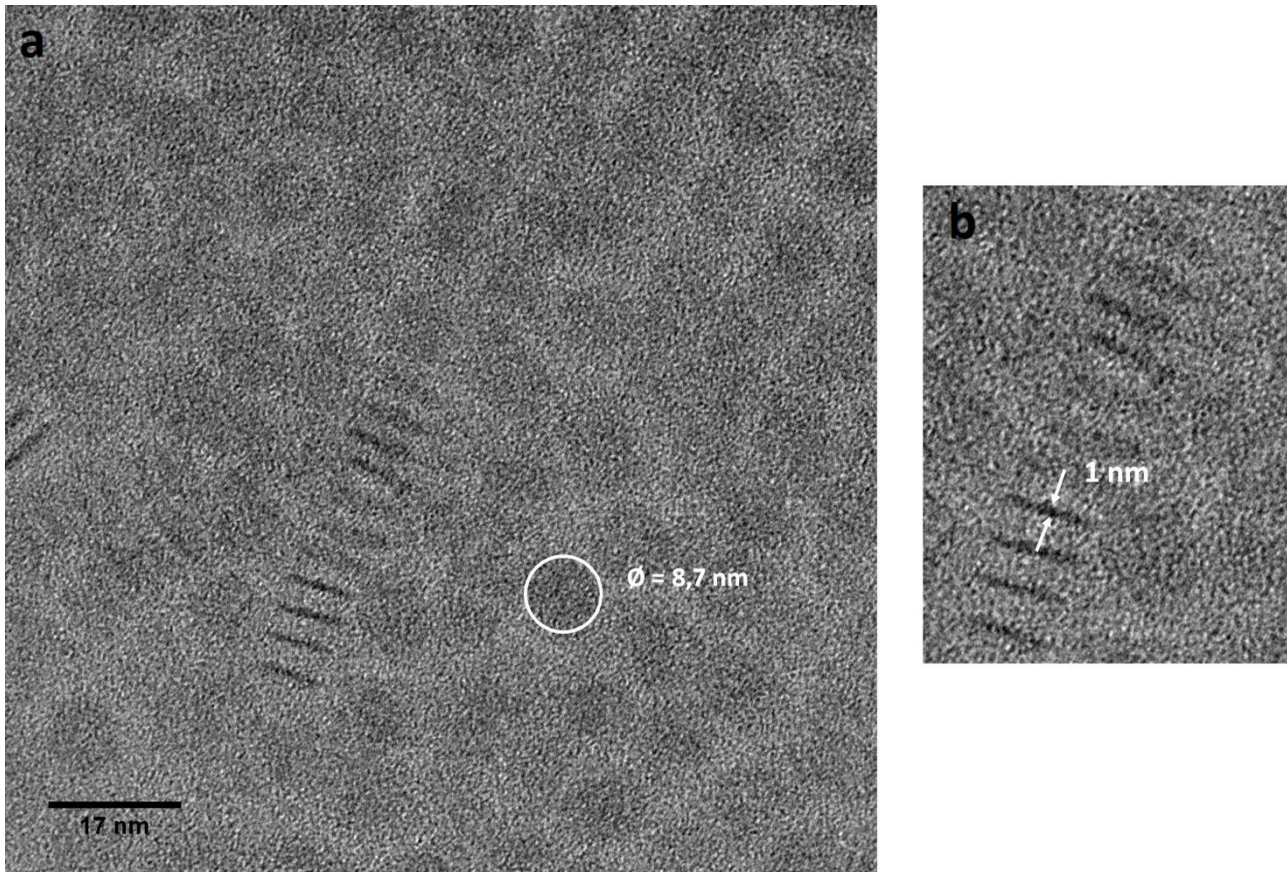
Figure 26: Yb^{3+} and Er^{3+} doped Gd_2O_3 nanodisk: diameter (a), thickness (b).

By observing the image acquired at TEM (X 150K, figure 26) it is possible to estimate the dimension of the nanodisks which have a diameter of 8.7 nm and a thickness of 1 nm (figure 26b). It is also noted that the sample has the same characteristics, in terms of mono-dispersion and self-assembly, seen in the previous undoped samples.

In addition to a direct observation of the nanoparticles' shape, TEM analysis allows to qualitatively evaluate the composition of the sample under examination. Specifically, this technique is called EDS (Energy Dispersion Spectrometry); the results obtained on various region of the doped sample did not show the presence of any of the dopant ions.

As a result of these analyses, the method used leads to the formation of undoped Gadolinium oxide nanoparticles, however the low amounts of dopant ions which has been used may not be sufficient to introduce visible morphological changes.

On the basis of this consideration and wanting to explore the doping with less used lanthanides, a series composed of three samples with increasing concentration of doping agent was produced. The ion chosen for this series of samples was Praseodymium and the concentration adopted were 5%, 10% and 15%. The three

samples were produced using the same synthetic procedure used in the preparation of the undoped nanoparticles: all the precursors were added at the start of the reaction and at room temperature; at the end of the reaction they were subjected to the washing protocol and to the morphological-structural characterizations already used for previously described samples.

Figure 27 illustrates the diffraction profile of the series of samples produced with different concentration of Pr^{3+}.
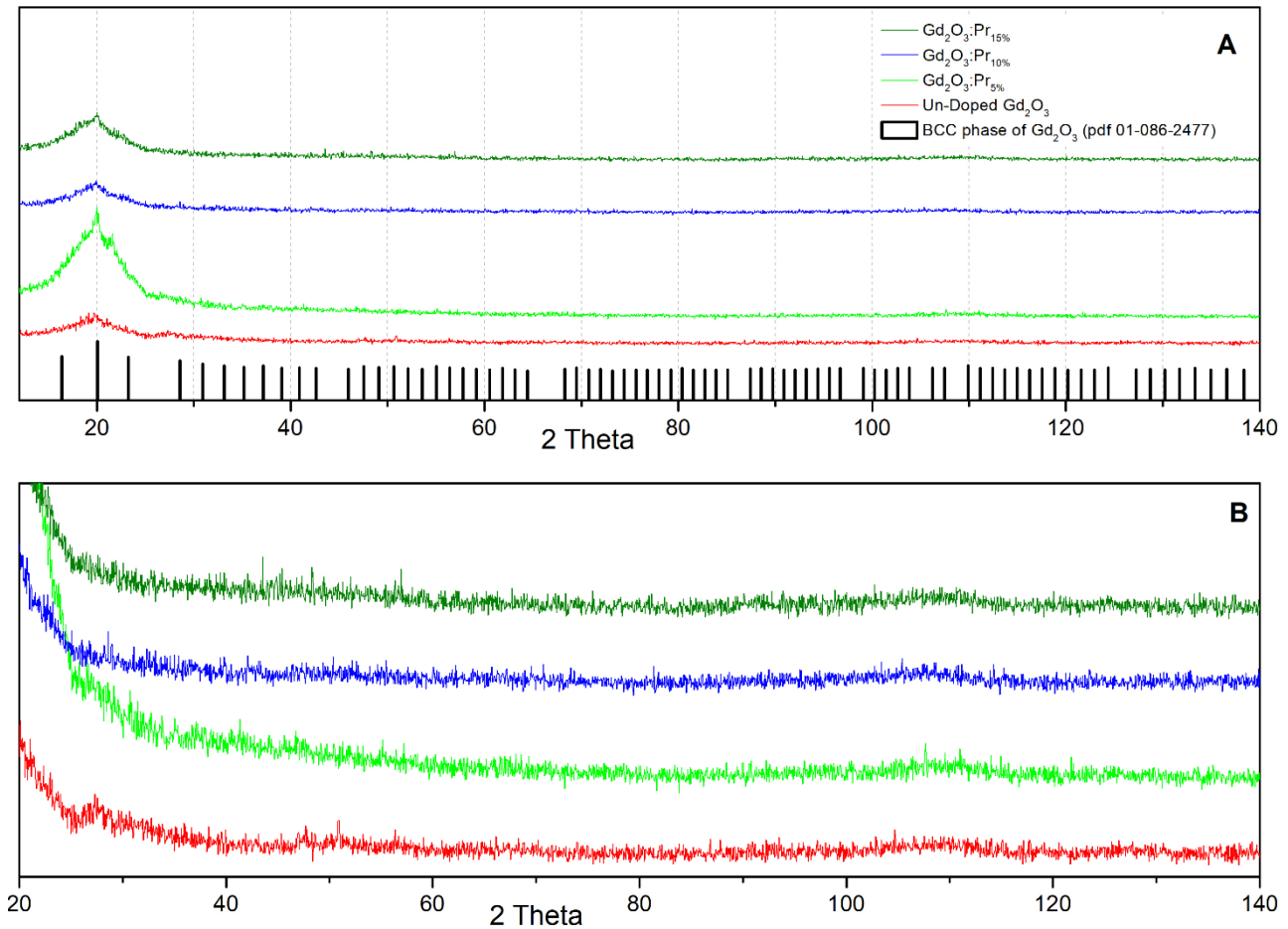
Figure 27: *XRD pattern of Gd₂O₃: Pr at different concentration: (A) comparison with XRD pattern of pure Gd₂O₃ nanoparticles and bulk material; (B) comparison among doped particles.*

Comparing the experimental data with the bulk material profile (pdf 01-086-2477) it is easily ascertainable that the synthesis carried out leads to the formation of a single crystalline phase. Regardless of the concentration of dopant ion, the nanoparticles have a cubic lattice with a centred body and apparent disc-shape morphology.

By comparison of the diffraction profile of the doped sample with that of the un-doped samples, observing in detail the spectra in figure 27b, we note that the relative intensities of the peaks located at angles greater

than 20 degrees follow the same scheme seen in the sample produced in the absence of doping agents. This fact suggests that also in this case, the nanoparticles have a disc-shape morphology.

In order to understand if the synthetic method used allows the doping of the Gadolinium Oxide matrix with the Pr^{3+} ion, the XRD spectra of each sample were subjected to refinement using the Rietveld method.

The graphic results of this processing are reported in appendix B while the numerical results are summarized in table 12

Sample name	Composition	Phase	Space Group	Edge of cell (Å)	Dimension by Sherrer's equation <D> (nm)
MFGdOPr5	Gd2O3:Pr5%	BCC	Ia-3	10,804 ± 0,006	9,1 ± 0,3
MFGdOPr10	Gd2O3:Pr10%	BCC	Ia-3	10,968 ± 0,006	5,4 ± 0,3
MFGdOPr15	Gd2O3:Pr15%	BCC	Ia-3	10,83 ± 0,01	3,8 ± 0,3

Table 12: *numerical results of refinement on the Pr-doped Gadolinium oxide nanoparticles xrd pattern*

Observing the numerical values referring to the lattice parameter, we note an anomalous trend within the same series: in fact, the increasing of the concentration of dopant should cause a proportional increase (or decrease) in the lattice size. If we compare the lattice parameters of the doped samples with the dimension of the elementary cell of the undoped one, this fluctuation trend is more evident (Figure 28).
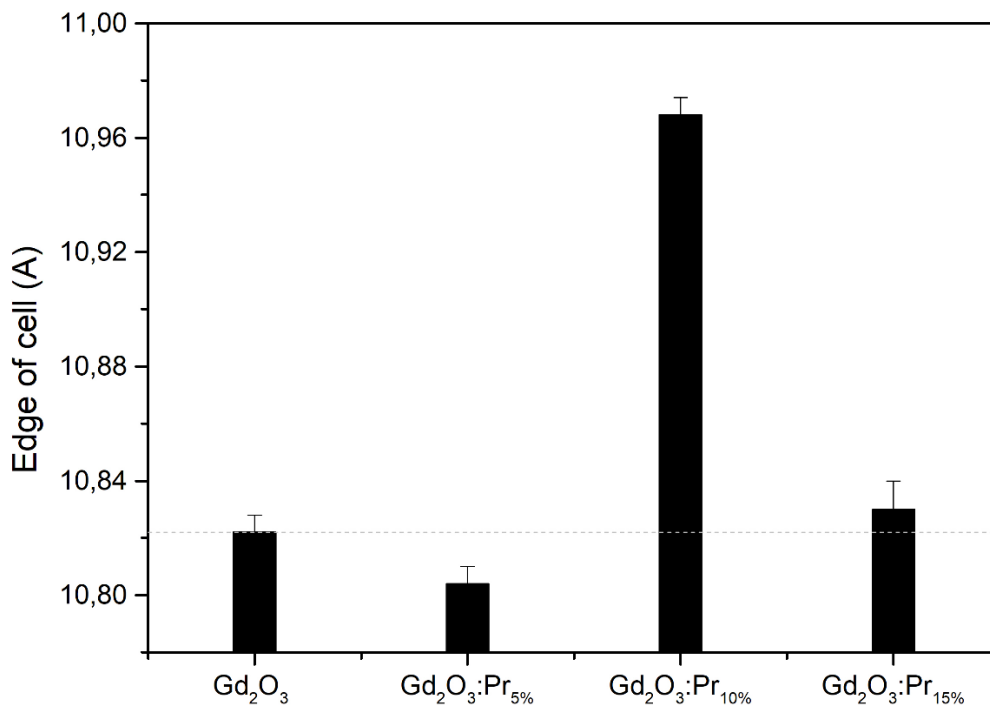

Figure 28: *fluctuation of the edge of cell in the Praseodymium doped samples*

As previously stated, to hypothesize in which direction the peak position should be shifted, it is advisable to consider the ionic radius of Praseodymium in the oxidation state 3+. According to what it is reported in table 1 (see introduction, paragraph 1.2.1) the ion Pr^{3+} has an ionic radius equal to 113 pm while the Gadolinium in the same state of oxidation has a value equal to 107.8 pm. If Praseodymium ions were present within the crystalline structure of the host material, the lattice should expand and therefore the unit cell should be larger if compared to that of dopant-free lattice.

Experimental data relative to the samples doped with 5% and 15% respectively, go in the opposite direction, showing a smaller unit cell parameter respectively equal to 10.804 ± 0.006 Å and 10.83 ± 0.01 Å.

The unit cell contraction seen in these samples could be explained considering the particularity of the Praseodymium element that can be easily oxidized to the 4+ state. The element in this state of oxidation has a smaller ionic radius (99 pm), when compared to that of Gd^{3+}, and so if it enters inside the crystal structure this should lead to the compression of the elementary unit cell. Furthermore, the presence of the Pr^{4+} ion would cause a charge failure that could be balanced by vacancies in oxygen atoms that could deform the crystal lattice and reduce its size.

In order to verify this hypothesis, these samples should be subjected to further analysis capable of discriminating the oxidation state of the atoms constituting the nanoparticles, which is out of the scope of this thesis.

Contrary to what was found for the two samples with 5 and 15% of dopant ion, the 10% doped specimen follows a trend that is in line with what is expected from the ionic radius. In fact, from the XRD refinement results for the MFGdOPr10 sample (figure 22) we found that the lattice parameter is equal to 10.968 ± 0.006 Å that is 0.4 Å larger than the one for the undoped sample. This result, however, does not constitute a certain proof of the presence of dopant in the crystal lattice as all the XRD data refinement could be affected by error coming from the high noise affecting the experimental data.

Since the XRD characterization does not allow a univocal determination of the presence of the doping agents into the crystalline structure of the Gadolinium oxide nanoparticles, doped samples were observed using TEM-EDS.

Praseodymium was found only in the sample containing 15% of dopant. The doped samples with 5% and 10% on the other hand did not show any signal related to the Praseodymium.

Since the analysis carried out on the sample with maximum dopant concentration revealed the presence of only traces for Pr, it is possible that during the synthesis the organic precursor of the rare earth is oxidized at different times with respect to the other precursors used in the synthesis. According to this hypothesis the low concentration of dopant in the first two samples of the series would not be sufficient to allow the formation of hybrid material.

The morphological and size analysis performed by the direct observation through TEM is presented below (figure 29).
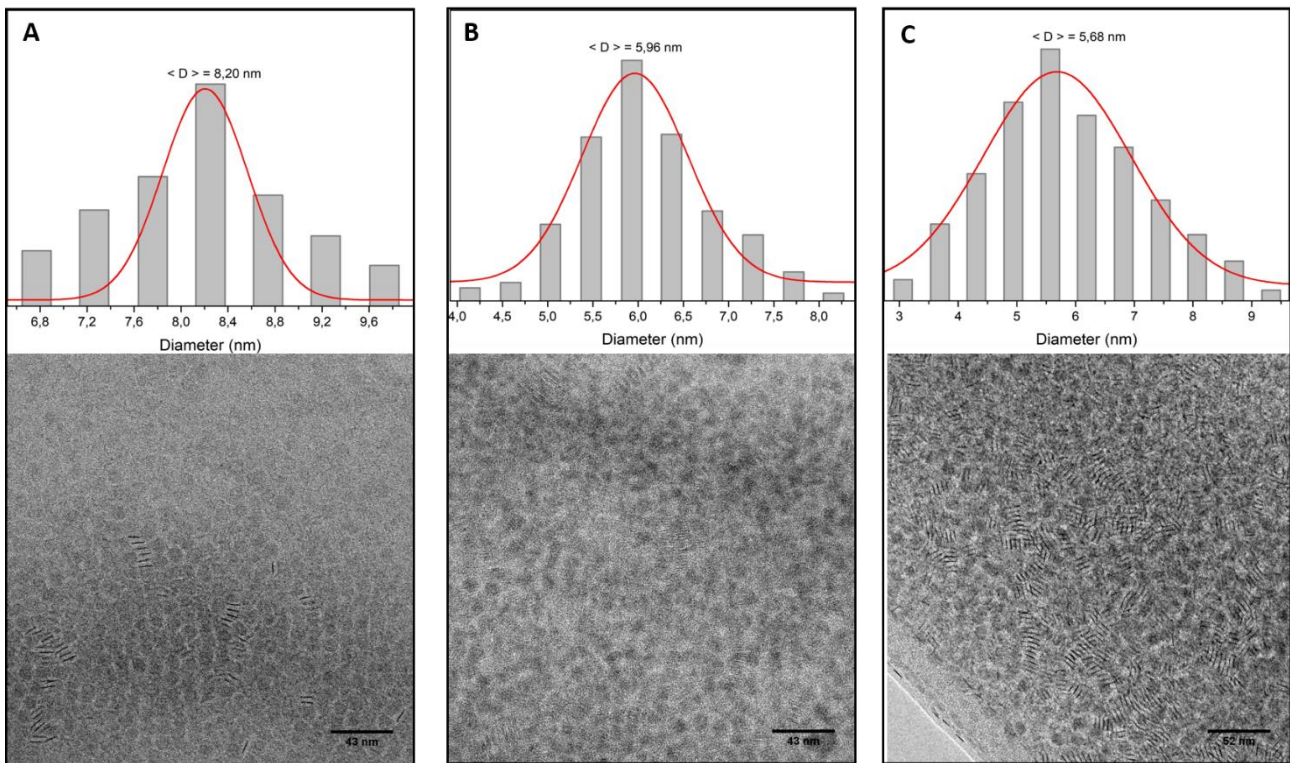
Figure 29: TEM image and size distribution of Gd2O3:Prx nanoparticles with x = 5% (A), 10%(B), 15% (C).

As reported at the beginning of this paragraph, assuming that the dopant ions are substitutional to the main lanthanide constituting the matrix, it is useful to investigate the crystallographic nature of pure Praseodymium oxide. For this reason, a sample of this material, called PrO, was synthetized and was characterized by X-ray diffraction.

According to the existing literature Praseodymium can form two different oxides having formula Pr_6O_{11} and Pr_2O_3 respectively. The first compound has a cubic lattice [63] in which the lanthanide is in the oxidation state 4+; the second, instead, has an hexagonal lattice [64] where the Praseodymium is present in the 3+ oxidation state.

Combining this information with the fact that high-temperature synthesis could oxidize Pr^{3+} to Pr^{4+} it is reasonable to expect that the synthetized nanoparticles (PrO), will crystallize in both structures.

The experimental data collected (the XRD pattern is reported in appendix B) show a profile similar to that of Gadolinium oxide, in which there are reflections probably belonging to the hexagonal phase and other reflection belonging to a cubic phase. However, the high background noise that affects the measurement does not allow a clear and immediate identification of the crystal structure of the sample under examination.

In light of these considerations, the question about whether "the modified digestive ripening method is able to allow the synthesis of doped nanoparticles" remains open.

The use of Praseodymium as a doping element is rare in literature, in fact, it is difficult to stabilize in the trivalent state and has optical properties that are not easy to evaluate. It did not turn out to be the ideal candidate to perform doping tests on the Gd_2O_3 matrix.

The most widely used lanthanide in this field and for which there is extensive literature [65] [66] [67] [68] is Europium. For this reason, a new specimen labelled as MFGdOEu10 and containing 10% of Eu^{3+} as a doping agent was synthetized following the same procedure already reported. Immediately after the synthesis and the relative washing procedure, the sample was observed under UV radiation (λ_{ec} = 365 nm) showing a lively red-magenta coloration characteristic of the doping ion. This emission, qualitatively, indicates the probable presence of the Eu^{3+} ion within the crystal lattice of the matrix. In order to confirm the qualitative hypothesis outlined before, the sample was characterized by XRD and TEM.

Unfortunately, the XRD pattern showed very broadened reflections indicating very small crystallites and low signal to noise ratio (SNR) which makes the identification of crystalline phase very difficult. Moreover, due to the low SNR an evaluation of possible peak shifts, which would provide evidence of the presence of Europium in the structure, is extremely complicated; for this reason, the refinement Rietveld method was not applied to this sample and consequently the lattice parameters and the average size were not calculated.

The morphological-structural analysis was performed by direct observation of nanoparticles through TEM analysis. In figure 28 the doped nanoparticles with Eu^{3+} are shown; it is observed that they have a disk-shape morphology with a diameter about 6 nm and thickness of 1 nm (figure 28b).
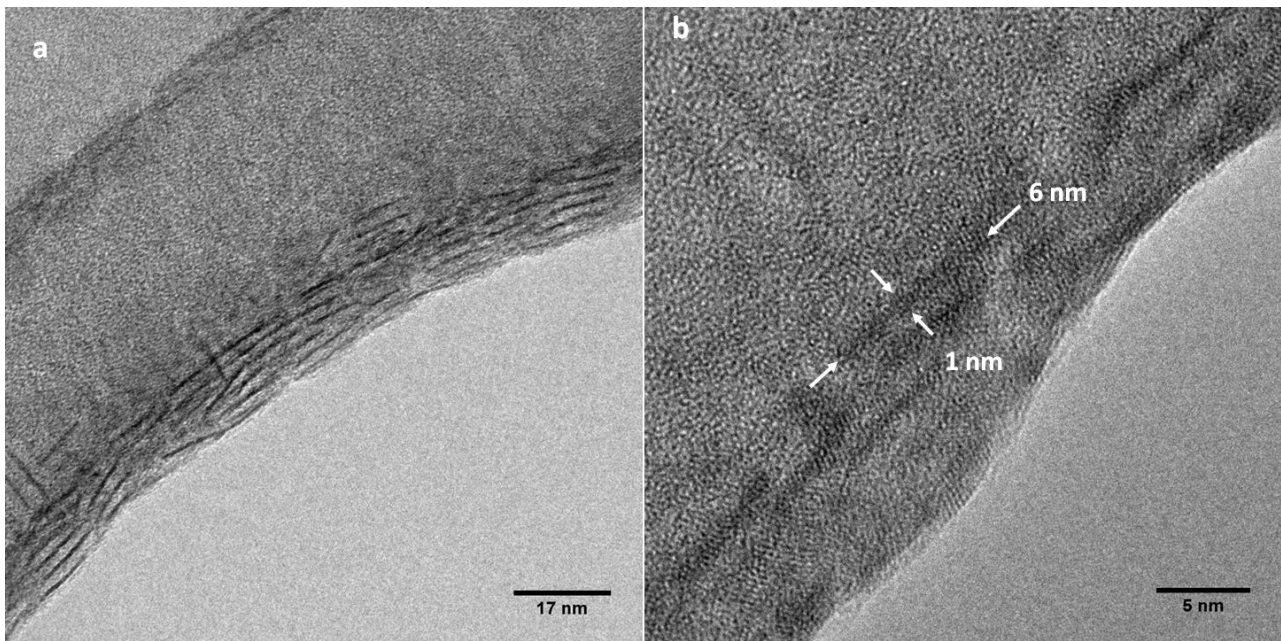
Figure 30: Tem image of Gd$_2$O$_3$:Eu10% nanodisk (a); HRTEM (b)

Comparing these values with the ones for pure Gadolinium oxide sample, we note that both samples are dimensionally similar. However, it is not possible to determine the crystallographic phase of the NPs for the doped sample. The results of EDS analysis showed the presence of Gadolinium as a major element and a lower intensity signal falling at energy very close to the one pertaining to Gd making difficult to discriminate

between the two signals; in fact, the energy difference between the two, if compared with the resolution of the measurement, is too low and consequently the two signals are displayed as a single wide band.

In all the samples analyzed, regardless of the type of dopant ion used, a columnar arrangement is observed where the nanoparticles are stacked one on the top of the other in a uniform and orderly manner, showing at the observer the thickness of the disc. Furthermore, the average distance between two consecutive particles is equal to 2.4 nm, that is equal to the length of the aliphatic chain constituting the capping agent (figure 29)
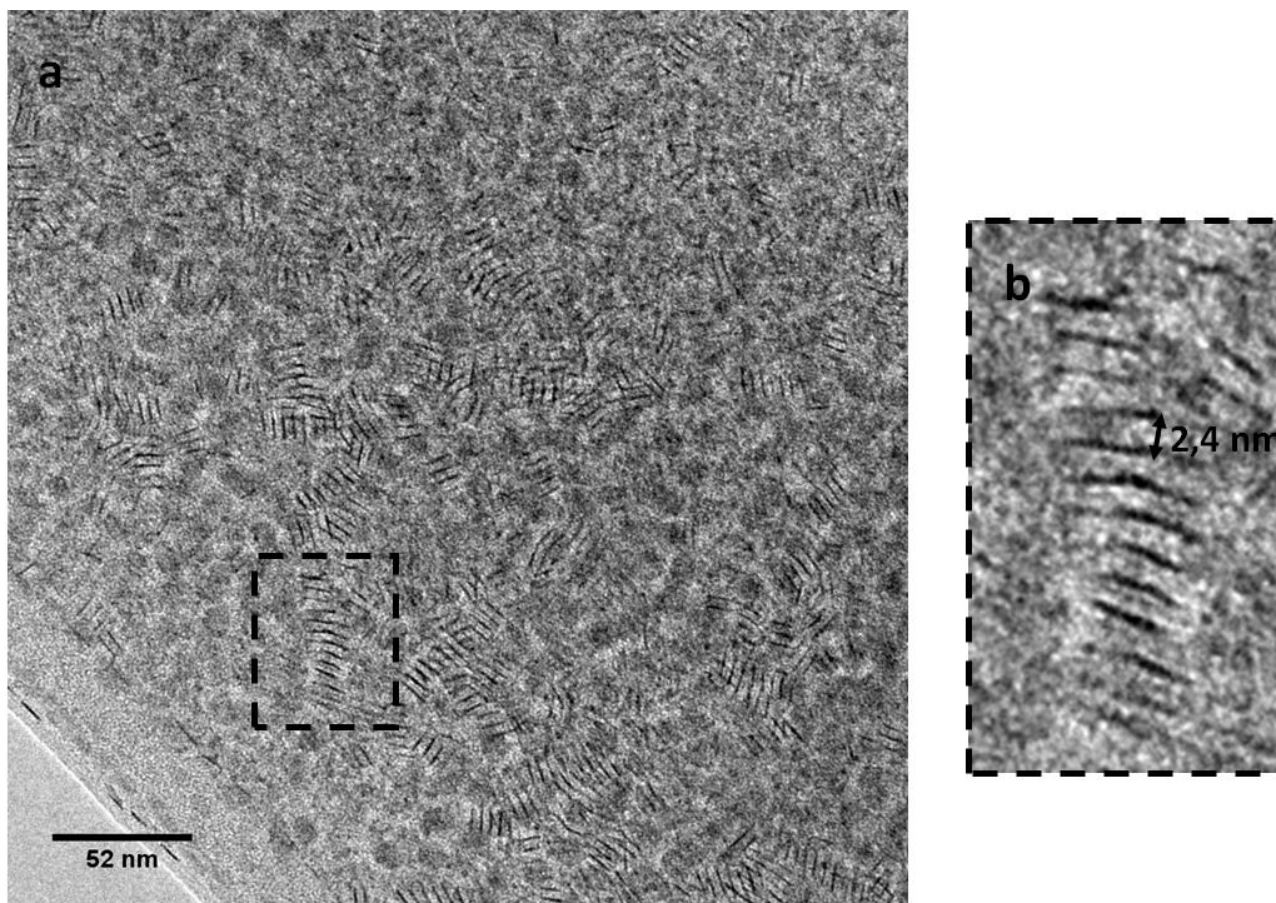
Figure 31: *Self-assembly of nanoparticles (a); detail of gap [nm] (b)*

An explanation of the mechanism by which the observed self-assembly takes place is given by considering the conformation of Oleic acid. In fact, it has a double bond in position 9 which diverts the chain in another direction not orthogonal to the surface of the nanoparticles. This three-dimensional conformation forms a "comb" linked to nanoparticles; between two consecutive "teeth" it is possible to insert a "tooth" of another ligand molecule belonging to an adjacent particle. Short-range interactions stabilize the system that, in this case, has the lowest energy configuration.

Conclusion

The work carried out and argued in this thesis has been divided into three parts. In the first one (chapter 3) the precursors reagents of the rare earth, necessary for the subsequent experimental parts, were produced and characterized. In particular, the complex acetylacetonate of Gadolinium, Ytterbium, Erbium and Europium were prepared. These compounds were characterized by Fourier Transform Infrared Spectroscopy (FT-IR); the spectra obtained were compared with literature data [69]. The comparison confirmed that the compounds produced are the rare earth acetylacetonate complexes mentioned above (the results obtained are presented in detail in appendix A).

The complexes produced were used as reagents in the synthesis of "pure" and doped Gadolinium Oxide nanoparticles, formed respectively the second and third part of this thesis (chapter 4).

The second part of this work saw, as protagonist, the synthesis of two nano-structured system based on Erbium and Gadolinium oxide nanoparticles using a "new" synthetic method: the digestive ripening process. The digestive ripening process uses oleylamine, with the dual role of solvent and capping agent, and oleic acid as a digestive agent. The sample consisting of Er_2O_3 was produced in order to determine which of the two organic molecules coat the nanoparticles after synthesis by FT-IR spectroscopy.

The acquired spectra showed the presence of both organic compounds however only oleic acid appears to be bound to the surface of the nanoparticles. This implies that the oleylamine must be removed. To this end, some washing tests were performed with solvents of different polarity (in ascending order hexane, toluene, diethyl ether and ethanol) and with a 1:3 solution of toluene/acetone.

The nonpolar solvent (hexane) and the two solvents with greater polarity (diethyl ether and ethanol) were unsuitable for an efficient purification of the nanoparticles from oleylamine residues. An excellent result was obtained using toluene as a washing solvent: the IR spectra, recorded in the three washing cycles, shows a complete removal of the amine. This was deduced form the disappearance of the signals relating to the –NH and C-N stretching characterizing the organic molecule. Given the efficiency in cleaning the nanoparticles, the use of toluene makes it difficult to isolate them, so a solution of toluene and acetone (in a 1:3 ratio) was used, which allows to eliminate impurities and isolate only the lanthanide oxide nanoparticles.

Using the same method, a sample consisting on Gd_2O_3 was produced whose characterization highlighted the formation of a poly-disperse anisotropic crystal system.

The structural analysis by x-ray diffraction identified two different populations of particles with cubic and monoclinic crystallographic structures respectively. The same analysis showed that these populations have different size. The application of Rietveld's method, for the refinement of the diffraction profile, confirmed the non-uniformity of the sample size by quantifying the average size and the lattice parameters of the two populations. The first family of particles have an edge of cell equal to 10.81 ± 0.01 Å and with average dimension of 9 ± 1 nm; the second one has average size of 6.2 ± 0.9 nm.

The same sample was analyzed by transmission electron microscope (TEM); this analysis in addition to confirm the results obtained by x-ray diffraction, revealed a poor definition of the shape of the nanoparticles. On the basis of these consideration, in agreement with the literature, two new series of samples were produced using a transition metal, as a definer of shape and size, in the synthetic process.

The first series of samples saw the use of Zn(II) while in the second series Nickel was used. Both transition metals have been used as acetylacetonate complexes.

In both series of samples, the results show that the use of the transition metal significantly increases the definition of the shape of the nanoparticles which appear as disks with a diameter of 5.4 ± 0.4 nm (sample produced with Zn^{2+}) and 6.1 ± 0.6 nm (sample synthesized with Ni^{2+}).

Furthermore, the dimensional analysis carried out on the images acquired by TEM shows a narrow size distribution, indicating the effectiveness of the metal to producing a mono-dispersed system in the final product.

However, both x-ray and electron microscopy characterization revealed the presence of ZnO in the sample produced with this metal. In fact, it is formed simultaneously with Gadolinium oxide and forms a second crystalline phase of greater dimensions equal to 58 ± 9 nm.

Zinc oxide, having an absorption in the ultraviolet region of the electromagnetic spectrum, must be removed from the sample as it would prevent a correct evaluation of the optical properties of the nano-material in view of potential application in the biomedical field. Nevertheless, the ZnO is an integral part of the sample and its removal is difficult.

For this reason, in the subsequent syntheses the Zn(II) has been replaced with the Ni(II) which has shown the same properties in the definition of morphology and dimensional distribution of the nanoparticles and has the advantage of being easily removed. The separation of Ni from the Gd_2O_3 nanodisks, takes place by natural precipitation during the first washing cycle which has been done using a solution of toluene and acetone in 1:3 ratios.

The use of a metal ion (Zn or Ni) in addition to the advantages discussed above allows the stabilization of the cubic phase with respect to the monocline one during the digestive ripening process.

The third part of this experimental work has been the synthesis of Lanthanide doped Gadolinium Oxide nanoparticles. In particular, samples of Gd_2O_3 doped with Yb^{3+}/Er^{3+}, Pr^{3+} at three different concentrations (5, 10 and 15%) and with Eu^{3+} were produced.

The bi-doped sample with Yb^{3+} and Er^{3+} respectively at 3% and 1% has a cubic crystal structure of BCC type similar to the one formed for the pure sample of Gd_2O_3.

The comparison of the XRD patterns does not reveal any peak shifts thus suggesting the absence of dopant ions in the crystal lattice of Gadolinium oxide matrix. This is confirmed also by the Rietveld refinement of the experimental XRD profile: the calculated lattice parameters are analogous to the ones found for the un-doped sample.

Similar results were also found for the doped sample series with increasing concentration of Pr^{3+} ion. The XRD experimental data show the presence of a single crystalline phase, however the low SNR does not allow to appreciate any displacement of the diffraction peaks.

The refinement of the diffraction profile for each of the samples showed an anomalous trend of the reticular parameters with respect to the dopant concentration: the 10% doped sample shows unit cell parameters greater than the ones of the doped samples at 5% and 15% respectively. An explanation could be hypothesized considering the the following aspect: Lanthanide Praseodymium, is present at the beginning in the reaction environment as Pr(III), but can then rapidly oxidize to Pr(IV) and enter into the lattice in this oxidation state. Since in the state 4+ the ionic radius of Pr (99 pm) in smaller than that of the Gd3+ (107.8 pm,) this could explain the unit cell compression observed for the doped samples at 5% and 15.

According to this line of thought, the lattice expansion seen in the 10% doped sample should be a symptom of the presence of the doping ion in 3+ oxidation state.

Nevertheless, considering that all the syntheses were carried out using the same experimental conditions, the possibility described above in unlikely.

The non-linear trend of the lattice parameters of this series of samples is more likely to derive form an incorrect refinement of the diffraction profiles. More precisely, since the experimental data have a low SNR it's possible that the simulation of the background does not allow a precise refinement of the position of the peak positions thus causing an error in the estimation of the lattice parameters.

The high background noise found in the XRD profile of aforementioned samples, was also found of the XRD pattern of the doped sample with Eu^{3+}; this high noise did not permit the identification with absolute certainty neither of the crystalline structure nor the possible shifting of the peaks of this sample.

Observing the $Gd_2O_3:Eu_{10\%}$ under a UV lamp, we note an interesting magenta-red coloration which, qualitatively, indicates the presence of Europium in the crystal structure.

To verify the effective presence of the doping ion, it is necessary to perform photoluminescence analysis: in this way the presence of doping would be confirmed, but this is out of the scope of the thesis. If this were the case, it would prove that the modified digestive ripening method is able to produce, not only nanoparticles based on lanthanide oxides with a well-defined shape and precise dimensional distribution, but also doped nanoparticles with the same characteristics.

All the samples synthesized grown in the final form of nano-disks with a diameter between 8 nm and 5 nm and with a thickness of about 1 nm.

The TEM micrographs showed a high ordering of nanoparticles known as self-assembly. This is due to the short-range interactions between the organic molecules bound to the surface of adjacent particles and between the same molecules and the solvent in which they are dispersed, this self-assembly phenomenon represents an excellent starting point for future studies.

BIBLIOGRAPHY

[1] I. 27867, *Nanotechnologies - Terminology and definnitions of nano object, nanoparticle, nanofibre and nanoplate.,* 2008.

[2] S. 2456-06, *Standard Teminology Relating to Nanotechnology.*

[3] SCENIHR, *Scientific Basis for the Definition of the term nanomaterials.*

[4] D. L. S. R. S. W. S. a. S. Z. B. Bhushan, Handbook of Nanomaterials Properties, Sprineer, 2014.

[5] J. H. a. P. D. Lisa J, "Chapter 10 - Nanoparticles and Nanosized Structure in Diagnostics and Therapy," in *Precision Medicine: Tools and Quantitative Approaches*, 2018, pp. 229-252.

[6] M. C. I. I.-B. a. M. M. María Vallet-Regí, "Mesoporous Silica Nanoparticles for Drug Delivery: Current Insights," *Molecules,* vol. 23, no. 47, pp. 1-19, 2018.

[7] Q. L. M. W. J. O. X. L. a. M. M. X. Liangpeng Ge, "Nanosilver particles in medical applications: syntheis, performance and toxicity," *International journal of Nanomedicine,* vol. 9, pp. 2399-2407, 2014.

[8] E. B. a. D. Astruc, "Gold nanoparticles in nanomedicine: preparations, imaging, diagnostics, therapies and toxicity," *Chemica Society Reviews,* vol. 38, no. 6, p. 1759, 2009.

[9] S. P. S. H. Dai, "Multifunctional FeCo-graphitic carbon nanocrystals for combined imaging, drug delivery and tumor-specific photothermal therapy in mice," *Nano Research,* vol. 4, no. 12, pp. 1248-1260, 2011.

[10] M. L. X. J. S. L. Yujuan Si, "Recent advances in Fe-Pt nanoparticles for biomedicine," *Journal of Nanomaterials,* vol. 21, no. 2, p. 22, 2015.

[11] L. W. H. G. Y. a. Y. H. S. Zi Fei Yin, "Recent progress in biomedical applications of titanium dioxide," *Physical Chemistry Chemical Physics,* vol. 15, no. 14, p. 4844, 2013.

[12] O. S. K. Y. M. S. S. M. T. O. M. N. Y. F. K. Senthilkumar, "Preparation of ZnO nanoparticles for bio-imaging applications," *Basic solid state physic,* vol. 246, no. 4, pp. 885-888, 2009.

[13] N. A. M.-R. R. A. J. P. D. R. J. N. W. T. S. J. M. S. S. A. S. Karakoti, "Nanoceria as antioxidant: Synthesis and biomedical applications," *Overview Biological Materials Science,* vol. 60, no. 3, pp. 33-37, 2008.

[14] H. Z. M. Z. I. u. H. A. R. P. J. S. A. a. A. H. Attarad Ali, "Synthesis, characterization, application and challenges of iron oxide nanoparticles," *Nanotechnology Science and Application,* no. 9, pp. 49-67, 2016.

[15] K. M. a. S. A. M. Tofail, "Nanoparticles in biomedical applications," *Advances in Physics: X,* vol. 2, no. 1, pp. 54-88, 2017.

[16] J. D. R. R. C. H. a. W. L. Kathryn M. L. Taylor-Pashow, "Hybrid nanomaterials for biomedical applications," *The Royal Society of Chemistry,* vol. 46, pp. 5832-5849, 2010.

[17] S. L. Z. M. a. J. Q. Yingxin Hao, "Understanding differences in Er3+–Yb3+ codoped glass and glass ceramic based on upconversion luminescence for optical thermometry," *Royal Society of Chemistry,* no. 8, pp. 12165-12172, 2018.

[18] P. Y. F. H. S. G. G. Y. ,. Y. D. Z. H. J. L. Ruichan Lv, "An imaging-guided platform for synergisticphotodynamic/photothermal/chemo-therapy with pH/temperature-responsive drug release," *Biomaterials,* no. 63, pp. 115-127, 2015.

[19] H. K. P. D. J. H. G. Wakefielda, "Structural and optical properties of terbium oxide nanoparticles," *Journal of physics and chemistry of solids,* no. 60, pp. 503-508, 1999.

[20] H. A. K. P. J. D. a. J. L. H. G. Wakefield, "Synthesis and Properties of Sub-50-nm Europium Oxide Nanoparticles," *Journal of colloid and inteface science,* no. 215, pp. 179-182, 1999.

[21] M. F. C. L. K. L. W. Z. C. D. S. R. B. M. G. L. E. B. P. P. a. O. T. R. Bazzi, "Synthesis and properties of europium-based phosphors on the nanometer scale: Eu2O3, Gd2O3:Eu and Y2O3:Eu," *Journal of Colloid and Interface Science,* no. 273, pp. 191-197, 2004.

[22] S. Cotton, Lanthanide and Actinide Chemistry, Wiley, 2006.

[23] F. A. F. a. E. M. V.A.G. Rivera, "Localized Surface Plasmon Resonances: Noble Metal Nanoparticle Interaction With Rare-Earth Ions," in *Plasmonics - Principle and Applications*, 2012, pp. 283-312.

[24] M. F. Reid, "Theory of Rare-Earth Electronic Structure," in *Handbook on the Physics and Chemistry of Rare Earths*, 2016, pp. 47-64.

[25] P. l. R. a. C. P. Bernard Geffroy, "Organic light-emitting diode (OLED) technology: materials, devices and display technologies," *Polymer international,* vol. 55, no. 6, pp. 572-582, 2006.

[26] R. M. M. F. N. S. H. F. E. E. T. a. S. P. M. Back, "Energy transfer in color-tunable water-dispersible Tb–Eu codoped CaF2 nanocrystals," *Journal of Material Chemistry C,* no. 4, pp. 1906-1913, 2016.

[27] H. Q. P. N. P. X. C. Guanying Chen, "Upconversion Nanoparticles: Design, Nanochemistry, and Applications in Theranostics," *ACS Chemica Reviews,* vol. 114, no. 10, pp. 5161-5212, 2014.

[28] L. A. B. M. v. d. E. T. J. H. V. a. A. M. Janne-Mieke Meijer, "Downconversion for solar cells in YF3:Nd3+, Yb3+," *Physical Reviews B,* no. 81, p. 35107, 2010.

[29] P. Weiss, "Variation du ferromagnetism du temperature," *Comptes Rendus ,* pp. 1136-1149, 1906.

[30] [Online]. Available: https://en.wikipedia.org/wiki/Magnetic_susceptibility.

[31] K. Y. D.-N. V. C. J. K. R. W. N. B. K. G. R. M. C. Wang D, "Synthesis and oxygen storage capacity of two-dimensional ceria nanocrystals," *Angewandte Chemie international edition,* vol. 50, no. 19, pp. 4378-81, 2011.

[32] C. L. P. Y. a. J. L. Shili Gai, "Recent Progress in Rare Earth Micro/Nanocrystals: Soft Chemical Synthesis, Luminescent Properties, and Biomedical Applications," *ACS Chemical Reviews,* vol. 114, pp. 1242-1289, 2014.

[33] S. X. S. R. Y. L. a. Y. C. Zhang YW, "Single-crystalline and monodisperse LaF3 triangular nanoplates from a single-source precursor," *Journal of American chemistry society,* vol. 127, no. 10, pp. 3260-3261, 2005.

[34] C. L. P. Y. Z. S. H. a. J. L. Zhenhe Xu, "Rare Earth Fluorides Nanowires/Nanorods Derived from Hydroxides: Hydrothermal Synthesis and Luminescence Properties," *ACS Publications Crystal growth & design,* vol. 9, no. 11, pp. 4752-4758 , 2009.

[35] J. W. S. a. F. C. J. M. v. Veggel, "Near-infrared Emission of Redispersible Er3+, Nd3+, and Ho3+ Doped LaF3 Nanoparticles," *ACS Publications Nano Letters,* vol. 7, no. 733-737, p. 2, 2002.

[36] L. Y. J. L. Xiaoming Liu, "Synthesis and Luminescent Properties of LaAlO3:RE3+ (RE = Tm, Tb) Nanocrystalline Phosphors via a Sol—Gel Process," *The journal of physical chemistry C,* vol. 113, no. 19, pp. 8478-8483, 2009.

[37] G. W. C. L. L. Y. L. Jian-Ping, "Formation of Disperse Nanoparticles at the Oil/Water Interface in Normal Microemulsions," *Chemistry a European journal,* vol. 12, no. 25, pp. 6552-6558, 2006.

[38] F. H. S. G. C. L. X. Z. S. H. a. P. Y. Na Niu, "Rapid microwave reflux process for the synthesis of pure hexagonal NaYF4:Yb3+,Ln3+,Bi3+ (Ln3+ = Er3+, Tm3+, Ho3+) and its enhanced UC luminescence," *Journal of material chemistry,* vol. 22, pp. 2113-2162, 2012.

[39] A. Taubert, "(Sub)Micron CaF2 Cubes and Hollow Rods From Ionic Liquid Emulsions," *Acta Chim. Slov,* vol. 52, pp. 168-170, 2005.

[40] V. K. D. R. H. L. V. K. LaMer and R. H. Dinegar, "Theory, production and mechanism of formation of monodispersed hydrosols," *Journal of American Chemistry Society,* vol. 72, no. 11, pp. 231-252, 1950.

[41] V. P. W., "The theory of Ostwald ripening," *Journal of statistical physics,* vol. 38, no. 1-2, pp. 231-252, 1985.

[42] C. Murray and D. J. a. B. M. G. Norris, "Synthesis and characterization of nearly monodisperse CdE (E = sulfur, selnium, tellurium) semiconductor nanocrystallites," *Journal of American Chemistry Society,* vol. 115, no. 19, pp. 8706-8715, 1993.

[43] M. W. M. B. D. S. D. J. W. R. Brust, "Synthesis of thiol-derivatised gold nanoparticles in a two-phase liquidliquid system," *Journal Chemical Society, Chemical Communication,* vol. 0, no. 7, pp. 801-802, 1994.

[44] X. M. S. C. M. K. K. J. Lin, "Digestive ripening, nanophase segregation and superlattice formation in gold nanocrystal colloids," *Journal of nanoparticles research,* vol. 2, no. 2, pp. 157-164, 2000.

[45] S. P. J. L. a. N. H. D.K. Lee, "A theoretical model for digestive ripening," *Acta Mater,* vol. 55, no. 15, pp. 5281-5288, 2007.

[46] D. S. S. a. B. L. V. P. Jayesh R. Shimpi, "Digestive Ripening: A Fine Chemical Machining Process on the Nanoscale," *Langmuir,* no. 33, pp. 9491-9507, 2017.

[47] S. J. a. P. B. L. V., "Bromide ion mediated modification to digestive ripening process: Preparation of ultra-small Pd, Pt, Rh and Ru nanoparticles," *Nano Research,* no. 9, pp. 2007-2017, 2016.

[48] N. K. M.-G. K. a. W. K. Jinhoo Jeong, "Generic Synthetic Route to Monodisperse Sub-10 nm Lanthanide Oxide Nanodisks: A Modified Digestive Ripening Process," *ACS Publication Chemistry of Material,* no. 28, pp. 172-179, 2016.

[49] A. K. H. P. C. V. P.-O. K. a. K. U. M. Engstrom, "High proton relaxivity for gadolinium oxide," *Magnetic Resonance Material in Physics,* vol. 19, pp. 180-186, 2006.

[50] D. W. B. A. F. Z. Y. A. K. M. A. M. V. N. R. V. Y. S. A. A. E. E. Z. K. D. A. Zatsepin, "Electronic structure, charge transfer, and intrinsic luminescence of gadolinium oxide nanoparticles: Experiment and theory," *Mesoscale and Nanoscale physics,* 2017.

[51] E. G. V.-L. L. A. D.-T. H. D. J. L. R.-L. a. E. P. Octavio Meza, "Luminescence Concentration Quenching Mechanism in Gd2O3:Eu3+," *The journal of physical chemistry A ,* no. 118, pp. 1390-1396, 2014.

[52] "https://subversion.xray.aps.anl.gov/trac/pyGSAS/wiki/WikiStart," [Online].

[53] J. J. B. a. V. P. K.A. Gschneidner, Handbook on the Physics and Chemistry of Rare Earths, vol. 35, Elsevier, 2005, pp. 123-125.

[54] N. K. M.-G. K. a. W. K. Jinhoo Jeong, "Generic Synthetic Route to Monodisperse Sub-10 nm Lanthanide Oxide Nanodisks: A Modified Digestive Ripening Process," *Chemistry of Materials,* vol. 28, pp. 172-179, 2016.

[55] "AIST: spectral database for organic compound, SDBS," [Online]. Available: https://sdbs.db.aist.go.jp/sdbs/cgi-bin/cre_index.cgi.

[56] Y. Z. X. C. a. Y. M. Fengzhu Lv, "Composition and Fluorescence of Gadolinium(III) Acetylacetonate Derivates by Solvothermal Method," *Internation Journal of Optics and Photonic Engineering,* vol. 2, no. 5, pp. 1-8, 2017.

[57] R. H. H.-C. G. Ling Zhang, "Oleic acid caoting on the monodisperse magnetite nanoparticles," *Applied surface science,* 2006.

[58] "ImageJ software," [Online]. Available: https://imagej.nih.gov/ij/.

[59] S. R. K. a. N. G. Satyanarayana Talam, "Synthesis, Characterization, and Spectroscopic Properties of ZnO Nanoparticles," *IRSN Nanotechnology,* 2012.

[60] "https://en.wikipedia.org/wiki/Zinc_oxide," [Online].

[61] Y.-W. Z. L.-P. Y. a. C.-H. Y. Rui Si, "Rare-Earth Oxide Nanopolyhedra, Nanoplates , and Nanodisks," *Angewandte Chemie Internation Edition: Nanocrystals,* vol. 44, no. 21, pp. 3256-3260, 2005.

[62] https://en.wikipedia.org/wiki/Ionic_radius, "Ionic radius," [Online].

[63] S. Z.-A. a. M. Salavati-Nisari, "Preparation and characterization of nanocrystalline praseodymium oxide via a simple precipitation approach," *Journal of Mater Science,* vol. 26, pp. 5812-5821, 2015.

[64] R. Z. B. B. A. H. a. T. P. O. Greis, "The crystal structure of the low-temperature A-type modification of Pr2O3 form x-ray powder and electrin single crystal diffraction," *Journal of Alloys and Compounds,* vol. 216, no. 2, pp. 255-258, 1995.

[65] H. F. B. X. X. W. C. D. a. Y. Q. Maofeng Zhang, "Synthesis, Characterization, and Luminescence Properties of Uniform Ln3+-Doped YF3 Nanospindles," *Journal of physical chemistry C,* vol. 111, pp. 6652-6657, 2007.

[66] H. A. K. P. D. a. J. L. H. G. Wakefield, "Synthesis and Properties of Sub-50-nm Europium Oxide Nanoparticles," *Journal of colloid and interface science,* vol. 215, pp. 179-182, 1999.

[67] X. W. X. L. Y. C. C. D. a. M. Y. Shaoshuai Zhoua, "Temperature sensing based on the cooperation of Eu3+and Nd3+inY2O3nanoparticles," *Sensor and Actuators B: Chemical,* vol. 246, pp. 352-357, 2017.

[68] M. A. F. C. L. K. L. W. Z. ,. C. D. S. R. B. M. G. L. E. B. P. P. a. O. T. R. Bazzia, "Synthesis and properties of europium-based phosphors on the nanometer scale: Eu2O3, Gd2O3:Eu, and Y2O3:Eu," *Journal of Colloid and Interface Science,* vol. 273, no. 1, pp. 191-197, 2004.

[69] H. A. a. A. E.-A. F.M. Abdel Kerim, "Infrared absorption spectra of some lanthanide acetylacetonate complexes," *Indian Academy of Sciences ,* vol. 86, no. 6, pp. 559-566, 1997.

IR SPECTRA OF LANTHANIDE ACETYLACETONATE COMPLEXES

In the following text the IR spectra, of all lanthanide complexes that are synthesized, will be illustrated.
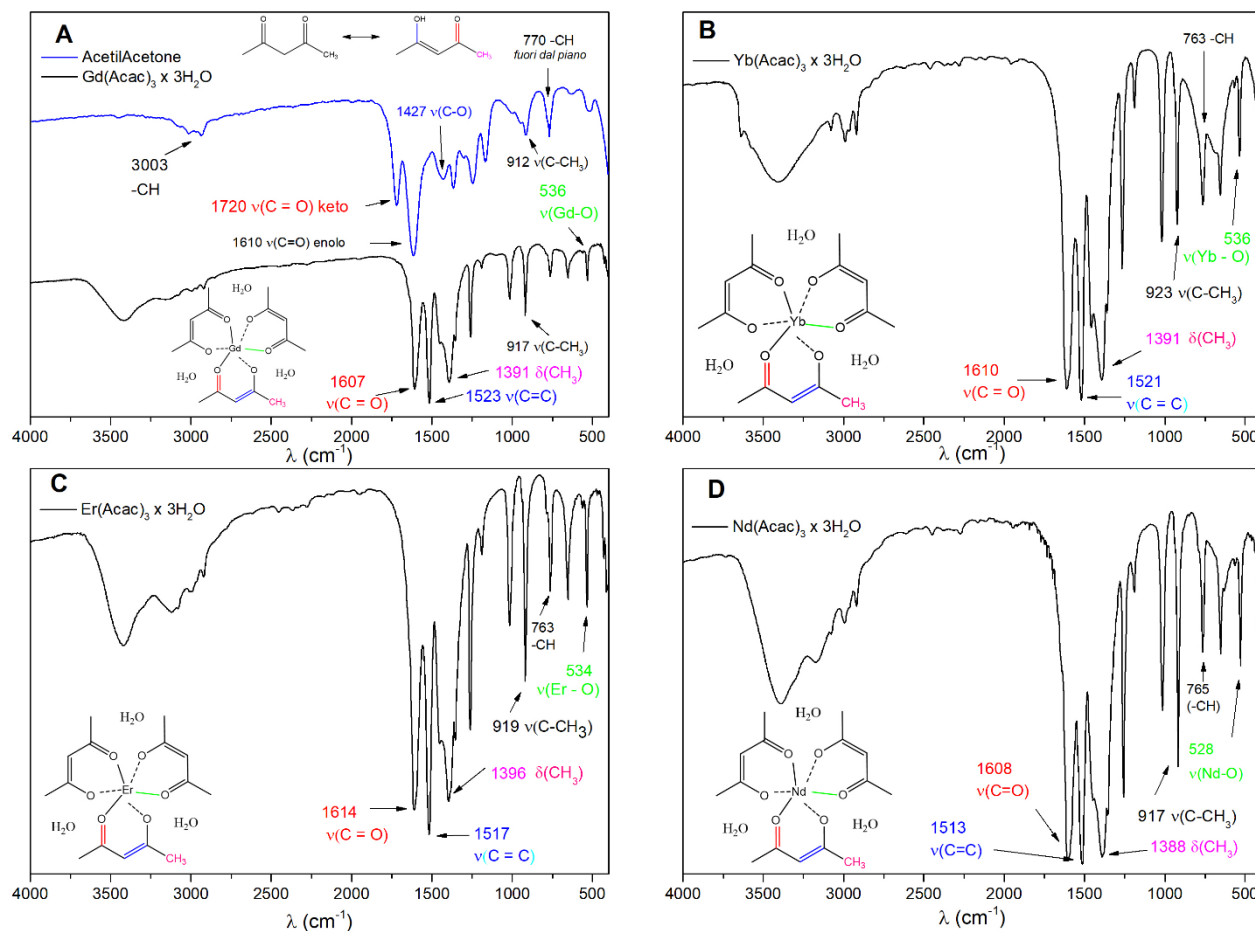

Figure 32: IR spectra of Gd(Acac)$_3$ x 3H$_2$O and pure Acetylacetone (A), Yb(Acac)$_3$ x 3H$_2$O (B), Er(Acac)$_3$ x 3H$_2$O (C) and Nd(Acac)$_3$ x 3H$_2$O (D)

Figure 32 shows the four IR spectra of the synthetized acetylacetonate complexes. The same figure shows the position of the main active IR signals and the relative functional groups from which the structure, of the complex, is described.

IR spectroscopy allows to obtain qualitative information such as product identification and its structure. identification takes place by recognizing the position of the IR active vibrational modes of particular functional groups present in the molecule under examination. For this purpose, in figure 31, a comparison between the four spectra recorded is reported.
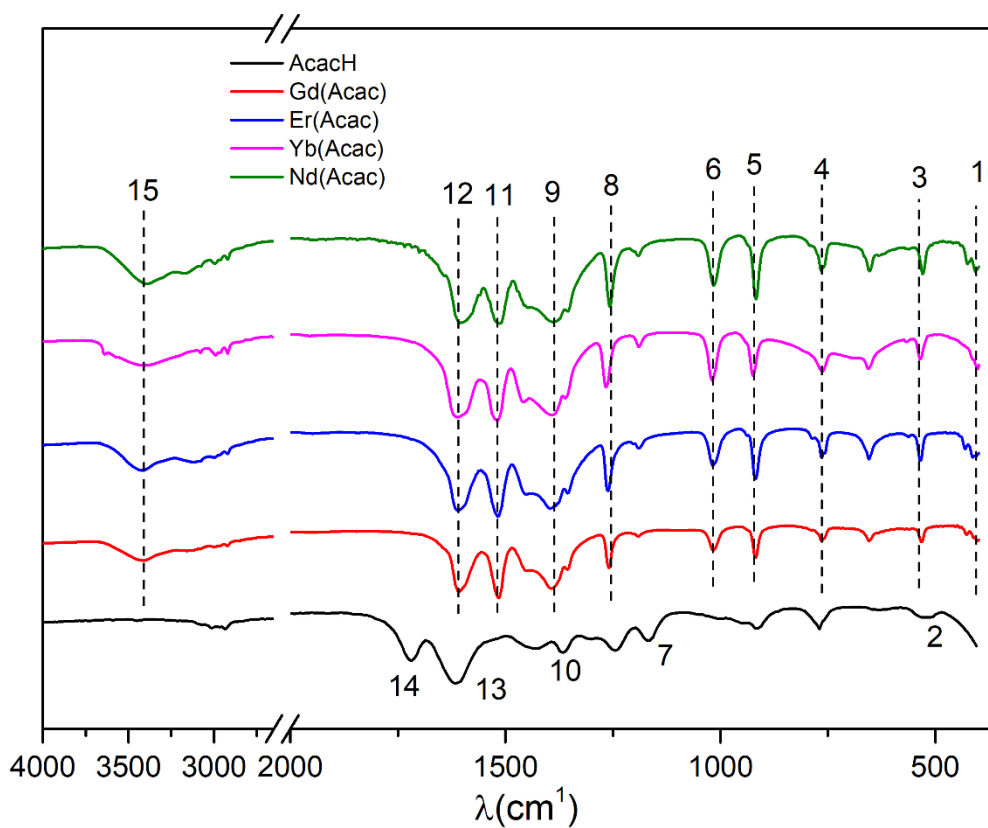
Figure 33: *IR spectra of the four Acetylacetonate complexes*

In the spectra of the four acetylacetonate complexes (figure 33) the main signals have been numbered from 1 to 15. The following table shows the experimental position of these signals which will be compared with literature data [69] (theoretical position in table 13).

		Theoretical			RI	Vibrational modes	Experimental				#
	AA	Nd	Gd	Yb			Nd	Gd	Yb	Er	
Region 1		410	411	410	m	v(Ln-O)	408	404	406	410	*1*
	510				m	CH-ring					*2*
		529	**532**	**534**	**m**	**v(Ln-O)**	**528**	**536**	**536**	**534**	*3*
Region 2	**760**	**735**	**760**	**762**	**m**	**CH *out of plane***	**765**	**763**	**763**	**763**	*4*
	910	**910**	**920**	**918**	**s**	**v(C-CH$_3$)**	**917**	**917**	**923**	**919**	*5*
		1018	1020	1020	s	γ(CH$_3$)	1014	1018	1018	1016	*6*
	1170				s	δ(CH) + (CH$_3$)					*7*
	1250				s	δ(CH)					*8*
		1390	**1390**	**1390**	**s**	**δ(CH$_3$)**	**1388**	**1391**	**1391**	**1396**	*9*
	1430				s	v(C-O) + CH$_3$					*10*
Region 3		**1520**	**1524**	**1520**	**vs**	**v(C = C)**	**1513**	**1523**	**1521**	**1517**	*11*
		1608	**1613**	**1615**	**vs**	**v(C = O)**	**1608**	**1607**	**1610**	**1614**	*12*
	1630				vs	v(C = O) *enolo*					*13*
	1760				vs	v(C = O) *chetone*					*14*

Table 13: *IR active vibrational modes of acetylacetonate complexes: expected (theoretical), synthesized (experimental). RI (Relative intensity: m: medium; s: strong; vs: very strong. Vibrational modes: v: stretching; δ: bending; γ: rocking.*

Looking at the figure 31 it can be seen that the spectra of the four complexes are replaced by the same signals, it is therefore possible to divide the spectrum into four regions. Region 1 from 400 cm^{-1} to 700 cm^{-1} contains the signals related to the vibration of the covalent lanthanide-oxygen bond, in particular the Ln – O stretching signals are placed at 528 cm^{-1} for Neodymium, at 536 cm^{-1} for Gadolinium and Ytterbium and at 534 cm^{-1} for Erbium complexes.

Region 2 from 700 cm^{-1} to 1500 cm^{-1} contains the signal of aliphatic functional group such as –CH and –CH$_3$ that are present in the ligand molecule. In this region a particularly important signal is that related to the stretching out of plane of the –CH group placed in α-position with respect to the two carbonyl groups of the α,β-diketone.

The third region, which extend from 1500 cm^{-1} to 2000 cm^{-1}, sees the presence of the active IR signals related to the system π coordinating with the ion Ln^{3+}. Signal 11, positioned at about 1520 cm^{-1} and the signals 12 at 1610 cm^{-1} indicate that the binder is present in the form of enolate, this it possesses a negative charge resonating between the two oxygen atoms and the carbon atom in beta position.

Finally, the region 4 (from 2000 cm^{-1} to 4000 cm^{-1}) contains the stretching of –OH groups which indicate the presence of water. Since the intensity of these signals is weak it's possible to state that the synthesis products contain water of crystallization.

Using these consideration (ligand molecule in enolic form, covalent Ln – O bond and stretching –CH out of plane) it is possible to hypotize the three-dimensional structure of the complex acetylacetonate of rare earth produced. This structure is illustrated in figure 34 and it is in agreement with the work of Fengzhu et al. [56].
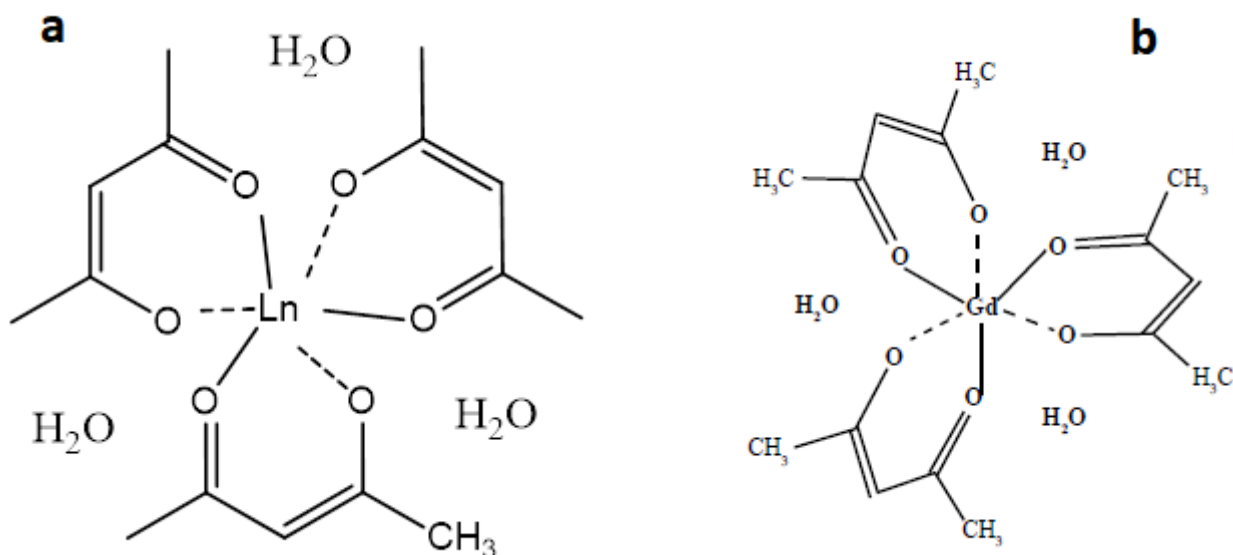
Figure 34: *structure of Ln(Acac)^3 x 3 H^{2}O (Ln:Gd^{3+}, Er^{3+}, Yb^{3+} and Nd^{3+}) projection on plane (a) and tri-dimensional (b).*

The structure of the complexes is presented with the trivalent ion Ln^{3+} (where Ln^{3+} = Gd, Er, Yb or Nd) placed at the center of a coordinating system. This system is formed by the π electrons of β-di-ketone in its enolic form, which also has a negative charge. The trivalent metal center is then stabilized by three ligand molecules which form three covalent bonds, signal ν(Ln – O), and three dative bonds.

Since the electrons of π-system belong to the orthogonal plane of the ligand molecule, the structure of the complex can be seen in the three dimension (figure 32b). this is supported by the presence of the –CH signals (out of plane stretching) at about 736 cm^{-1}.

The FT-IR analysis carried out, however, is able to provide qualitative information from which a possible structure is extrapolated. In order to determine with certainty, the architecture of the acetylacetonate complexes of the rare earth produced it is necessary to carry out an x-ray diffraction analysis.

Appendix B

X-RAY POWDER DIFFRACTION PATTERN AND RIETVELD REFINEMENT

In the following text the x-ray powder diffraction patterns, the calculated profile by Rietveld method and the structural data extrapolated by the same method of $Gd_2O_3{:}Yb_{3\%}Er_{1\%}$ and $Gd_2O_3{:}Pr_x$ (x = 5%, 10% and 15%) will be illustrated.
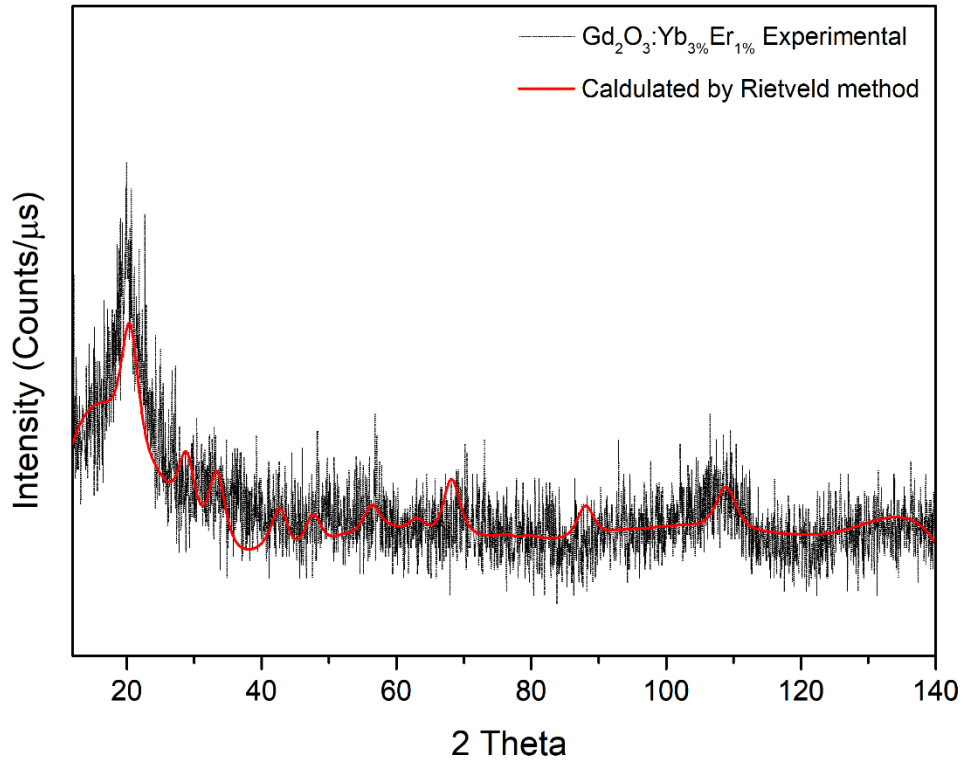

Figure 35: *Experimental xrd pattern and calculated profile by Rietveld of $Gd_2O_3{:}Yb_{3\%}Er_{1\%}$*
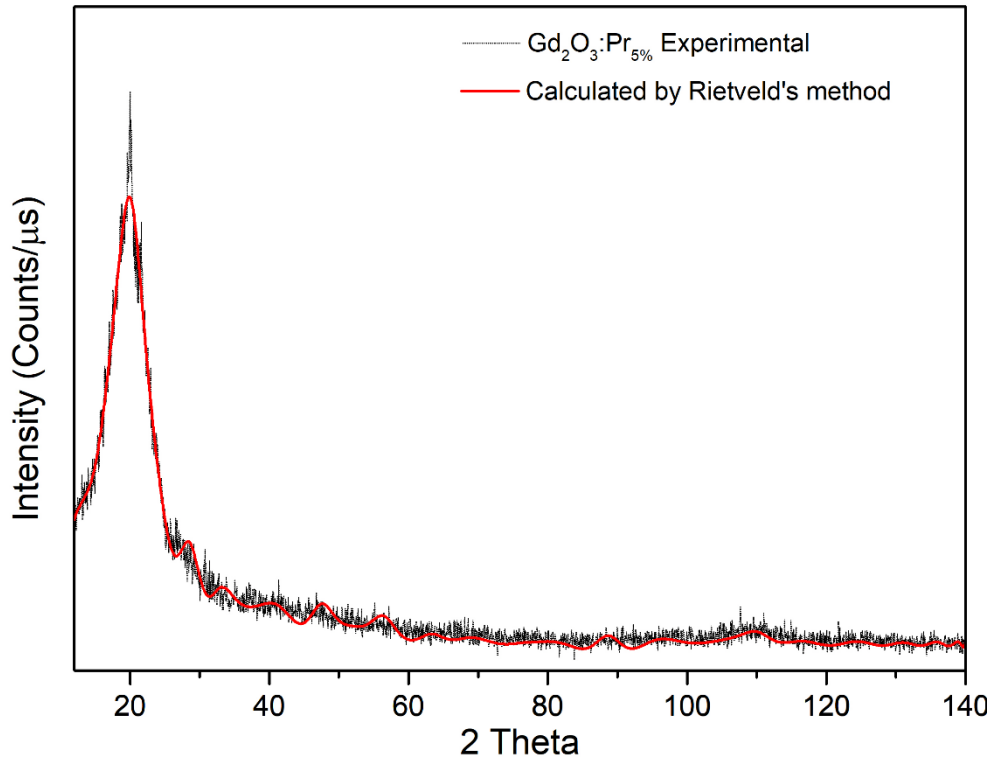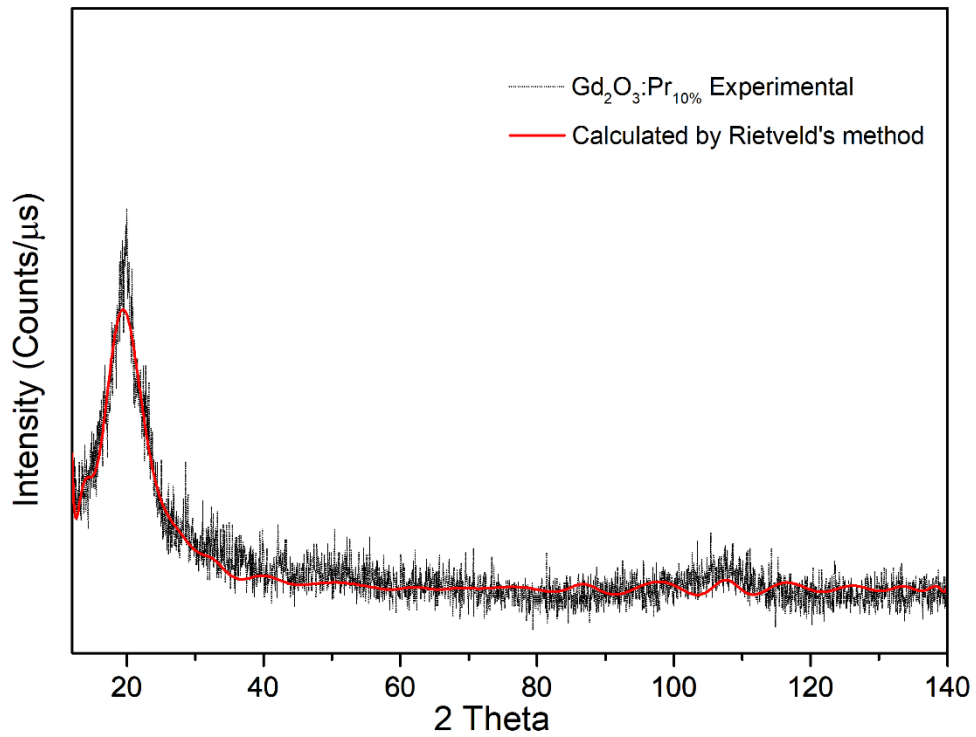
Figure 36: *Experimental xrd pattern and calculated profile by Rietveld of Gd$_2$O$_3$:Pr$_{5\%}$*

Figure 37: *Experimental xrd pattern and calculated profile by Rietveld of Gd$_2$O$_3$:Pr$_{10\%}$*
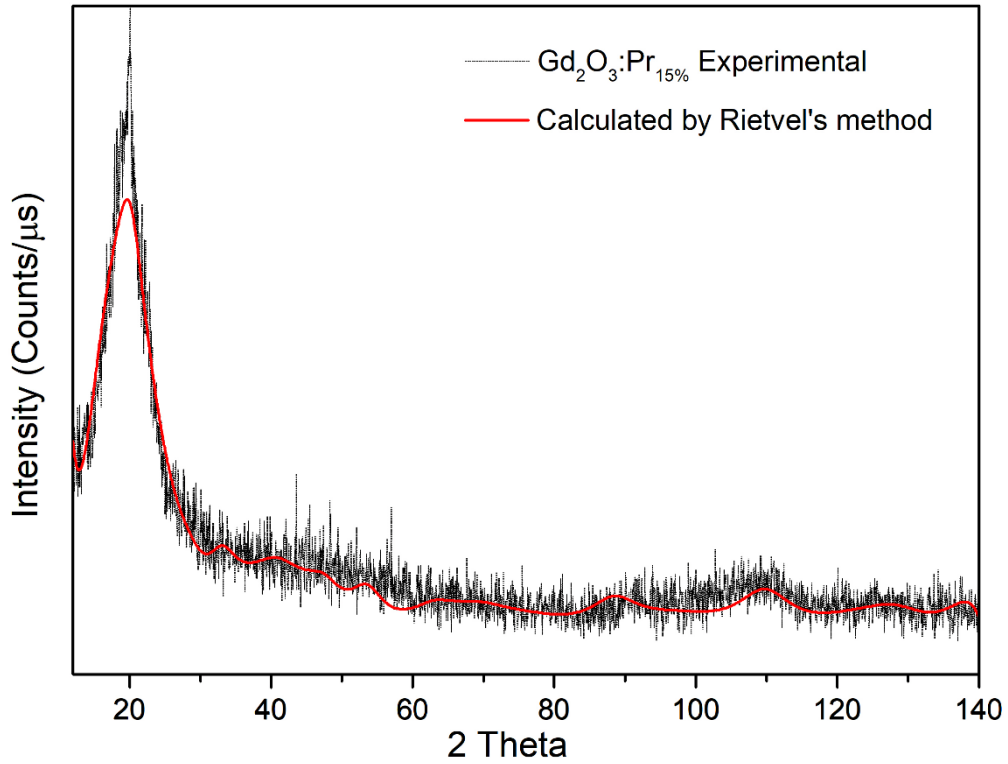
Figure 38*: Experimental xrd pattern and calculated profile by Rietveld of Gd$_2$O$_3$:Pr$_{15\%}$*

In the table 14, the structural data extrapolated from Rietveld refinement of the bi- and mono- doped samples are reported.

Sample name	Composition	Phase	Space Group	Edge of cell (Å)	Dimension by Sherrer's equation <D> (nm)	Figure
MFGdO_YbEr	Gd$_2$O$_3$:Yb$_{3\%}$Er$_{1\%}$	BCC	Ia-3	10,910 ± 0,009	8,8 ± 0,1	35
MFGdOPr5	Gd2O3:Pr5%	BCC	Ia-3	10,804 ± 0,006	9,1 ± 0,3	36
MFGdOPr10	Gd2O3:Pr10%	BCC	Ia-3	10,968 ± 0,006	5,4 ± 0,3	37
MFGdOPr15	Gd2O3:Pr15%	BCC	Ia-3	10,83 ± 0,01	3,8 ± 0,3	38

Table 14*: structural data extrapolated from Rietveld refinement.*

Finally, the xrd pattern of Gd_2O_3:$Eu_{10\%}$ and relative crystalline phase (in agreement with pdf 01-073-6953) is illustrated in figure 39.
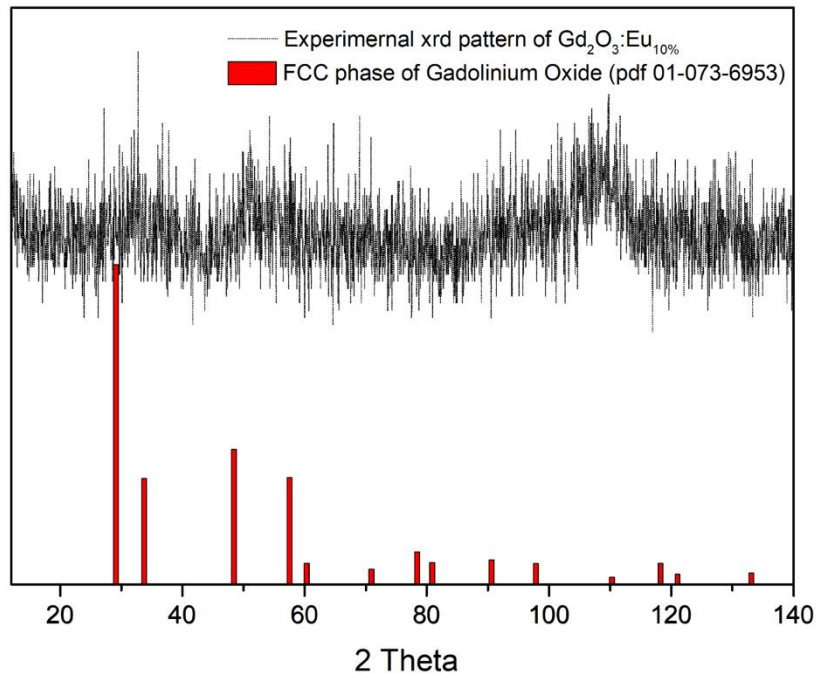

Figure 39: *xrd pattern and crystalline phase of Gd$_2$O$_3$:Eu$_{10\%}$*